THE UNIVERSITY OF MICHIGAN
COLLEGE OF ENGINEERING
Department of Electrical Engineering
Space Physics Research Laboratory

Scientific Report No. HS-1

THEORETICAL AND EXPERIMENTAL INVESTIGATION OF RADIOACTIVE IONIZATION GAUGES

Prepared on behalf of the project by:

Mohammad A. El-Moslimany

UMRI Projects 2096, 2406, 2597, 03554

The research reported in this document has been sponsored by the Geophysics Research Directorate of the Air Force Cambridge Research Center, Air Research and Development Command, under Contracts Nos. AF 19(604)-545, 1511, 1948, 6162.

administered by:

THE UNIVERSITY OF MICHIGAN RESEARCH INSTITUTE ANN ARBOR

May 1960

This report has also been submitted as a dissertation in partial fulfillment of the requirements for the degree of Doctor of Philosophy in The University of Michigan, 1960.

TABLE OF CONTENTS

TABLE OF CONTENTS (Concluded)

LIST OF FIGURES

LIST OF FIGURES (Continued)

LIST OF FIGURES (Continued)

LIST OF FIGURES (Continued)

LIST OF FIGURES (Concluded)

LIST OF SYMBOLS

a	rate of electron attachment.
a_1	coefficient used in Eq. (3.97).
A	coefficient in current polynomial, Eq. (3.63).
A'	coefficient in current polynomial, Eq. (3.102).
b	dimensionless parameter, Eq. (3.65).
b_1	coefficient used in Eq. (3.97).
b_∞	effective radius of collisions for gas particles at $T = \infty$.
B	coefficient in current polynomial, Eq. (3.63)
B'	coefficient in current polynomial, Eq. (3.102).
c_e	random velocity of electrons.
c_g	random velocity of gas particles.
c_i	random velocity of ions.
c_n	random velocity of negative ions.
c_p	random velocity of positive ions.
c_1	coefficient used in Eq. (3.97).
C	constant of integration, Eq. (3.42).
C_1	constant of integration, Eq. (3.56).
C_2	constant of integration, Eq. (3.92).
C_3	constant of integration, Eq. (3.95).
d_o	radius of sphere of active attraction, Eq. (2.20).
D	diffusion coefficient.
D_e	diffusion coefficient of electrons.

D_n diffusion coefficient of negative ions.

D_p diffusion coefficient of positive ions.

E electric field intensity.

$\vec{E}$ electric field intensity, a vector quantity.

E_x component of electric field intensity.

f collection efficiency, Eq. (3.1).

f_k molar fraction of the kth gas component.

F attractive force between an ion and a molecule, Eq. (2.5).

F_i effective molar fraction of ith component gas, Eq. (3.118).

g average rate of volume ionization.

g_o average rate of initial volume ionization, Eq. (2.1).

g' average rate of volume ionization defined by Eq. (3.81).

G mobility constant, Eq. (2.3).

i total current.

i_o total saturation current.

J total current density.

J' net ionic current density, Eq. (3.82).

J_m saturation current density, Eq. (3.4).

$\vec{J}$ total current density, a vector quantity.

$\vec{J}_e$ current density due to flow of electrons, a vector quantity.

$\vec{J}_n$ current density due to flow of negative ions, a vector quantity.

$\vec{J}_p$ current density due to flow of positive ions, a vector quantity.

k Boltzmann's constant, value 1.38×10^{-23} joules/°K.

ℓ_e electron mean free path.

ℓ_{e_a} average random free path for electron attachment.

ℓ_{e_o} standard-of-comparison electron mean free path.

ℓ_{e_R} Ramsauer electron mean free path.

ℓ_g mean free path of gas particles.

ℓ_i mean free path of ith type of ions.

ℓ_n mean free path of negative ions.

ℓ_p mean free path of positive ions.

m_e mass of an electron.

m_g mass of a gas particle.

m_i mass of an ion.

M_o molecular weight.

n_e concentration of free electrons.

n_n concentration of negative ions.

n_p concentration of positive ions.

N_o number of ion pairs initially produced per unit length, Eq. (2.1).

N_∞ number of ions, per unit length, escaping columnar ionization, Eq. (2.17).

N_A Avogadro's number, value 6.025×10^{26}.

N_q Loschmidt's number, value 2.687×10^{25} molecules per cubic meter.

p total electric dipole moment.

p_i induced electric dipole moment.

p_p permanent electric dipole moment.

P gas pressure in millibars.

q ionic charge.

q_e electronic charge, value 1.6×10^{-19} coulomb.

r	distance between ions and gas particles, Eq. (2.4).
r_e	rate of electron-ion recombination, Eq. (3.19).
r_i	rate of ion-ion recombination, Eq. (3.19).
r_m	radius of deflecting cross sections of an electron in a gas.
r_1, r_2	inner and outer diameter of two coaxial cylinders.
s	random distance in gas.
s_o	spacing between parallel plates.
t	time elapsed in seconds.
T	gas temperature on Kelvin scale.
T'	temperature constant, Eq. (2.23).
u	velocity of ionizing particles.
v_e	electron drift velocity.
v_i	ion drift velocity.
V	total voltage between electrodes.
V_n, V_o, V_p	regional potential differences between electrodes, Eqs. (3.60), (3.61), and (3.59).
V_T	kinetic temperature, Eq. (3.27).
V_0, V_1, V_2	regional potential differences, Eqs. (3.101), (3.99), and (3.100).
w	total probability that one of two ions will collide with a gas molecule within the sphere of their active attraction.
w_n	probability of collision of a negative ion with a gas molecule within the sphere of active attraction of a positive ion.
w_p	probability of collision of a positive ion with a gas molecule within the sphere of active attraction of a negative ion.
W	slope of the squared value of the field x-component, Eq. (3.41).
W_i	energy required to produce an ion pair in the ith gas.

x	distance variable.
x	dimensionless parameter, Eq. (2.18).
y	arbitrary substitution for E_x^2, Eq. (3.41).
$\frac{3}{16Y}$	function of a variable ζ, as illustrated in Fig. 2.3.
z	ratio of distance of active attraction to mean free path of an ion, Eq. (2.21).
z_e	collision frequency between electrons and gas molecules.
α	first Townsend coefficient.
α	escape constant for radon, Appendix.
β_0	dimensionless parameter, Eq. (3.47).
β_1	dimensionless parameter, Eq. (3.92).
β_2	dimensionless parameter, Eq. (3.95).
γ	total molecular polarizability, Eq. (2.8).
γ	dimensionless parameter, Eq. (3.112).
δ	gas density.
δ_0	gas density at normal temperature and pressure.
δ_e	probability of electron attachment.
ϵ_r	relative permittivity of a gas.
ϵ_0	permittivity of free space, value $\frac{10^{-9}}{36\pi}$ farad/meter.
ζ^2	ratio of K.E. to P.E. of polarized molecule at ion-molecule impact.
η	negative-ion-formation factor, Eq. (3.81).
η_0	rate of electron attachment per unit length, Eq. (4.1).
θ	angle between ionizing-particle track and direction of electric field.
$\lambda, \lambda_1, \lambda_2$	thickness of space charge layers.

λ_i decay constant of the ith radioactive isotope.

μ, μ_i ionic mobility.

μ_e electron mobility.

μ_n mobility of negative ions.

μ_p mobility of positive ions.

ξ dimensionless parameter, Eq. (3.14).

ξ_{cyl} dimensionless parameter, Eq. (3.16).

ρ recombination coefficient.

ρ_e coefficient of electron-ion recombination.

ρ_i coefficient of ion-ion recombination.

σ_a cross section of electron attachment.

σ_g solid elastic collision cross section for gas molecules.

σ_m collision cross section, in a gas, for electron deflection.

τ_a mean lifetime of a free electron, Eq. (2.40).

ABSTRACT

In measuring densities and temperatures at high altitudes, rocket-borne radioactive ionization gauges have several merits. This type of gauge is characterized by its physical ruggedness, good response to density change, and freedom from damage when exposed to higher densities. Its usable range, however, is limited by several factors. At low densities, the linear gauge characteristic is marred by the relatively high residual (dark) current, and at higher densities, by a decrease in the collected current due to the loss of ions by recombination.

This dissertation is intended to be a contribution towards a systematic study of the properties and behavior of radioactive ionization gauges. The chief ionic and electronic processes encountered are briefly reviewed. Then a relationship between the collected ion current and the gas pressure is analytically developed for a planar configuration, considering the probability of electron attachment as a function of the electric field intensity and the gas pressure. In calculating the theoretical current-pressure curves, the numerical values used for ionic mobilities and the recombination coefficient are those derived from kinetic theory; Bloch and Bradbury's theoretical values of electron attachment are used for different mixtures of nitrogen and oxygen. Experimental current-pressure curves are found to be in fair agreement with the theoretical results.

It is indicated that the hysteresis phenomenon, sometimes exhibited by ionization gauges, may be caused by:

a. Temperature dependence of the main electronic processes inside the gauge.
b. Variation in the environmental conditions which may result in a change in the composition of one or more of the present electronegative gases.

It is shown that the primary ionization by alpha particles, in a gas of constant density, increases as the temperature decreases.

The results led to the design of two radioactive ionization gauges; one uses alpha particles emitted from a radium source as the ionizing agent and the other employs beta particles from a tritium source.

The general agreement of the theoretical and experimental current-pressure curves also points to the validity of Bloch and Bradbury's theory of electron attachment in diatomic molecules. This agreement confirms the steep rise of attachment probability as well as the peak value predicted by them at low electron energies.

In carrying out the experimental investigations, it is found that the planar gauge used would be a useful tool in the study of ionization of gases by electron collisions.

CHAPTER I

INTRODUCTION AND STATEMENT OF THE PROBLEM

1.1. INTRODUCTION

For a number of years, a research program in the Department of Electrical Engineering of The University of Michigan has been aimed at determining upper-atmosphere ambient pressures and temperatures through the use of sounding rockets.[1,2] The research has been concerned chiefly with measurements at altitudes above those readily attainable with balloons, and thus has been concentrated on the development of techniques and instruments which can perform reliably in a high-velocity rocket. The general measurement procedure is to determine the air pressures at selected points on the surface of the rocket nose cone, from which the flow Mach number may be determined. Subsequent interpretation of the Mach number with knowledge of rocket trajectory, combined with certain reasonable assumptions, permits calculation of ambient air temperature. The pressure measurements there have been made mostly by radioactive ionization gauges.

1.2. DESCRIPTION OF A SIMPLE RADIOACTIVE GAUGE

In a simple radioactive ionization gauge, shown in Fig. 1.1, the gap between two parallel plane electrodes is irradiated by X-rays or alpha-particles emitted from a radioactive source such as radium. The number of ion pairs generated in a unit volume of the gas per second, i.e., rate

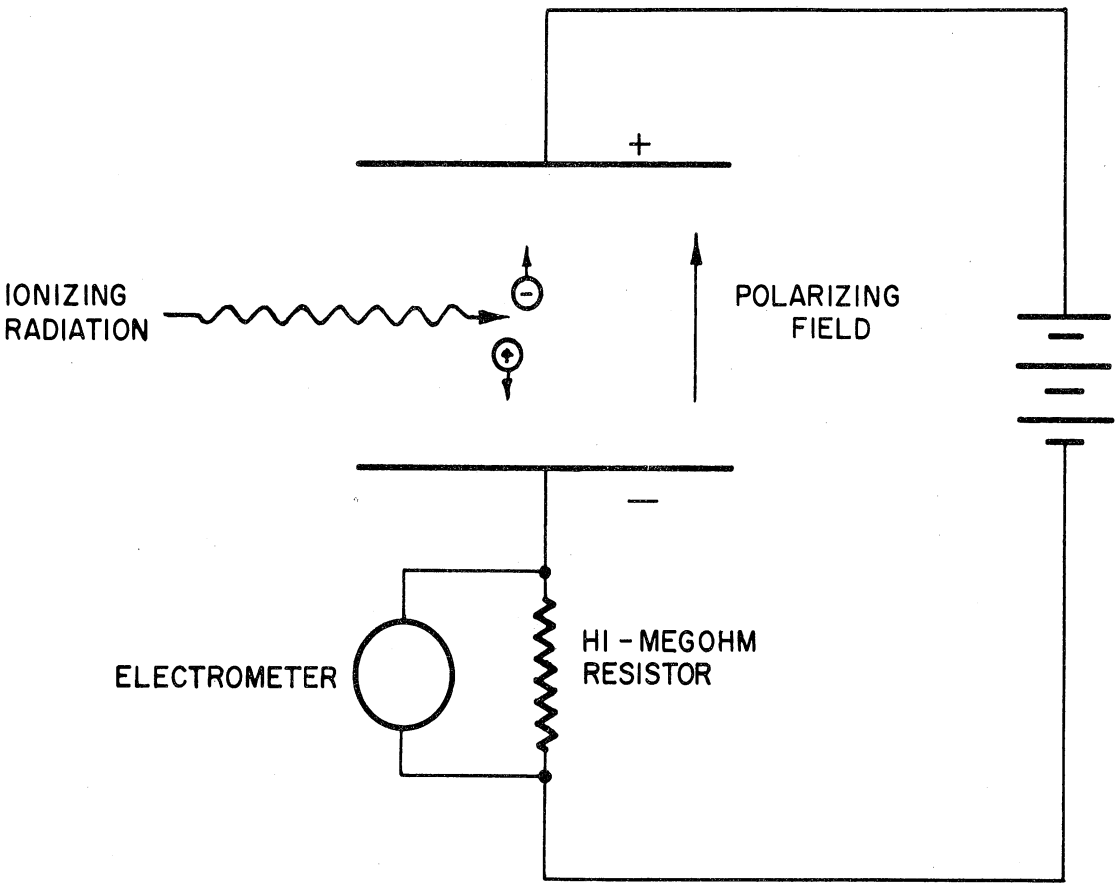

Fig. 1.1. Schematic diagram of a planar radioactive ionization gauge.

of ionization, is characteristic of the type of gas used, its density, and the initial intensity of the ionizing radiation.[3] If the applied field is strong enough, all ions produced in the gap will be swept toward their respective electrodes, thereby setting up a current, known as the saturation current, in the outer circuit. The magnitude of this current, however minute it may be, is found to be directly proportional to the gas density and hence to pressure, provided the temperature remains constant. Therefore, the value of the ionization current may be related graphically to the pressure at a known and constant temperature, as indicated in Fig. 1.2. In weak fields, however, only a portion of the ions produced can reach the electrodes because a large number of ions of unlike sign will recombine, that is, neutralize their charges in the gas, before having reached an electrode. For this reason the pressure-current characteristic becomes nonlinear at the high end of the pressure range. This is illustrated in Fig. 1.3.

Throughout this study, the word "pressure" is often used in place of "density" for convenience. This is permissible only if the temperature is maintained constant. The gas temperature is therefore always assumed to be standard (273°K), unless stated otherwise.

1.3. MERITS AND DRAWBACKS OF RADIOACTIVE GAUGES

Although several types of ionization gauges can be employed over portions or all of the pressure range concerned in the rocket-sounding investigations, the radioactive ionization gauge is often used for many reasons,

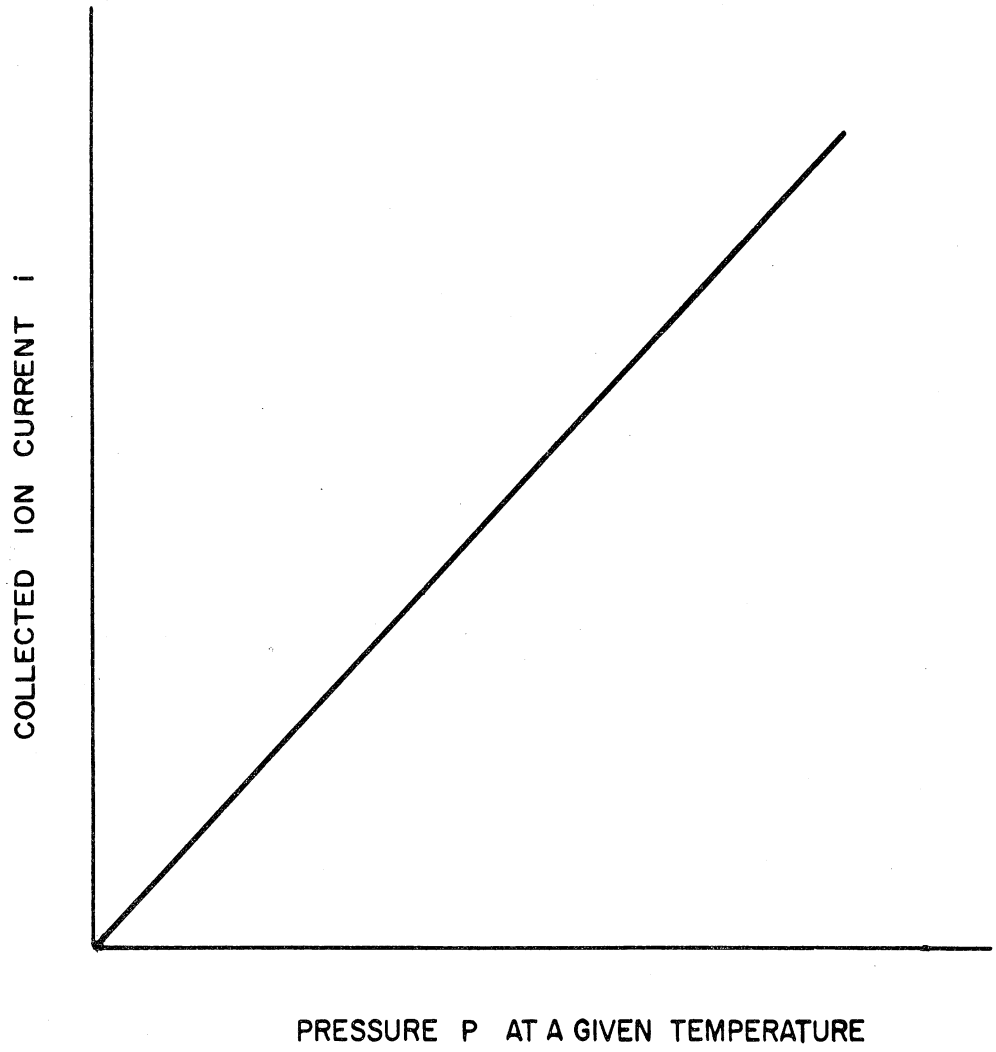

Fig. 1.2. Ideal current-pressure characteristic of radioactive ionization gauge.

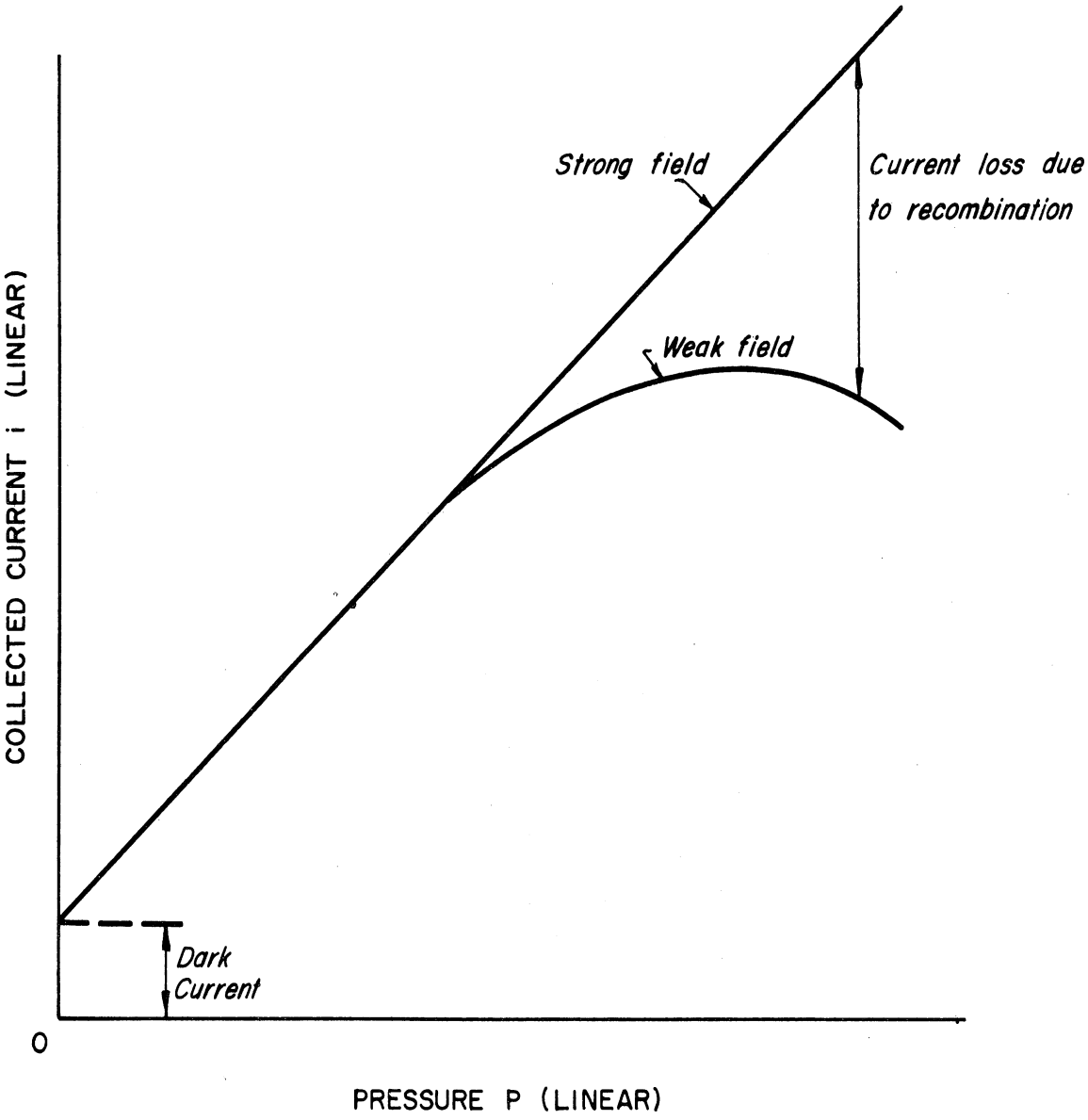

Fig. 1.3. Typical current-pressure curve of radioactive ionization gauge.

including the following:[2]

(1) It is physically rugged.

(2) It responds adequately over the desired pressure range.

(3) It can be operated without damage at atmospheric pressures.

(4) It responds without delay to density change.

(5) Its current-density characteristic is linear over a considerable range.

However, it has certain drawbacks:

(1) The presence of a radioactive source constitutes a potential health hazard, especially if gamma radiation is present.

(2) The signal level is quite low, requiring appreciable electronic circuitry.

(3) In a certain portion of the operating range, the output current appears not entirely dependent on the gas density, in that the curve for a rising pressure is not always retraced during the lowering of the pressure. This is designated by the broken line in Fig. 1.4. This phenomenon will be referred to in the course of this work as hysteresis. However, a word of caution about such nomenclature is in order. Unlike magnetic or mechanical hysteresis, the above phenomenon is believed to be due to slight changes in the apparently constant experimental conditions between rise and fall rather than to an influence of history under constant environmental conditions.

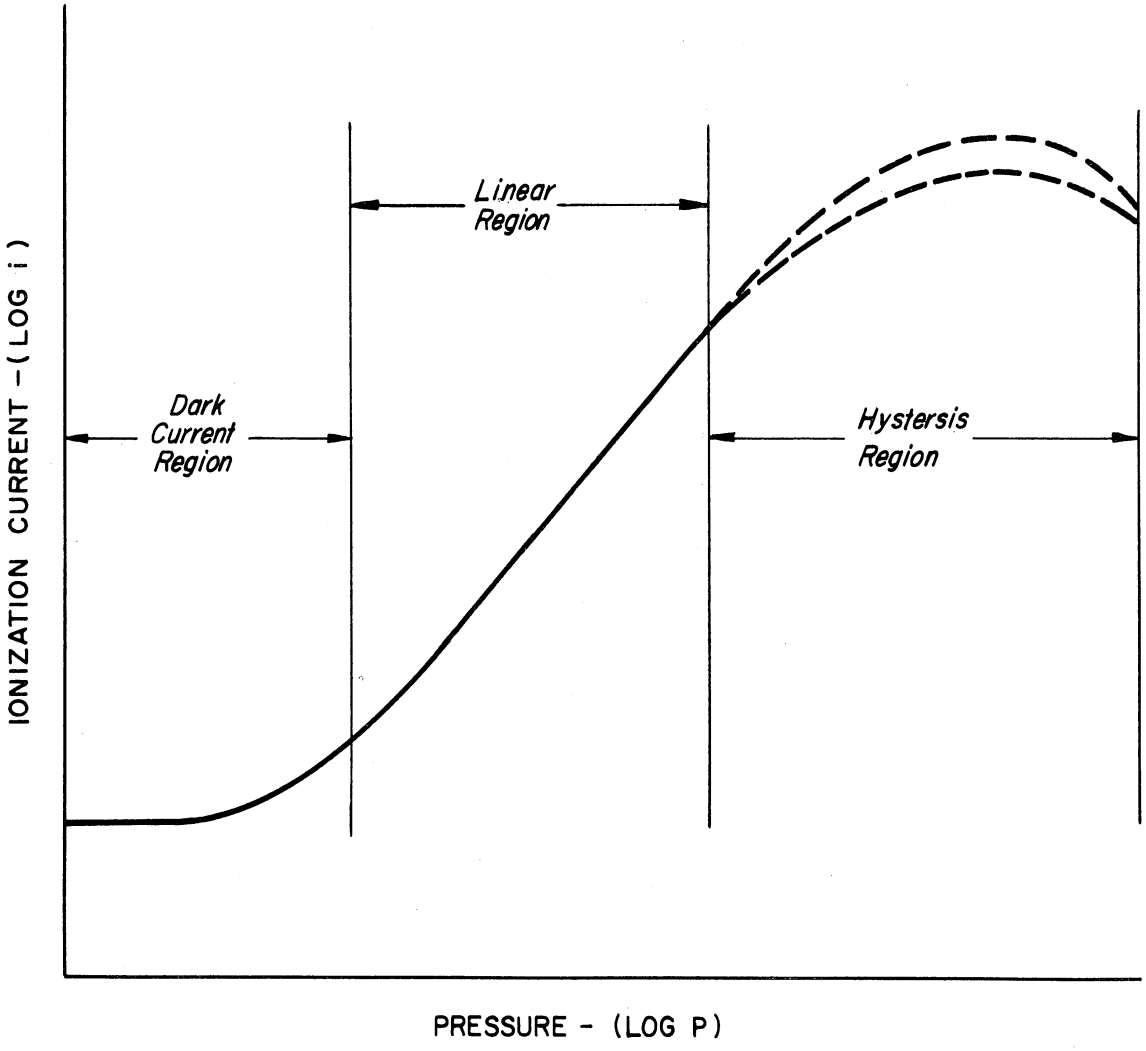

Fig. 1.4. Actual i-P characteristic showing the hysteresis and dark current regions.

1.4. OBJECTIVES

The purpose of the work reported here was to study systematically the general properties of radioactive ionization gauges. Such a study is necessary to achieve a better understanding of the potentialities as well as of the limitations of this device for measuring pressure. It may then be possible to improve the general performance of the gauge and in particular to:

(1) Extend the linearity of the current-pressure relationship to both higher and lower pressures.

(2) Reduce or eliminate the causes of the undesirable hysteresis effect experienced at high pressures.

1.5. PROCEDURE

(1) In Chapter II, the general properties and behavior of the different charge carriers are reviewed, especially those properties pertaining to pressure, temperature, and nature of gas. The production of ions, their mobilities, and their loss by recombination are also discussed.

(2) In Chapter III, two relations between the current and pressure are analytically derived, assuming, first, complete electron attachment, and then variable attachment. Gas temperature, gauge configuration, and collector voltage appear as parameters in both relations.

(3) Finally, in Chapter IV, the theoretical results of Chapters II and III are compared with experimental results. The most probable causes of the hysteresis phenomenon are also discussed.

CHAPTER II

SURVEY OF IONIC PROCESSES ENCOUNTERED IN A RADIOACTIVE IONIZATION GAUGE

2.1. INTRODUCTION

A gas becomes a conductor of electricity if free charges such as ions, electrons, or heavy charged particles are present. Positive ions are atoms, molecules, or groups of molecules which have lost one or more electrons and thus carry single or multiple charges. Negative ions are atoms, molecules, or groups of molecules to which electrons, usually only one, have become attached. A negative ion which arrives at a positive electrode will deliver the electron which has been attached to it, and in general the resulting neutral molecule returns to the gas.

On the other hand, if a positive ion arrives at the negative electrode, it picks up an electron from the metal and then returns, as a neutral molecule, to the gas. It follows that the contribution of a newly formed ion to the current in the outside circuit will depend on the time during which the ion stays in the gas as a free entity. Therefore, before deriving an expression for the output current as a function of pressure for a radioactive gauge, it is in order to give a brief account of the most important properties and characteristics of the basic processes which take place inside the gauge with special attention to the effect of pressure, temperature, and electric field upon them. The main processes

encountered are: (a) production of ions, (b) motion of ions and electrons, (c) recombination of oppositely charged carriers, and (d) electron attachment and formation of negative ions.

2.2. PRODUCTION OF IONS

2.2.1. General Considerations.—Ionization in gases can be produced by irradiating with X-rays, by bombarding with alpha or beta particles, and in several other ways. In a radioactive pressure gauge, the ionizing agent may be alpha, beta, or gamma rays emitted from a radioactive material usually deposited on a plate and mounted inside the gauge chamber. The number of ion pairs produced by the passage of any of these rays through a gas varies greatly between the three cases, being roughly in the ratio 10,000 : 100 : 1, respectively.[4] Since the contribution of gamma rays to ionization is so minute compared to the other rays, most of the sources used in such gauges are either alpha- or beta-particle emitters. In either case the average number of ion pairs produced per unit path length (called the specific ionization) depends on the gas density, the nature of the gas, and the velocity or residual range of the particle.

2.2.2. Ionization by Alpha Particles.—A typical long-life alpha-particle emitter employs a gold-radium alloy containing approximately 0.2 to 0.5 mg of radium. The amount depends on the volume of gas to be ionized, the desired pressure range, and the lowest desired output current.[5] To make the active area a highly efficient alpha-particle emitter and yet with a relatively low emanating power, the radium alloy is electroplated

with a very thin film of metal such as nickel. The nickel film acts as a seal which retains radon gas (the first decay product of radium) and its subsequent decay products, which yield three additional alphas for every alpha particle originally emitted from the radium. This film should be very thin so that the particles lose only a small fraction of the total energy in penetrating into the gas in the chamber. The degree of constancy of source activity can be determined by the use of Bateman's equations for radioactive decay and the well-known values of the half-lives for the daughter products of the radioactive series.[6] The buildup in the activity of radium source as an alpha emitter is analytically developed in the Appendix (case I). In Fig. 2.1 the ratio of total alpha-particle activity to the initial value (i.e., of radium only), is plotted as a function of time. It can be seen that after one month the source activity remains almost constant; the slow increase is caused by the buildup of polonium, with its consequent activity.

Alpha particles are positively charged particles initially projected from the radioactive substance with high velocity, which varies for different substances between 1.4×10^7 and 2.2×10^7 meters per second. Normally the alpha particles at the moment of expulsion carry two positive charges and are to be identified with the nuclei of helium atoms. They are distinguishable from other radiations by their absorbability; they are completely stopped by less than 10 cm of air under standard temperature and pressure or by 1/10 mm of aluminum. An alpha particle possesses an appreciable kinetic energy, 7.7 Mev in the case of those emitted from

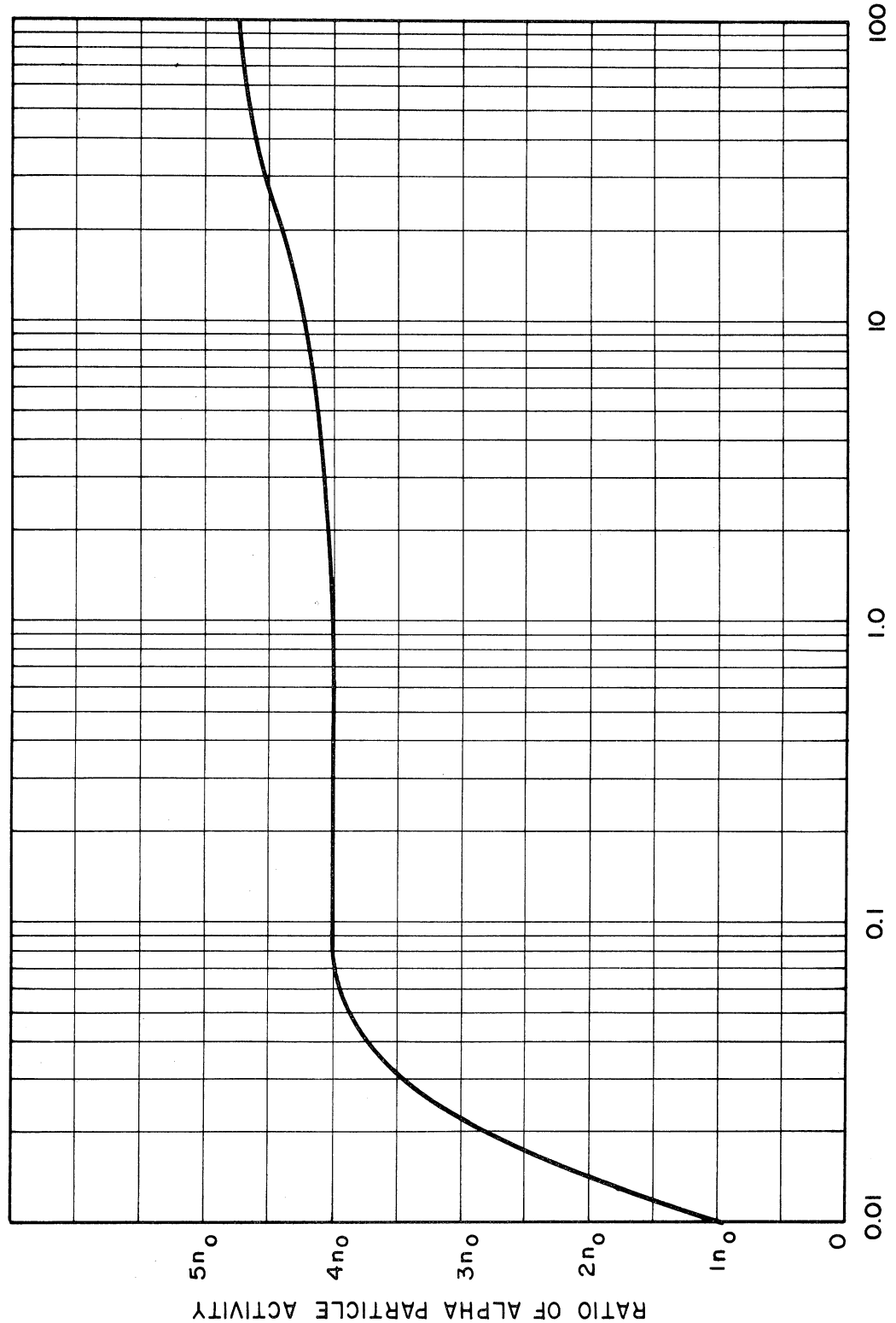

Fig. 2.1. A plot of the calculated alpha-particle activity for a source that is initially radium alone (emitting n_o particles/sec) and retains all of its decay products.

radium C'. Because of their great energy, they pass freely through the electronic structure of the atoms in their path, and it is only rarely that they pass close enough to the nucleus to experience a sensible deflection.

In consequence of its charge, when an alpha particle passes close to an atom or penetrates it, it must disturb the motions of the electrons in the atom, resulting in excitation and/or ionization of the atom. The primary ionization due to the incident particle is a consequence of the liberation of an electron from the atom or molecule. Depending on the closeness of collision, these electrons or delta rays, as they are often called, may have velocities between 0 and 2u, where u is the velocity of the incident particle. If the speed of the ejected electron is sufficiently high, it may in turn produce a number of ions in the gas before it comes to rest. This is known as secondary ionization. As a result of detailed calculation, Fowler[7] found that about three-quarters of the energy of a swift delta particle can be used in producing ions. The longest delta-particle tracks were found to be about .5 mm in air at standard conditions.[4] The primary ionization constitutes about one-third of the total ionization, whereas the major part thereof is due to the absorption of the energies of the secondary delta rays.

The average energy absorbed as observed experimentally in the formation of an ion pair by an alpha particle varies somewhat from one gas to another; it is between 20 and 40 electron volts for gases commonly encountered in gauges of the type under discussion. This energy is invari-

ably higher than the ionization potential of the gas involved for two reasons: (a) the incident particle may excite some atoms without ionizing them, and this requires energy; (b) the electrons freed from those atoms which are ionized are given some kinetic energy, and this, as well as the ionization energy, must be furnished by the alpha particle.

The number of ion pairs produced per unit length along the track of the particle depends on its velocity and increases rapidly as the velocity diminishes.[8] Although the charged particle exerts the same force of interaction on a given planetary electron regardless of the particle's velocity, the length of time during which this force is exerted is also important in determining whether or not the electron is to be freed from the atom. As a first approximation, the probability of freeing an electron would be proportional to the product of the force and time of interaction.[9] This is a very interesting point of view, which is used later in explaining the variation of specific ionization of a gas with temperature even for constant densities.

2.2.3.—Ionization by Beta Particles.—Ionization of gas inside a gauge can also be achieved by bombardment with beta particles (electrons) as emitted from radium or other radioactive substances. They are ejected from different radioactive materials with a wide range of velocities, the greatest approaching within about 2% of the velocity of light. Beta particles are distinguishable from alpha particles by their greater penetrating power for the same amount of energy.

With beta particles, too, ionization takes place along and around the

trajectory of the particle as a result of primary and secondary collisions. The number of ion pairs produced per unit length by a beta particle is considerably smaller than the corresponding number produced by an alpha particle. This is partly due to the higher velocity with which the beta particle travels through gas particles, thus decreasing the duration of interaction, and partly due to the smaller collision cross section compared to that of an alpha particle.

2.2.4. Columnar Ionization.—The ionization produced by either alpha or beta particles is characterized by a high concentration of ions very close to the particle track, thus forming what is known as columnar ionization. This occurs at pressures near atmospheric and above.[10,11] However, as the pressure drops below atmospheric, the size of the column increases as a result of the broadening in the range of secondary ionization around the main path, being about 3 mm at a pressure of 100 millibars (mb). Because 3 mm is much greater than the typical spacing between tracks, it seems justified to assume that the ionization is macroscopically uniform at and below this range of pressure.

Taking into account recombination within the column, the net rate of volume ionization for an entire region is given by[10]

$$g = \frac{g_o}{1 + \frac{\rho N_o}{8\pi D} f(x)} \qquad (2.1)$$

where

g_o = the average initial ionization, ion pairs per unit volume per second, throughout the region,

ρ = coefficient of volume recombination,

N_o = number of ion pairs initially produced per unit length,

D = coefficient of diffusion,

$f(x) = e^x \frac{i\pi}{2} H_o^{(1)}(ix)$; $H_o^{(1)}(ix)$ is the Hankel function and x is a dimensionless parameter depending on the mobility of the ion, the field, and its direction as described in section (2.5.2).

2.3. IONIC MOBILITY

2.3.1.—Definitions.—If ions of a certain type form a swarm so that the velocities of individual particles are equally distributed in all directions about an average velocity, the applied electric field acting on the swarm will move it as a group. The average speed with which the center of the swarm moves in the direction of the applied field is called the drift velocity. The ionic mobility, μ_i, is thus defined as the ratio of the drift velocity, v_i, to the field E causing it,

$$v_i = \mu_i E \quad , \qquad (2.2)$$

where μ_i is expressed in meter/second per volt/meter. A similar equation relating to electron motions is obtained by using the subscript "e" instead of "i."

At the gas densities and field strengths here considered, the mobility μ_i can be assumed a constant for the gas in question. Also, μ_i has been found to be inversely proportional to the gas density, δ; in other words, the mobility is inversely proportional to the pressure, P, at constant temperature, T. Thus

$$\mu = G\frac{\delta_o}{\delta} = G\left(\frac{1013}{P}\right)_T , \qquad (2.3)$$

where δ_o is the density of the gas used at a pressure of 760 mm Hg, and at a temperature of 273°K (called normal temperature and pressure), and G is the reduced mobility or mobility constant, which is a slowly varying function of temperature at normal conditions.

2.3.2. Langevin's Theory of Ionic Mobility.—The ionic mobility has been analyzed according to several theories which range from one based on the simple mechanistic approach using average free paths, average velocities, and assuming elastic collisions between ions and gas particles, to the more correct and generalized theoretical approach based on the Maxwell and Boltzmann procedures, using force fields instead of the simple mean free path concept. Langevin[12] made a thorough and complete theoretical study of ionic mobilities, in which he assumed solid elastic impacts of ions with molecules, and considered the fundamental role played by the dipole character of gas molecules. According to the theories preceding Langevin's work, a negative ion, for example, would travel in the force-field direction colliding only with molecules in its path. But in Langevin's theory an ion approaching a distant molecule displaces its electrons with respect to the positive nucleus, inducing an electric dipole in the molecule. Hence the ion is attracted by the positive end of the dipole and deflected toward this molecule, as illustrated in Fig. 2.2. So without colliding in the classical sense, an exchange of momentum between the negative ion and the neutral molecule takes place.

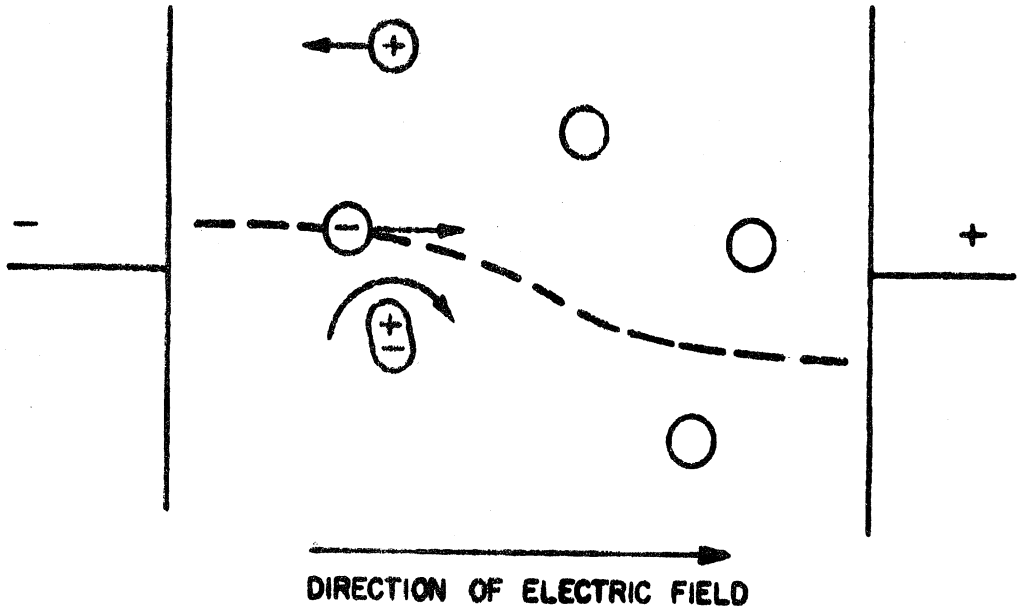

Fig. 2.2. Path of a negative ion under the influence of an induced electric dipole.

An ion of charge q_e has an electric field of strength

$$E = \frac{q_e}{4\pi \epsilon_o r^2} \text{ volts per meter} , \qquad (2.4)$$

at a distance r. This field is of the order of 10^8 volt/meter at intermolecular distances under atmospheric pressures. In fields of this magnitude, all molecules experience a displacement of their electron clouds relative to the nuclei, so as to produce an electrical dipole of moment, p_i. Certain molecules such as H_2O, NH_3, etc., possess an additional permanent electrical dipole moment, p_p. Thus an effective average moment, $p = \gamma E$, is induced on the molecules by the ionic force field at a distance r, with γ as the total polarizability of the molecule. Now this dipole with its axis aligned by the field E of the ion will experience an attractive force

$$F = \frac{2p\, q_e}{4\pi \epsilon_o r^3} . \qquad (2.5)$$

Since the dipole moment

$$p = \gamma E = \frac{\gamma\, q_e}{4\pi \epsilon_o r^2} , \qquad (2.6)$$

substitution in (2.5) gives the force between the molecule and ion:

$$F = 2\gamma \left(\frac{q_e}{4\pi \epsilon_o}\right)^2 \frac{1}{r^5} . \qquad (2.7)$$

This law is correct while r is sufficiently great, so that the field E is sensibly uniform within the space occupied by a gas molecule.

The total molecular polarizability is determined from the Clausius-Mossotti relation:

$$\frac{\epsilon_r-1}{\epsilon_r+2}\,\frac{M_o}{\delta} = \frac{N_A}{3\epsilon_o}\,\gamma \quad , \tag{2.8}$$

where

M_o = molecular weight,

δ = gas density in kg/m^3,

ϵ_r = relative permittivity of gas,

ϵ_o = permittivity of a vacuum, value $10^{-9}/36\pi$ farad/meter,

N_A = Avogadro's number, value 6.025×10^{26}, and

γ = the total polarizability per molecule.

Since the relative permittivity of the gas, ϵ_r, has a value very close to unity, $\epsilon_r + 2 \cong 3$, and the above relation becomes

$$(\epsilon_r-1)\,\frac{M_o}{\delta} \cong \frac{N_A}{\epsilon_o}\,\gamma$$

or

$$\gamma = \frac{\epsilon_o(\epsilon_r-1)\,M_o}{N_A\,\delta} \quad . \tag{2.9}$$

From (2.9) one can also write

$$\frac{(\epsilon_r-1)}{(\epsilon_r-1)_o} = \frac{\delta}{\delta_o} \quad , \tag{2.10}$$

where $(\epsilon_r-1)_o$ and δ_o are the dielectric constant and gas density, respectively, at normal temperature and pressure.

Langevin assumed, according to the relation (2.7), that the attractive force between an ion and a gas molecule obeys the fifth-power law, and thus his complete treatment led to the following form for the ionic mobility:

$$\mu_i = \left(\frac{3}{16Y}\right) \frac{3.16 \times 10^{-3} \sqrt{1 + (m_g/m_i)}}{\sqrt{(\epsilon_r - 1)\delta}} \quad \text{m/sec per volt/m} \quad , \tag{2.11}$$

where m_g and m_i are the mass of molecule and ion, respectively, and $(3/16Y)$ is a function of a variable ζ containing the effects of the integration over all classes of orbits involved in solid elastic impacts.

The relation between $(3/16Y)$ and ζ, as computed by Hasse,[13,14] is shown in Fig. 2.3. Here, ζ is given by

$$\zeta^2 = \left(\frac{\text{kinetic energy of molecule}}{\text{potential energy of polarized molecule}}\right)_{\substack{\text{at ionic} \\ \text{molecular} \\ \text{impact}}}$$

$$= \frac{32\, \epsilon_o\, \sigma_g^2\, P}{(\epsilon_r - 1) q^2}$$

where

σ_g = solid elastic collision cross section,

P = gas pressure, and

q = ionic charge.

At low temperatures, and with small ions and molecules, the value of $(3/16Y)$ approaches a limiting value of 0.51. On the other hand, as the temperature, and the radii of the molecules and ions, increase, the value of $(3/16Y)$ increases, reaches a maximum, and then decays to about 0.1.

In the derivation of Langevin's relation (2.11), it was assumed that the ionic drift velocity was small compared to the random velocities, and that the ions remain in thermal equilibrium with the gas molecule, i.e.,

$$\frac{1}{2} m_i \overline{c_i^2} = \frac{1}{2} m_g \overline{c_g^2} = \frac{3}{2} kT \quad , \tag{2.12}$$

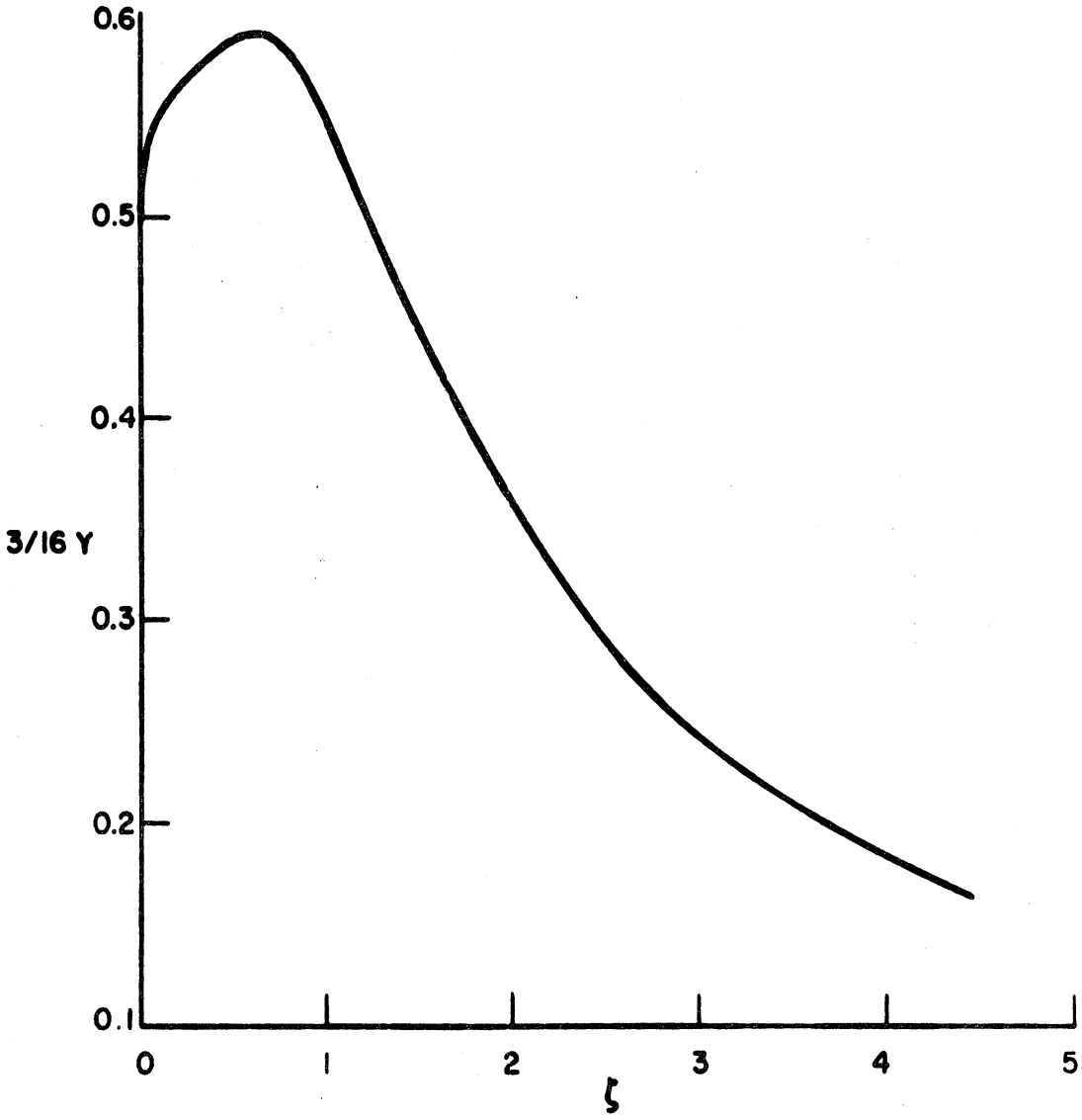

Fig. 2.3. Plot of Langevin's quantity (3/16Y) as a function of the parameter

$$\zeta = \sqrt{\frac{32\ \epsilon_0\ \sigma_g^{\ 2}\ P}{(\epsilon_r - 1)q^2}}\ .$$

where $\overline{c_i^2}$, $\overline{c_g^2}$ are the mean-square values of random velocities of ions and molecules, respectively, and k is Boltzmann's constant. The numerical agreement between Hassé's theoretical values and experiment has proven to be reasonably good.

Loeb put the mobility equation (2.11) in the more convenient form[15,16]

$$\mu = \frac{3}{16Y} \frac{4.62 \times 10^{-3} \sqrt{1 + (m_g/m_i)}}{(\delta/\delta_o)\sqrt{(\epsilon_r - 1)_o M_o}} \text{ m/sec per volt/m} \quad . \quad (2.13)$$

The ionic mobility behavior will now be summarized; for low values of E/P it is given adequately by Eq. (2.13).

(1) The ionic mobility is independent of the electric field strength, E, except at high values of E/P where the energy of the ion caused by the field begins to exceed thermal energies by a considerable amount, causing a reduction in the attractive-force action. Figure 2.4 shows the limiting value of E/P at which the mobility of N_2^+ ion in N_2 ceases to be independent of E/P.

(2) The mobility is inversely proportional to the gas mass density. This is illustrated by Fig. 2.5 in which the mobilities of different ions are plotted against their masses.

(3) At constant density, the mobility is a slowly rising function of temperature, usually changing insignificantly within the range of temperatures experienced in the laboratory. Figure 2.6 shows the effect of temperature on the mobility of N_2^+ ions in N_2 for constant pressure and for constant density; this is accounted for in the 3/16Y factor.

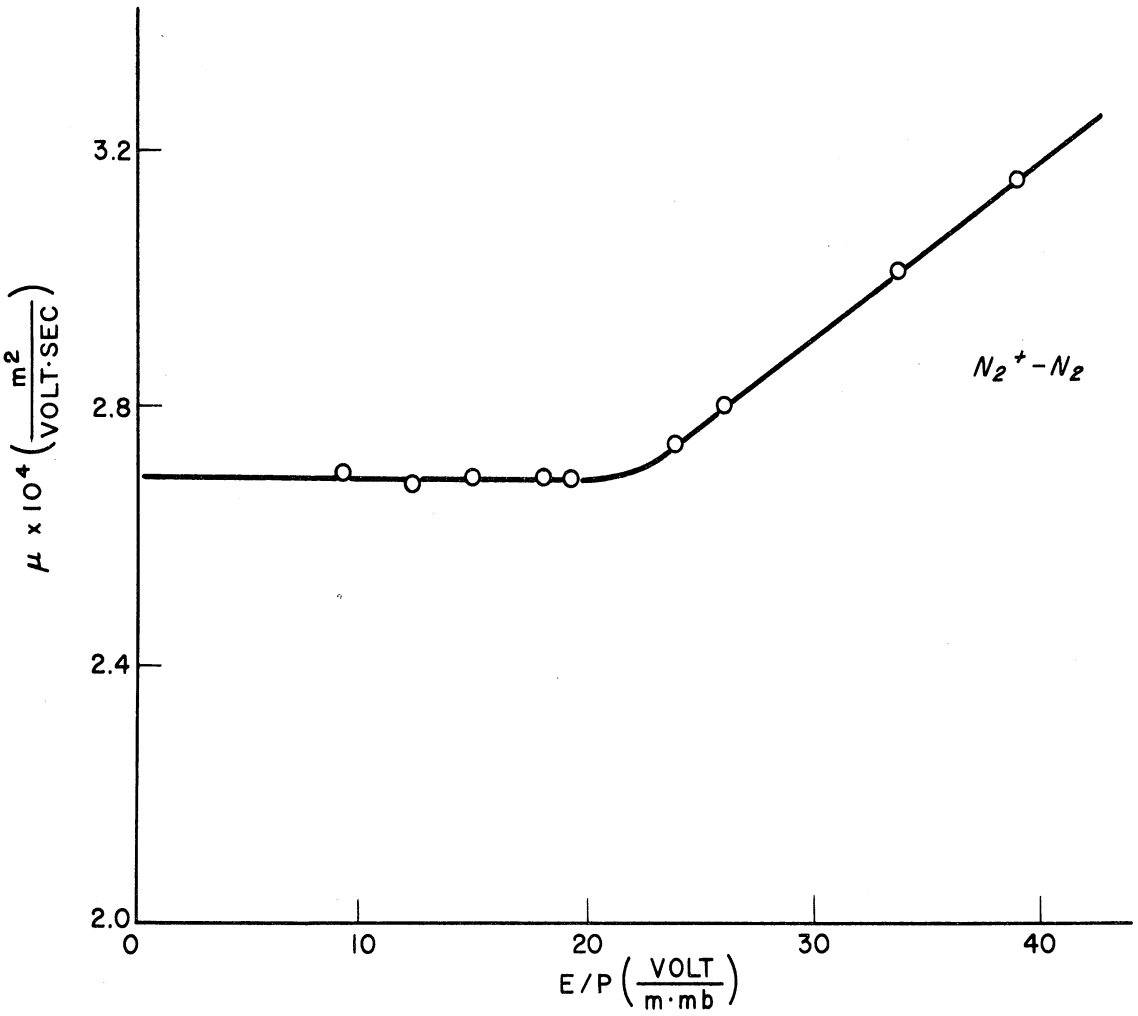

Fig. 2.4. Limiting values of E/P at which mobility of N_2^+ ions in N_2 gas ceases to be independent of E/P.

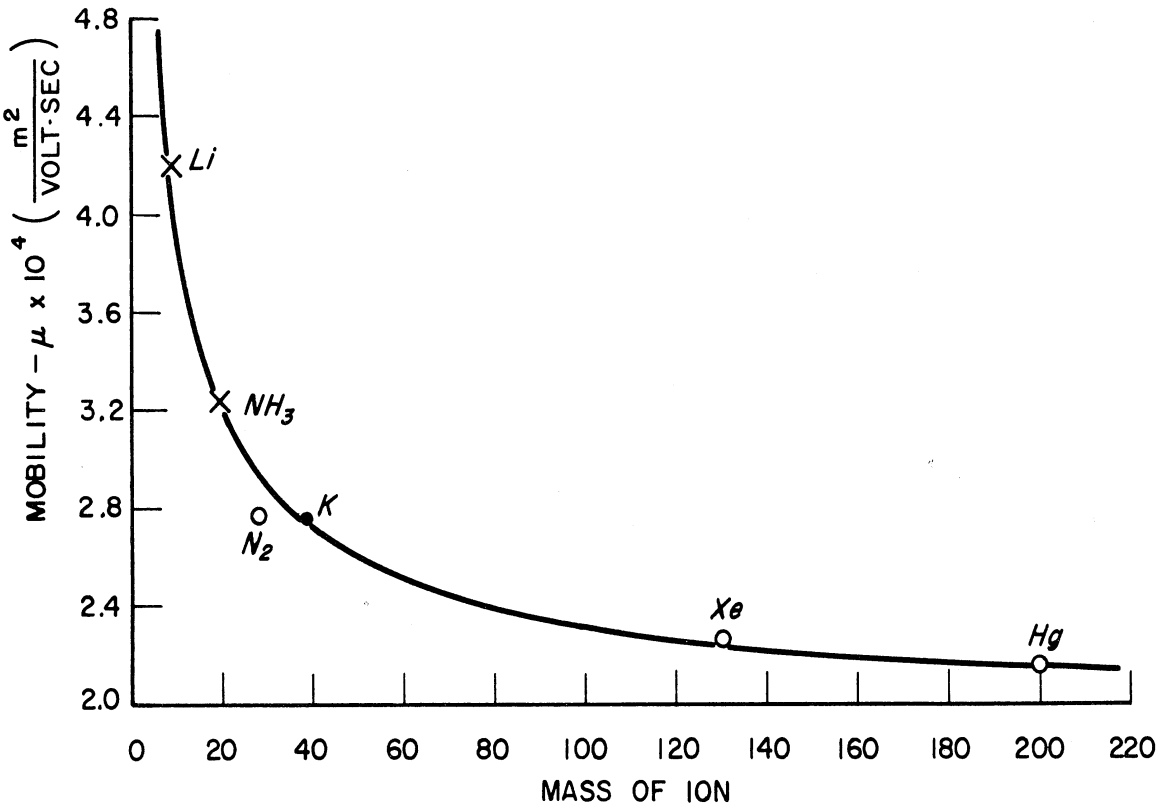

Fig. 2.5. Mass-dispersion curve of Langevin's theory and experimental values for various ions in N_2 gas.

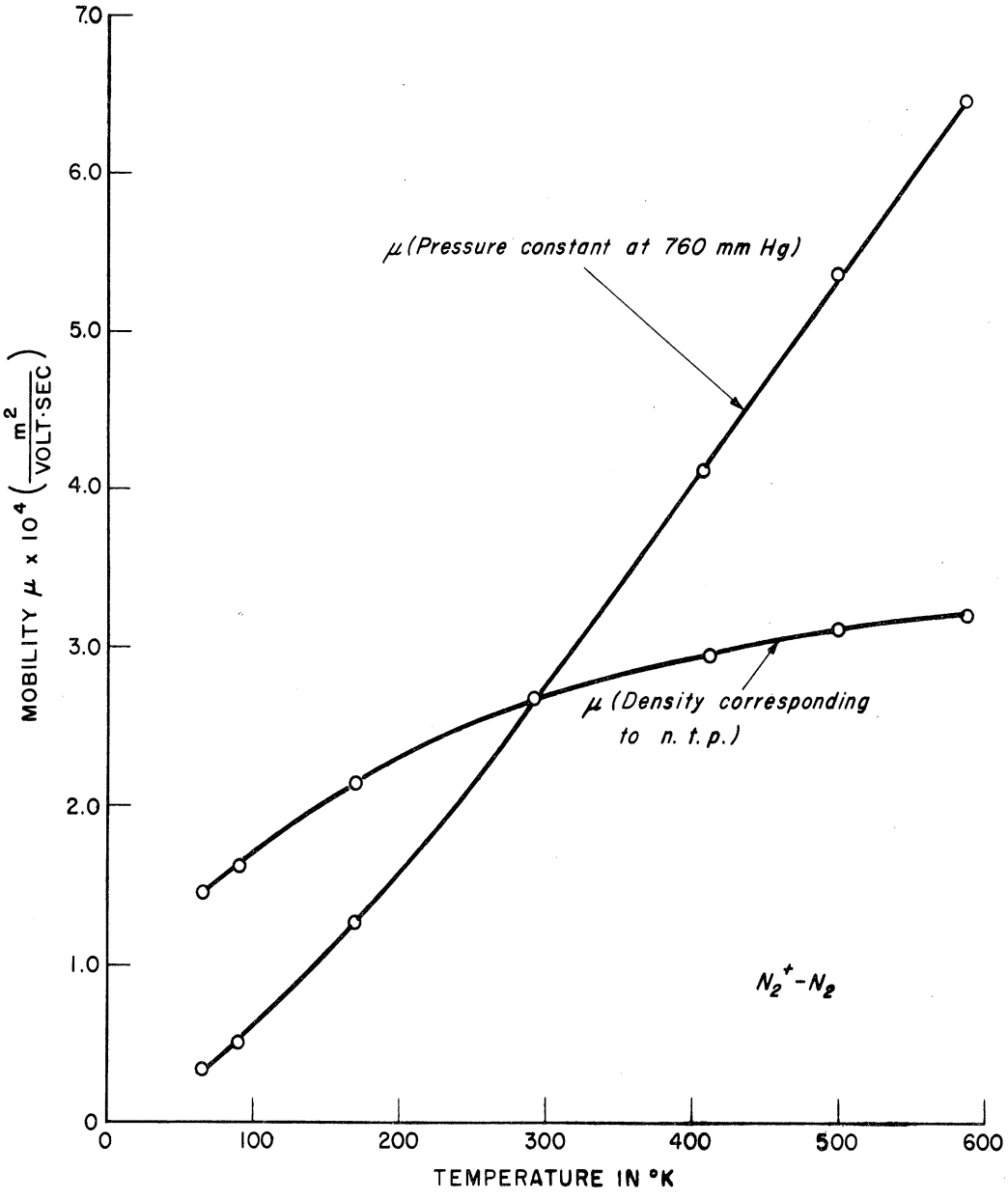

Fig. 2.6. Effect of temperature on mobility of N_2^+ in N_2 gas.

(4) The mobility depends on

$$\frac{\sqrt{1 + (m_g/m_i)}}{\sqrt{(\epsilon_r - 1)_o \, M_o}} \quad ,$$

which is a property of the gas; this prediction from the theory has been in good accord with observations.

2.4. ELECTRON MOBILITY

The electron mass is so small compared to molecules of the gases in which they find themselves that in elastic collision with the heavier molecules they rebound and retain a large fraction of their momentum. Thus even where low fields are present, the electrons retain energy gained from the field and thus possess energies different from those of the surrounding molecules. In this respect one expects them to behave differently from the more massive ions.

A simple expression for the electronic mobility, as derived by Langevin from the kinetic theory is[12]

$$\mu_e = \frac{3}{4} \frac{q_e}{m_e} \frac{\ell_e}{\overline{c_e}} \quad , \tag{2.14}$$

where $\overline{c_e}$ is the electron average random velocity, determined from electron temperature, and ℓ_e is the electron mean free path. The latter is given by

$$\ell_e = \ell_{e_R} \frac{1}{P} \frac{T_g}{273} \tag{2.15}$$

where ℓ_{e_R} is the Ramsauer electron mean free path in meters at 273°K and a pressure of 1 mb, a value which varies in a most complicated fashion

with electron energies.[17-19]

Compton's equation for electron mobility[20] will be used here as adapted by Bradbury and Nielsen,[21-23] and arranged in terms of standard-of-comparison mean free paths, ℓ_{e_o}, the electric field strength, E, the gas pressure, P, and the gas temperature, T. This equation reads:

$$\mu_e = \frac{1.825 \times 10^6 \, \ell_{e_o} \, (1/P) \, (T/273)^{1/2}}{[1 + \{1 + 9.82 \times 10^5 \, M_o \, \ell_{e_o}^2 \, (E/P)^2\}^{1/2}]^{1/2}} \quad \frac{m^2}{\text{volt-sec}} \tag{2.16}$$

where M_o is the molecular weight of the gas, and the pressure, P, is expressed in millibars.

2.5. RECOMBINATION OF IONS

2.5.1. Definitions.—Since the ions are in general oppositely charged particles, they attract each other according to the ordinary laws of electrostatics. When they collide, their charges may neutralize each other, and the ions again become neutral particles. The chance of a given positively charged ion, for example, meeting a negative ion in a given time is proportional to the number, n_n, of the negative ions present per unit volume, while the number of positive ions finding partners in a given time is proportional to the number n_p, of positive ions actually present per unit volume of the gas. The rate at which recombination goes on is thus proportional to $n_n \, n_p$. This rate is usually written as $\rho \, n_n \, n_p$, where ρ is constant under given conditions and is known as the coefficient of recombination.

There are various types of recombination,[24] such as preferential,

initial, columnar and volume recombination. In the radioactive gauges of the type considered here only two of these are of significance, viz., columnar and volume recombination.

2.5.2. Columnar Ion-Ion Recombination.—Ionization by high-energy particles is by no means isotropic, especially not at the high range of pressure. However, such anisotropy is removed (by diffusion) when pressure is lowered, as a result of the secondary ionization around each track. In columnar ionization the ions have their highest concentration along the particle's track, or column; hence columnar recombination is liable to take place there. The effect of such recombination is only on the value of saturation currents, i.e., on the net rate of ion production, g. This value is found to be dependent on the angle a column makes with the electric field. Maximum saturation currents are achieved when the field is perpendicular to the path of the ionizing particle and minimum when parallel.

Moulin[25] studied this phenomena and then Jaffé[10] developed his now well-known theory of columnar ionization and recombination. Jaffé assumed that electrons, just released in ionization process, diffuse outward; and at the end of 10^{-3} or more of a second, most of them will have attached to give negative molecular ions. Oxygen is a typical example of such electronegative molecules which can readily attach electrons to form negative molecular ions, as explained in Section 2.6. Jaffé also assumed that the negative and positive ions are symmetrically distributed radially about the track axis, with density declining radially outward, following a

Gaussian error curve, the form of which will not change by subsequent recombination. Under these conditions one finds that the number of ions, N_∞, escaping recombination is given by

$$\frac{N_\infty}{N_o} = \frac{1}{1 + \frac{\rho N_o}{8\pi D} f(x)} \tag{2.17}$$

where

N_o = number of ion-pairs initially produced per unit length,

ρ = coefficient of volume recombination,

D = coefficient of diffusion,

$f(x) = e^x \frac{i\pi}{2} H_o^{(1)}(ix)$,

$H_o^{(1)}(ix)$ is Hankel's function (for definition and tables see Watson, Bessel Functions, Cambridge, 1952), and x is a dimensionless parameter defined by

$$x = 2\left(\frac{\mu r_o E \sin\theta}{\pi D}\right)^2 \tag{2.18}$$

where μ is the ionic mobility, r_o, the average displacement of the Gaussian curve from the columnar axis, a function of pressure,[10] and θ the angle between the particle track and the direction of the electric field E. The agreement of this theory with experiment is good,[11] particularly at pressures above 1 atmosphere (Fig. 2.7).

In fact, the net saturation current is a result of ions escaping this type of recombination. Thus the net rate of ion production per unit volume is given by

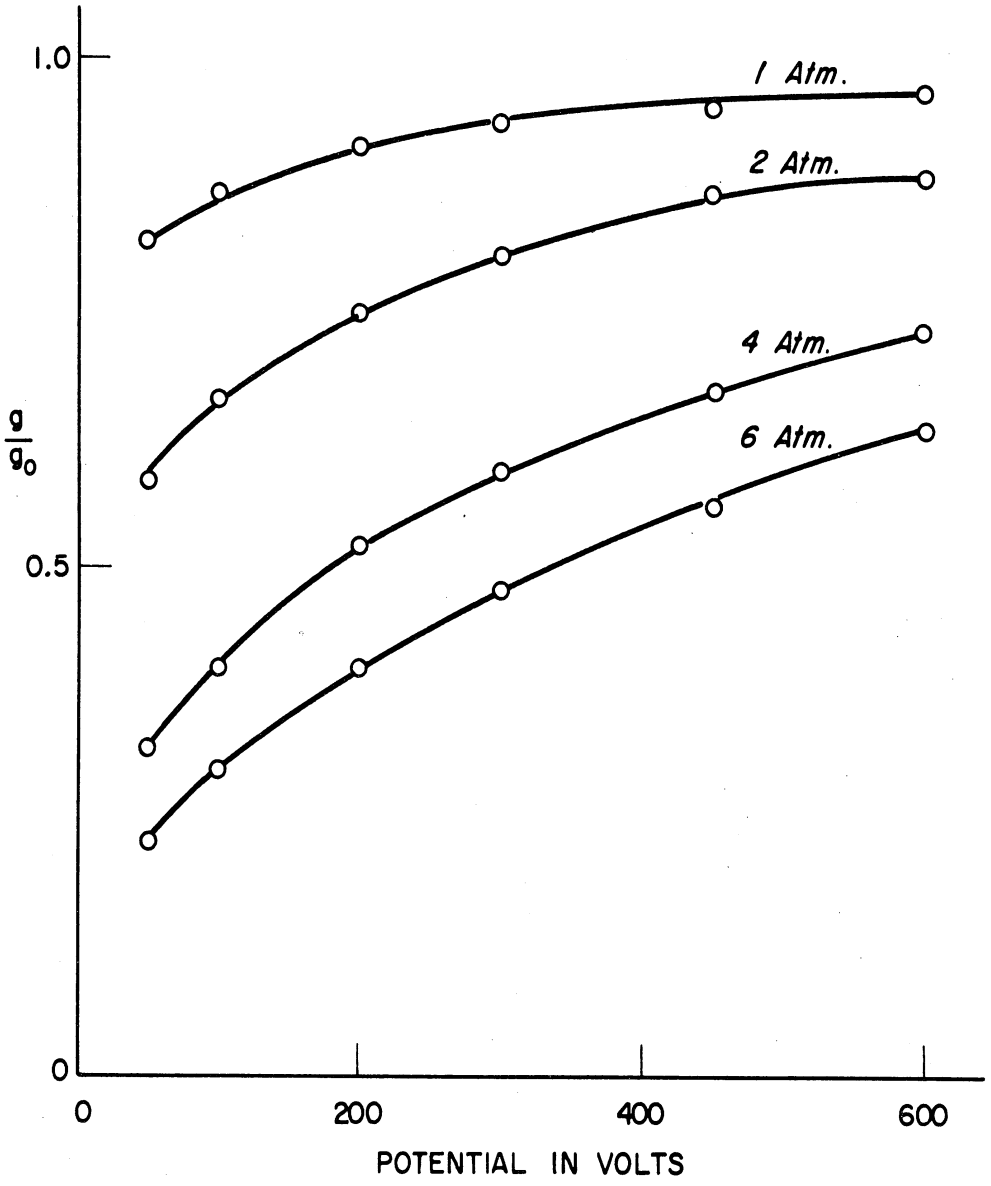

Fig. 2.7. Calculated theoretical saturation currents compared to experimental points.

$$g = \frac{g_o}{1 + \frac{\rho N_o}{8\pi D} f(x)} \tag{2.19}$$

where g_o is the average rate of initial production, assuming no recombination of any type, called the true saturation value.

2.5.3. Volume Ion-Ion Recombination.—Due to the diffusion of ions the ionization columns expand radially so that they touch and merge. The ions then are likely to be evenly distributed and the recombination from then on follows the relations for general volume recombination. Thus, following Thomson's calculations,[26] the coefficient of volume ion-ion recombination is given by

$$\rho = \pi d_o^2 w \sqrt{\overline{c_p^2} + \overline{c_n^2}} \quad , \tag{2.20}$$

where

$\overline{c_p}$ = the average velocity of positive ions,

$\overline{c_n}$ = the average velocity of negative ions,

d_o = the radius of sphere of active attraction, defined by

$$d_o = \frac{q_e^2}{6\pi \epsilon_o kT} \quad ,$$

w = the chance of recombination, given by

$$w = w_p + w_n - w_p w_n \quad ,$$

and

$$w_i = 1 - \frac{\ell_i^2}{2d_o^2}\left[1 - e^{-2d_o/\ell_i}\left(\frac{2d_o}{\ell_i} + 1\right)\right] \quad .$$

with ℓ_i as the mean free path of the ith type of ions. Assuming the ions and gas particles are in thermal equilibrium, we then have

$$\ell_n = \ell_p = \ell \quad .$$

Also $\overline{c_p} = \overline{c_n} = \overline{c}$, and consequently

$$w_p = w_n = w_o \quad .$$

Thus the recombination coefficient becomes

$$\rho = \pi d_o^2 \, \overline{c} \sqrt{2} \, w(z) \quad , \tag{2.21}$$

where

$$w(z) = 2w_o - w_o^2 \quad ,$$

$$w_o = 1 - \frac{2}{z^2} \left[1 - e^{-z} (z-1)\right]$$

and

$$z = \frac{2d_o}{\ell} \quad .$$

The distance of active interaction, d_o, depends solely on the thermal agitation, and therefore on the gas temperature,

$$d_o = 4.075 \times 10^{-8} \left(\frac{273}{T}\right) \text{ meters} \quad .$$

The ionic mean free path, ℓ, is affected by several complicating factors such as the attractive forces between the ions and neutral gas molecules, and the energy gained by ions in the presence of a strong electric field. However, most of the investigations here are made under such conditions that thermal equilibrium of molecular ions with gas molecules is usually assured; it is therefore permissible to assume

$$\ell \cong \ell_g \quad ,$$

where ℓ_g is the mean free path of gas molecules. ℓ_g is a function of temperature and pressure, and is given by[27]

$$\ell_g = \ell_{g_o} \frac{1}{P} \frac{T}{273} ,$$

where P is the pressure in mb and ℓ_{g_o} is the Maxwell's mean free path in meters at 273°K and a pressure of 1 mb and is given by

$$\ell_{g_o} = \frac{2.13 \times 10^{-24}}{b_\infty^2 (1 + T'/T)} , \qquad (2.23)$$

with b_∞ as the effective radius of collision at $T = \infty$, T' the temperature constant of gas; both constants have been determined for a large number of gases.[28] Air, for example, has

$$b_\infty = 1.57 \times 10^{-10} \text{ meter} ,$$

and

$$T' = 111.3°K .$$

Therefore, for air

$$z = 9.47 P \left(1 + \frac{111.3}{T}\right) \left(\frac{273}{T}\right)^2 \cdot 10^{-4} .$$

The average random velocity, $\bar{c}$, is given by

$$\bar{c} = 0.922 \sqrt{\frac{3kT}{m_g}} . \qquad (2.24)$$

Thus the final form of the coefficient of volume recombination is given by

$$\rho = 2.47 \times 10^{-11} \frac{1}{\sqrt{M}} \left(\frac{273}{T}\right)^{3/2} w(z) , \qquad (2.25)$$

where M is the molecular weight of the ions relative to hydrogen, chosen as 1. The above formula for the recombination coefficient, as a function of pressure and temperature, is in good agreement with actual values as

illustrated in Figs. 2.8 and 2.9 for pressure and temperature, respectively.

2.5.4. Electron-Ion Recombination.—So far we have considered only ion-ion recombination which is predominant under the prevailing conditions. Recombination of electrons and positive ions is a highly improbable process,[29] and consequently is neglected in the present investigation.

2.6. ELECTRON-ATTACHMENT AND FORMATION OF NEGATIVE IONS

2.6.1. General Considerations.—Negative ions appear in gases under different circumstances:[30]

1. They may be created in the gas largely through the attachment of free electrons to neutral atoms or molecules.
2. They may be introduced into the gas by interaction of fast particles of atomic mass with surfaces or by liberation of adsorbed and absorbed gas molecules from hot metallic surfaces such as filaments or oxide-coated cathodes.

The first type, however, is a predominant source of negative ions under the conditions usually encountered in the study of radioactive ionization gauges.

In general there are three widely varying types of behavior in regard to the formation of negative ions in different gases. The first of these may be characterized by the fact that no electron attachment is observed, for electrons having any value of kinetic energy, and can be explained as due to the absence of an electron affinity. Such cases are found in the rare gases, and in nitrogen and hydrogen. In the second type,

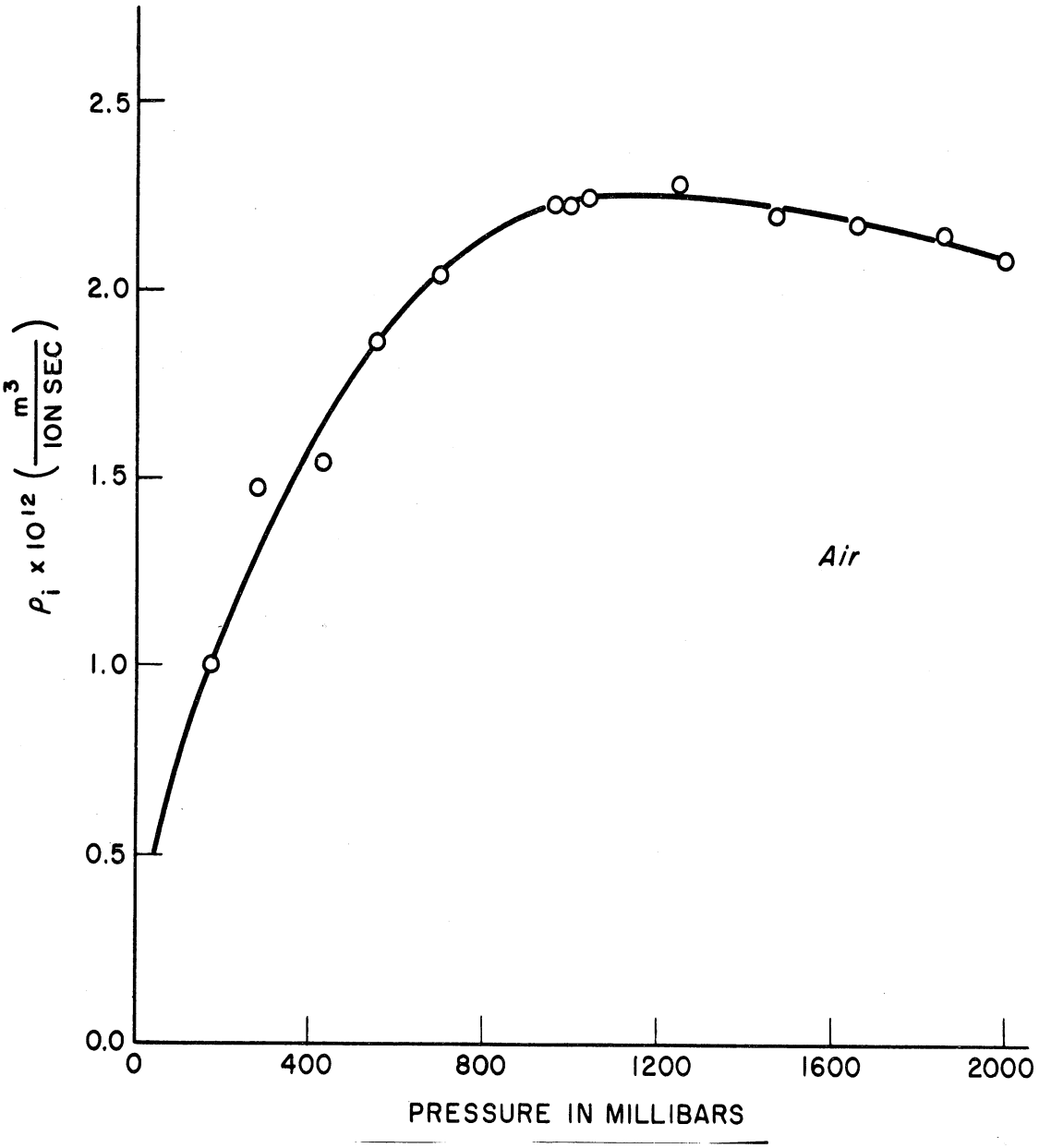

Fig. 2.8. Sayer's data of ρ_i in air as a function of pressure.[51] The full curve represents Thomson's theory for ρ_i in this range.

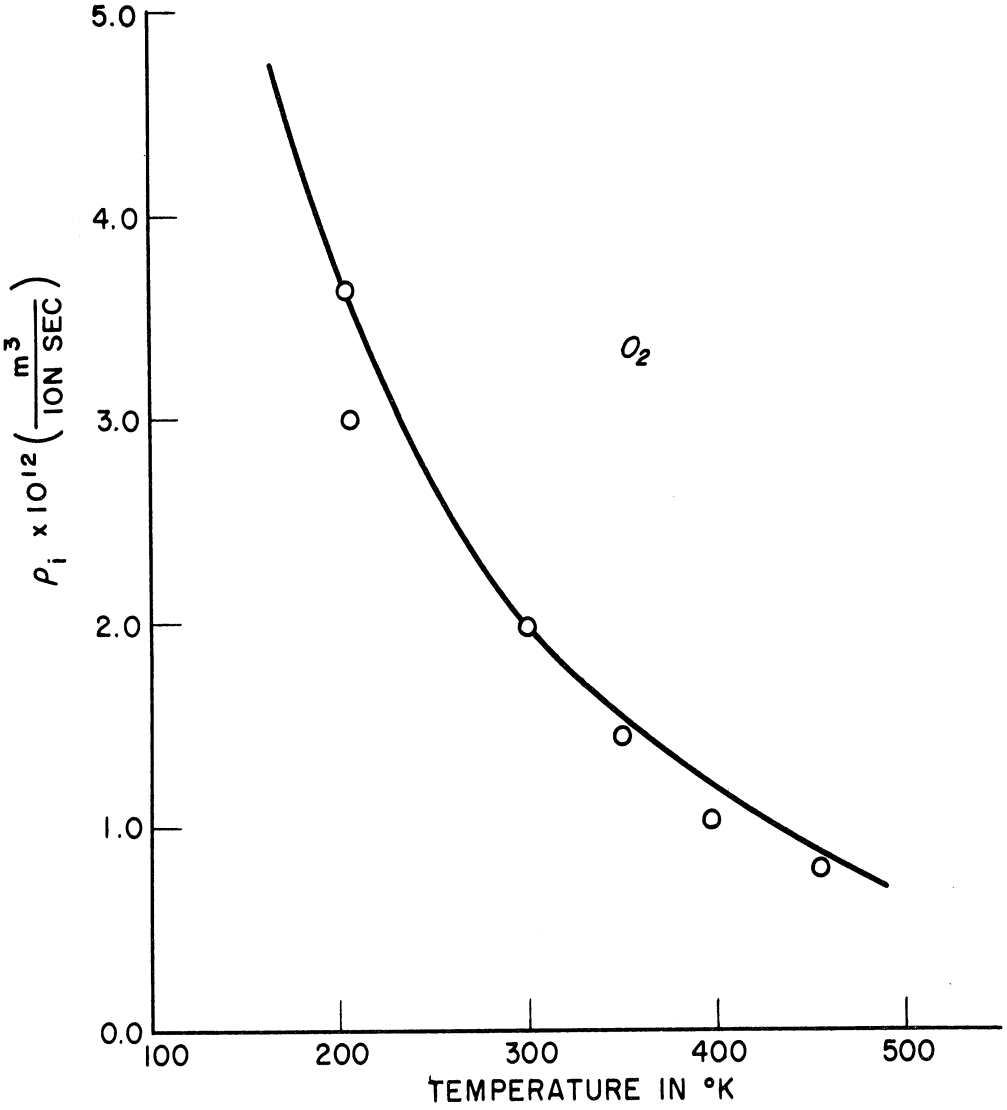

Fig. 2.9. Gardner's data of ρ_i in O_2 as a function of temperature at constant density, compared with calculations from Thomson's theory.[52]

negative ions are formed only by sufficiently high-energy electrons so that dissociation of gas molecules can occur. Examples of this are found in N_2O, NH_3, and HCl. The reaction of this type is

$$XY + e \rightarrow X^- + Y \quad .$$

Finally, there are gases in which electrons of very low kinetic energy can be captured, and in fact show a decrease of cross section with increasing energy of the electron. Oxygen and water vapor are good examples of gases possessing an electron affinity. This can be represented as

$$X_2 + e \rightarrow X_2^- \quad .$$

The electron affinity of an atom or molecule is defined physically as the difference in energy between the ground state of atom or molecule with a free electron at rest at infinity and the ground state of the corresponding negative ion.[31] For atoms, this is simply the binding energy of the extra electron on the negative ion, whereas in the case of molecules, the change in nuclear motion too must be taken into account. An example of molecular ion potential energy curves for oxygen is shown in Fig. 2.10. The electron affinity of O_2, by definition, corresponds to the difference in energy between the lowest vibrational and rotational levels of the O_2 ($^3\Sigma_g^-$) state (point A) and the O_2^- ($^2\Pi_g$) state (point B). However, the minimum energy required to detach an electron from an unexcited O_2^- molecule corresponds to the transition BC, for no change in the nuclear separation. This transition is known as vertical detachment, which is distinguished from the affinity BA.[32]

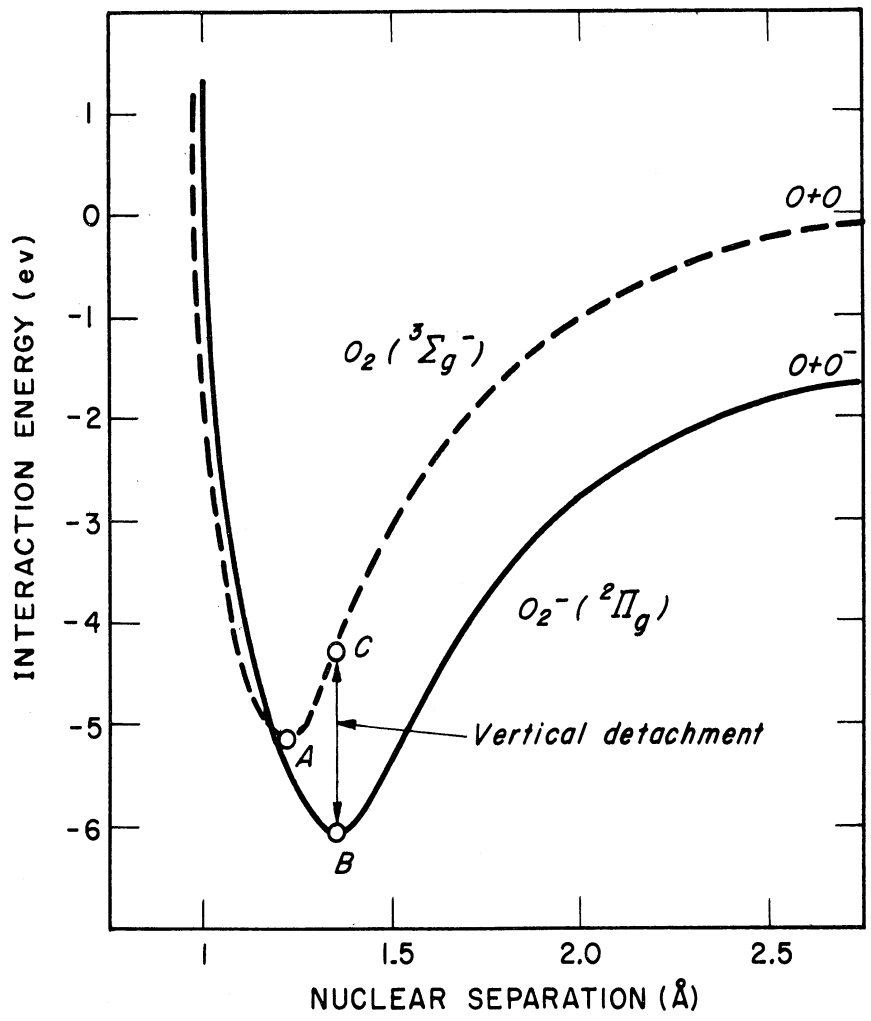

Fig. 2.10. A possible potential energy curve for O_2^-, compared with the known ground state of O_2 (dashed curve).

On the other hand, a negative electron affinity implies an extremely small or zero probability of formation of a negative ion. This is illustrated in Fig. 2.11 which shows the theoretical calculations of the potential energy curves for a hydrogen molecule (H_2) and its corresponding negative molecular ion (H_2^-).[33] From this figure one finds +0.9 ev for the vertical detachment energy, and -3.58 ev for hydrogen electron affinity. Negative molecular hydrogen ions have never been observed experimentally.

There is no experimental evidence of the existence of double-charged negative ions in the gas phase. If such ions exist, they are probably very unstable,[31] because small values of the electron affinities for attachment of single electrons make it improbable that a second electron could also be attached with a decrease of energy. In either direct or dissociative attachments, the excess energy of the attacking electron is removed either by (a) radiation, (b) subsequent collision with a third body, or (c) by resonance with an excited electronic, or vibrational or rotational state of the ion with subsequent loss of energy by radiation or collision.

2.62. Basic Theory of Attachment.—Following J. J. Thomson,[34] it is assumed that electrons do not readily attach to molecules to form negative ions, i.e., there is a certain small probability δ_e that, in a collision between an electron and a molecule, the electron will attach to the molecule, thus forming a negative ion. If the average random velocity of an electron is $\bar{c}_e$ and its mean free path is ℓ_e, then the collision frequency is $\bar{c}_e/\ell_e$. The drift velocity v_e of an electron in the direction of a field of strength E_x is $v_e = \mu_e E_x$, μ_e being the electron mobility.

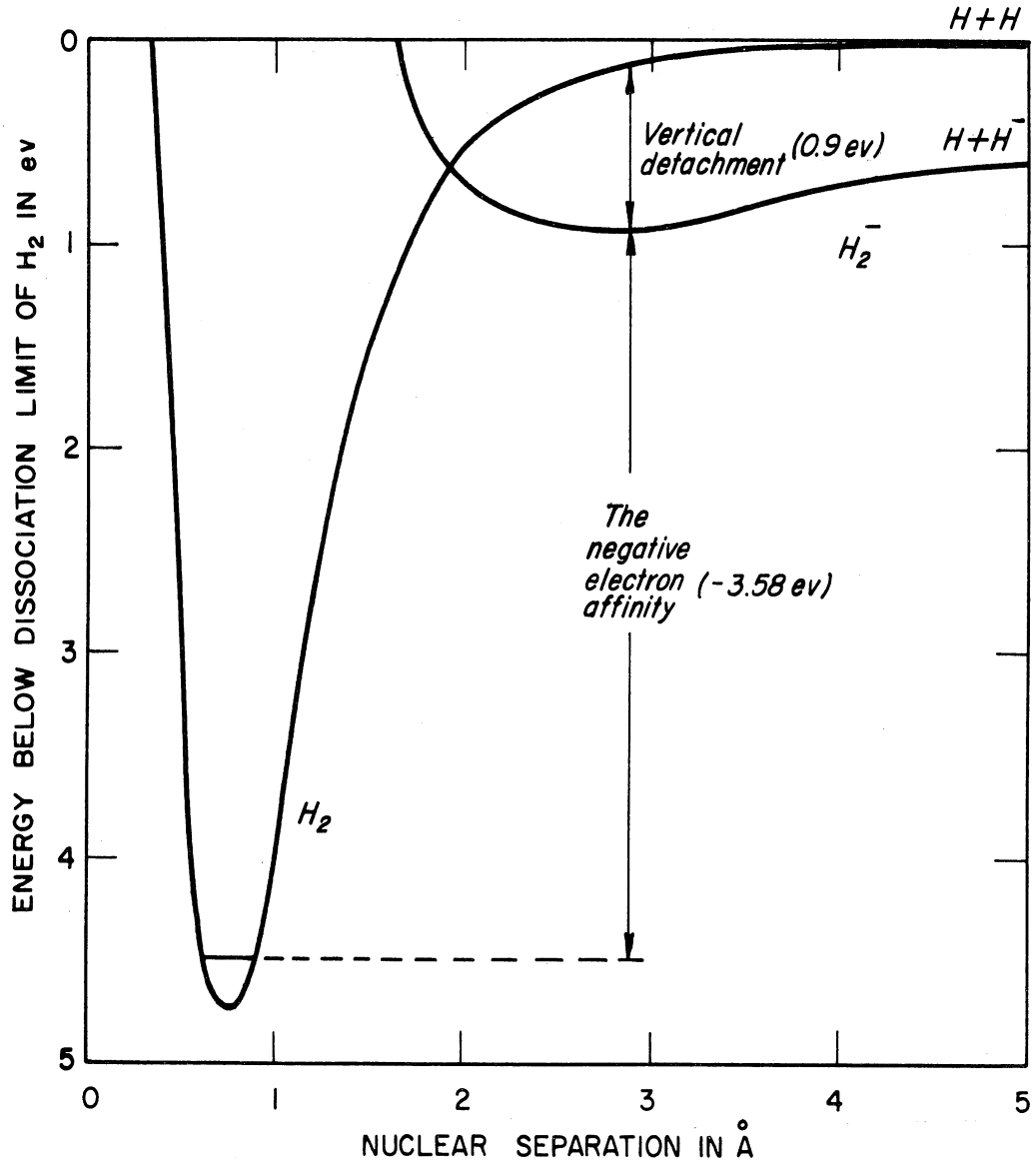

Fig. 2.11. Theoretical potential energy curve for H_2^-, compared with ground state of H_2.

Thus, in advancing a unit length in the field direction along the x-axis, the electron travels a time $t = 1/v_e$; it then makes $\bar{c}_e/(\ell_e v_e)$ collisions per meter. If the attachment process is a pure chance event, of probability δ_e that attachment will occur at any given collision, then out of n electrons starting from a point x at a time t = 0, the number of attachments dn occurring in a distance dx will be

$$dn = - \frac{\delta_e \bar{c}_e}{\ell_e v_e} n \, dx \quad . \tag{2.26}$$

Integrating and setting $n = n_o$ at x = 0, the number of electrons n, out of the initial n_o, that do not experience attachment within a distance x is given by

$$n = n_o \, e^{- \frac{\delta_e \bar{c}_e}{\ell_e v_e} x} \quad . \tag{2.27}$$

This shows that the number of electrons surviving attachment after traversing a distance x in the field direction is a negative exponential function of distance. The average distance $\bar{x}$ for attachment under the present conditions is thus given by

$$\bar{x} = \frac{\ell_e \, \mu_e \, E_x}{\delta_e \, \bar{c}_e} \quad . \tag{2.28}$$

This gives the average free path in the field direction before attachment. The electron drift velocity v_e, is, according to Compton or Langevin related to ℓ_e and $\bar{c}_e$ by the fundamental relation

$$v_e = 0.815 \, \frac{q_e \, E_x \, \ell_e}{m_e \, \bar{c}_e} \quad , \tag{2.29}$$

where the energy distribution is assumed to be Maxwellian. For other

types of energy distribution, only the numerical fraction in Eq. (2.29) is to be slightly modified, with values being, however, near unity. q_e and m_e are charge and mass of an electron, respectively.

From (2.29) we have

$$\frac{\ell_e}{\bar{c}_e} = \frac{m_e v_e}{0.815\, q_e E_x} , \tag{2.30}$$

so that the survival equation becomes

$$n = n_o e^{-\frac{0.815\, \delta_e q_e x}{m_e \mu_e^2 E_x}} . \tag{2.31}$$

The attachment process can also be described in terms of collision cross section for capture. An electron moving with average random velocity $\bar{c}_e$ among the relatively fixed gas molecules describes a random path of total length $\bar{c}_e$ meters in one second. All molecules, the centers of which lie within a distance r_m, collide with the electron, causing appreciable deflection in the otherwise straight trajectory. Thus a volume $\pi r_m^2 \bar{c}_e = \sigma_m \bar{c}_e$ is swept out in one second. Here σ_m is the collision cross section of one atom or molecule, for electron deflection, and is known as the collision cross section for electrons in a gas. Since there are N_q molecules per m^3 of a gas at temperature of 273°K and pressure of 1 mb, then the $N_q \sigma_m \bar{c}_e$ molecules lying within this broken cylinder will have collided with the electron in a second. But the total distance traveled in one second is $\bar{c}_e$. Therefore the average distance between collisions or the mean free path is

$$\ell_{e_o} = \frac{\bar{c}_e}{N_q \sigma_m \bar{c}_e} = \frac{1}{N_q \sigma_m} . \tag{2.32}$$

This is not a precise relation because of the Ramsauer effect; electron free paths are a rather complex function of energy and differ for each type of gas.

If P is the pressure in millibars and T the gas temperature in degrees Kelvin, then the survival equation for the n electrons, out of n_o, that have traversed a random distance, s, in the gas without a deflecting collision with molecules is

$$n = n_o e^{-s/\ell_e} = n_o e^{-N_q \sigma_m P(273/T)s} . \qquad (2.33)$$

The probability of attachment, δ_e, as defined by Thomson may now be stated more precisely in terms of collision cross sections. Thus

$$\delta_e = \frac{\sigma_a}{\sigma_m} \qquad (2.34)$$

or

$$\sigma_a = \delta_e \sigma_m . \qquad (2.35)$$

This enables σ_a, the attachment cross section, to be calculated if σ_m and δ_e are known from measurement. Since the collision cross section is inversely proportional to the mean free path, Eq. (2.34) could be written as

$$\delta_e = \frac{\ell_e}{\ell_{e_a}} = \frac{\ell_e/\bar{c}_e}{\ell_{e_a}/\bar{c}_e} \qquad (2.36)$$

$\ell_e/\bar{c}_e$ actually represents the mean time elapsed between two successive collisions, whereas $\ell_{e_a}/\bar{c}_e$ is the mean lifetime of a free electron before experiencing any attachment. Accordingly the coefficient of attachment, δ_e, could be redefined as

$$\delta_e = \frac{\text{mean time between collision}}{\text{mean lifetime of a free electron}} \quad . \tag{2.37}$$

Using Eqs. (2.35) and (2.36), it is then possible to express the survival equation for attachment in random motion in a gas as

$$n = n_o e^{-s/\ell_{e_a}} = n_o e^{-N_q P \sigma_a (273/T) s} \quad , \tag{2.38}$$

with

$$\ell_{e_a} = \frac{1}{N_q P \sigma_a (273/T)} = \frac{\ell_e}{\delta_e} \quad , \tag{2.39}$$

the average random free path for attachment.

It should be noted here that Eqs. (2.27) and (2.31), which deal with the distances, x, for attachment involving motion in the field direction, are not to be confused with Eqs. (2.33) and (2.38) dealing with distances, s, of random motions involved in attachment. A similar distinction applies to $\bar{x}$ of (2.28) and ℓ_{e_a} of (2.39). The average random free path for attachement, ℓ_{e_a}, can be determined directly from microwave techniques.[35]

Since the random path s is given by $s = \bar{c}_e t$, then substituting in the survival equations (2.38) renders

$$n = n_o e^{-(\bar{c}_e/\ell_{e_a})t} = n_o e^{-N_q \sigma_a (273/T) \bar{c}_e t}$$

$$= n_o e^{-t/\tau_a} \tag{2.40}$$

and

$$dn = -\frac{n_o}{\tau_a} e^{-t/\tau_a} \, dt \quad , \tag{2.41}$$

where $\tau_a = \ell_{e_a}/\bar{c}_e$ is the mean lifetime of a free electron.

2.6.3. Attachment in a Mixture of Gases.—It was stated in the previous section that the number of collisions in dt second is $(\bar{c}_e/\ell_e)dt$, with $\bar{c}_e$ the random velocity of electrons and ℓ_e the corresponding mean free path. In a mixture of gases, the calculation of the collision frequency is not so simple, for one must compute the relative number of impacts with each type of molecules, which will in turn be a function of the mean free path and the molar fraction of the respective gases. The attachment in air, for example (which consists of oxygen and nitrogen, and only the former with attaching molecules), is[36]

$$\delta_{e_{air}} = \frac{\delta_{e_{O_2}}}{1 + \frac{f_1 \ell_{e_2}}{f_2 \ell_{e_1}}} \tag{2.42}$$

where f_1 and ℓ_{e_1} are the molar fraction and the deflecting mean free path of nitrogen, and f_2 and ℓ_{e_2} the corresponding values of oxygen. Since the molar fraction is proportional to the partial pressure of the gas, Eq. (2.42) could be written as

$$\delta_{e_{air}} = \frac{\delta_{e_{O_2}}}{1 + \frac{P_1 \ell_{e_2}}{P_2 \ell_{e_1}}} \tag{2.43}$$

where P_1 and P_2 are the partial pressures of nitrogen and oxygen, respectively.

In general, for mixtures containing more than two gases, the effective attachment probability is given by

$$\bar{\delta}_e = \frac{\sum_k \delta_{e_k} \frac{P_k}{\ell_{e_k}}}{\sum_k \frac{P_k}{\ell_{e_k}}} \tag{2.44}$$

where δ_{e_k}, P_k, and ℓ_{e_k} refer to the kth gas in the mixture.

2.6.4. Attachment Properties of Oxygen and Water Vapor.—Examples of electron-attaching gases most likely to be found in air are molecular oxygen (O_2) and water vapor (H_2O). The attaching properties of both gases are summarized in the following.

It has been observed that in oxygen the attachment probability, δ_e, is not pressure-dependent above about 4 mb.[36-38] For oxygen it appears likely that the energy of attachment is taken up into the vibrational system for some period. If an impact does not remove this energy during the lifetime of the vibrational negative ion state, the electron will separate again. In this case the formation of a negative ion depends on two successive collisions so that the newly formed ion must collide with a neutral molecule before spontaneous separation of the electron takes place. In such a process the higher the energy of the electron, the less likely the initial attachment will be, and consequently δ_e quickly goes down as the energy of the attacking electron increases. Thus, a characteristic of this process is a rapid decline of δ_e with increase in E/P. This is illustrated by Bradbury's data[36] (Fig. 2.12). At low electron energies the attachment process in molecular oxygen is direct and can be represented by the reaction

$$O_2 + O_2 + e \rightarrow O_2^- + O_2 \quad ,$$

in which excess energy goes into vibrational state until it is lost in impact later. Another feature of the above data is the subsequent rise of the value of δ_e as the energy increases. This is believed to be due

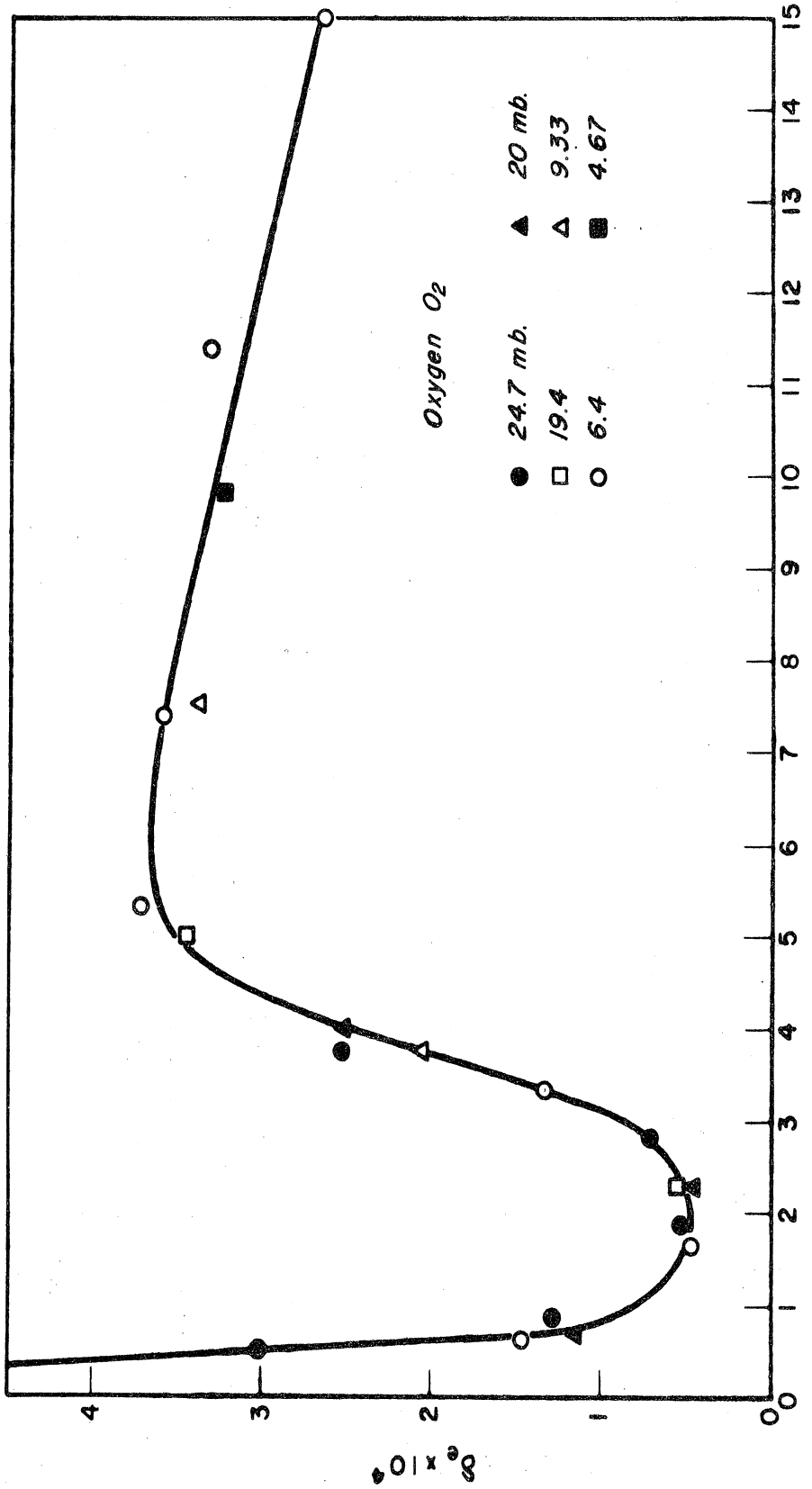

Fig. 2.12. Probability of electron attachment in oxygen as a function of E/P. The points indicate data taken at different pressures.

to an added different type of attachment, known as dissociative attachment, which may set in at higher electron energies. Under these circumstances the energy of the attacking electron is so great that the electron is captured and molecular dissociation occurs giving rise to neutral atomic oxygen and atomic negative ion. This type of attachment may be represented by the reaction

$$O_2 + e \rightarrow O^- + O \quad .$$

Bloch and Bradbury[39] developed quantum-mechanically a theory which accounted for the mechanism of capture of an electron by O_2, SO_2, or NO at low-energy values in which a dissociation process does not occur. They assumed that the capture of the electron is a uni-molecular process involving the excitation of molecular vibrational levels and subsequent loss of energy by collision or radiation. Their theoretical curve is compared with experimental data in Fig. 2.13. The theoretical curve has a peak at some lower energies. There has been no experimental evidence in the available literature to support this theoretical peak. Yet some of the experimental results obtained in the present work may be adequately explained if such a peak in the attachment probability is present.

Figure 2.14 is Bradbury's experimental curve for air.[36]

In the case of water vapor, at appropriate pressures of H_2O, the H_2O polymerizes to $(H_2O)_2$ and the equilibrium concentration of $(H_2O)_2$ is a function of pressure and gas temperature. Thus negative ions in H_2O are likely to be formed by an electron attachment to the $(H_2O)_2$ complexes with

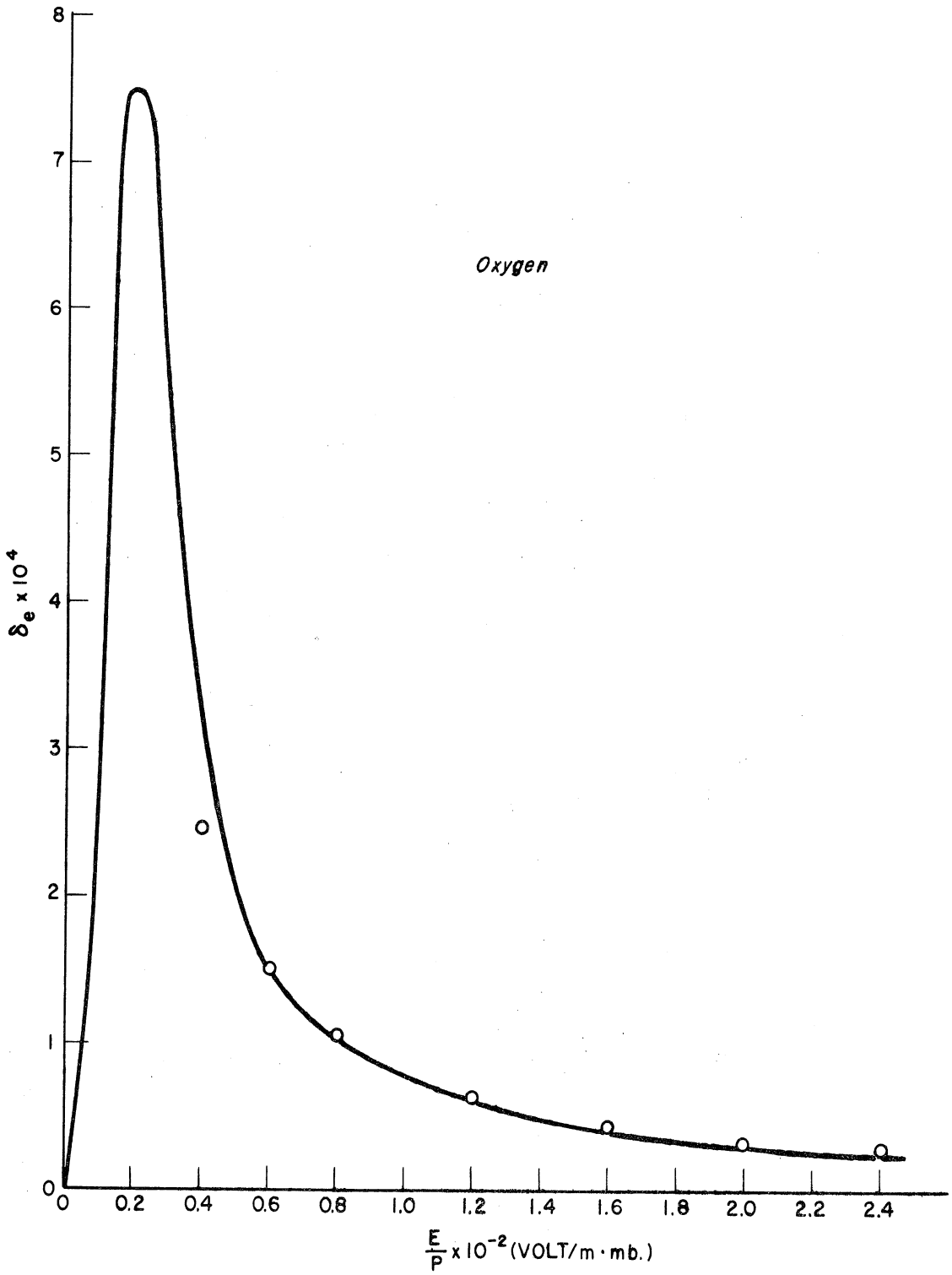

Fig. 2.13. Plot of δ_e as a function of E/P as given by Bloch and Bradbury's theory. The theory is fitted at one point. Note the peak and decline of theory at lower E/P.

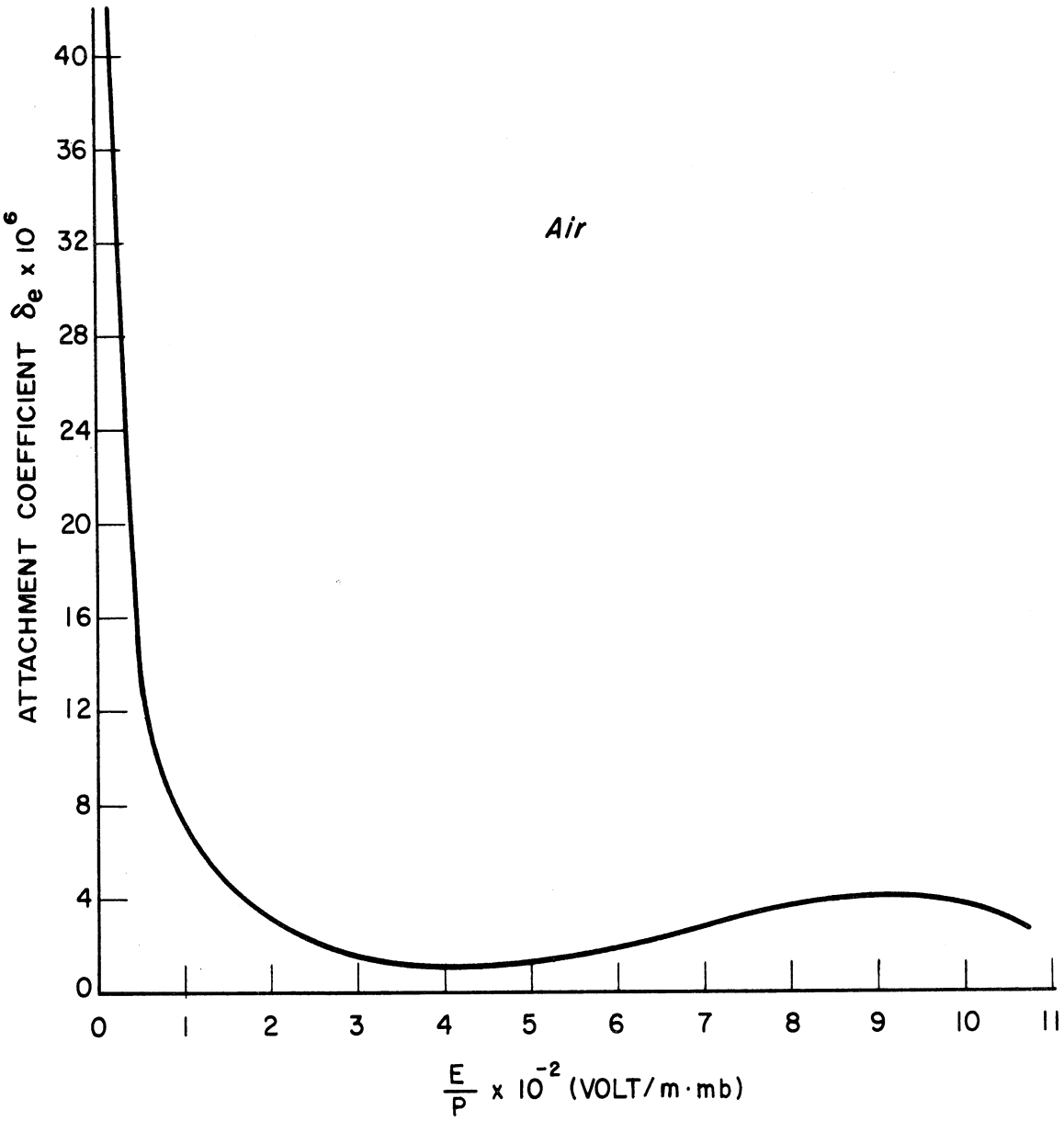

Fig. 2.14. Bradbury's values for δ_e as a function of E/P in air.

dissociation to give an H_2O^- ion and an H_2O molecule. At low values of E/P, the attachment probability, δ_e, is pressure-dependent (Fig. 2.15). In fact, at a fixed E/P, the value of δ_e increases approximately in a linear relation with pressure. The reaction in this type of attachment is

$$(2H_2O) + e \rightarrow (H_2O)^- + H_2O \quad .$$

Above an E/P of about 10^3 volt/meter per mb, a pressure-independent dissociative attachment occurs with a probability of the order 4×10^{-4}.

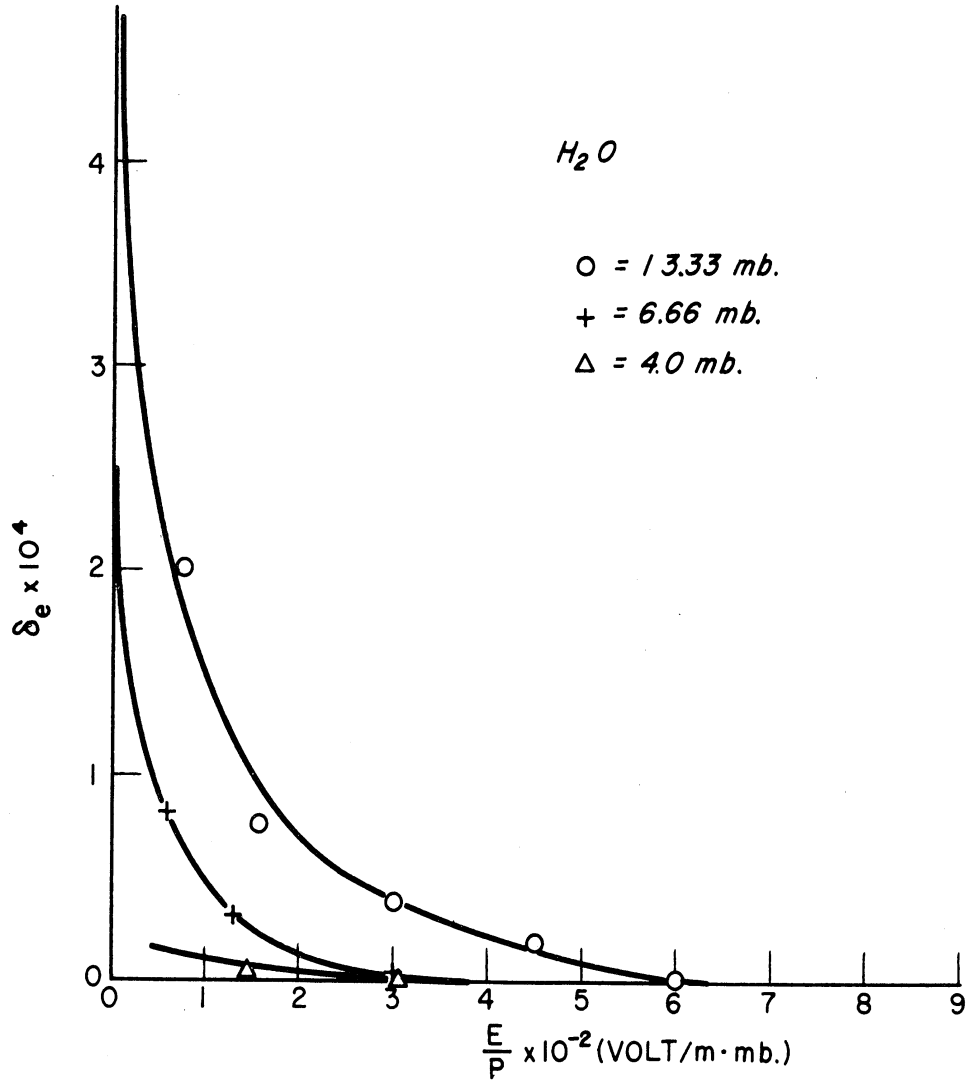

Fig. 2.15. Bradbury's values for δ_e in H_2O as a function of E/P.

CHAPTER III

THEORY OF RADIOACTIVE IONIZATION GAUGE

3.1. INTRODUCTION

In this chapter the current-pressure relation in a radioactive ionization gauge will be derived from the basic equations of current conduction and of electric field in weakly ionized gases. Two cases will be considered: (1) the case in which complete electron attachment is assumed and thus the conduction current is entirely due to ionic currents alone, and (2) the case in which the electron attachment is variable, and hence the electronic current in addition to the ionic is of importance in determining the conduction characteristics of the gauge.

Two methods are adopted in the derivation of the current-pressure relationship; first an approximate method in which the electric field is assumed constant, and then a general method in which the electric field is modified due to the presence of a thin layer of space charge in the vicinity of the electrodes.

3.2. APPROXIMATE METHOD

As mentioned in Chapter I, a simple form of a radioactive ionization gauge can consist of two parallel plates, between which there is an appropriate gas sample. One plate can be the ionizing source and if between this and the other plate an appropriate voltage is applied, the collected

ion-current can be taken as a measure of the gas pressure.

A first approximation of the problem can be achieved by assuming (1) a constant field throughout the gap between the two planes; (2) that the gas is weakly ionized so that there will be no space-charge effects; and (3) that the electric field is strong enough to effect collection of ions, yet too weak to accelerate the electrons to velocities sufficient to produce ionization by collision.

Let the gas be uniformly ionized and let g be the number of ion-pairs produced per unit volume in one second. As the space-charge field is negligible compared to the applied field, $E_o = V/s_o$, where V and s_o are the voltage and distance between the plates, respectively (Fig. 3.1), the ions of the same kind will have as a group a constant drift velocity, μE_o, where μ is the ion mobility.

In the ideal case, where there is no loss of ions by recombination, nor any additional ionization by collision, all the ions produced by irradiation are collected, giving a maximum value of current known as the saturation current. On the other hand, if some of the ions recombine during their drift towards the respective electrodes, the net current flow will be less than the saturation value and the collection efficiency, f, is thus defined by

$$f = \frac{\text{measured current}}{\text{saturation current}} . \qquad (3.1)$$

If there is no recombination loss, i.e., f = 1, the total number of positive ions crossing a unit area at a distance x from the positive plate is

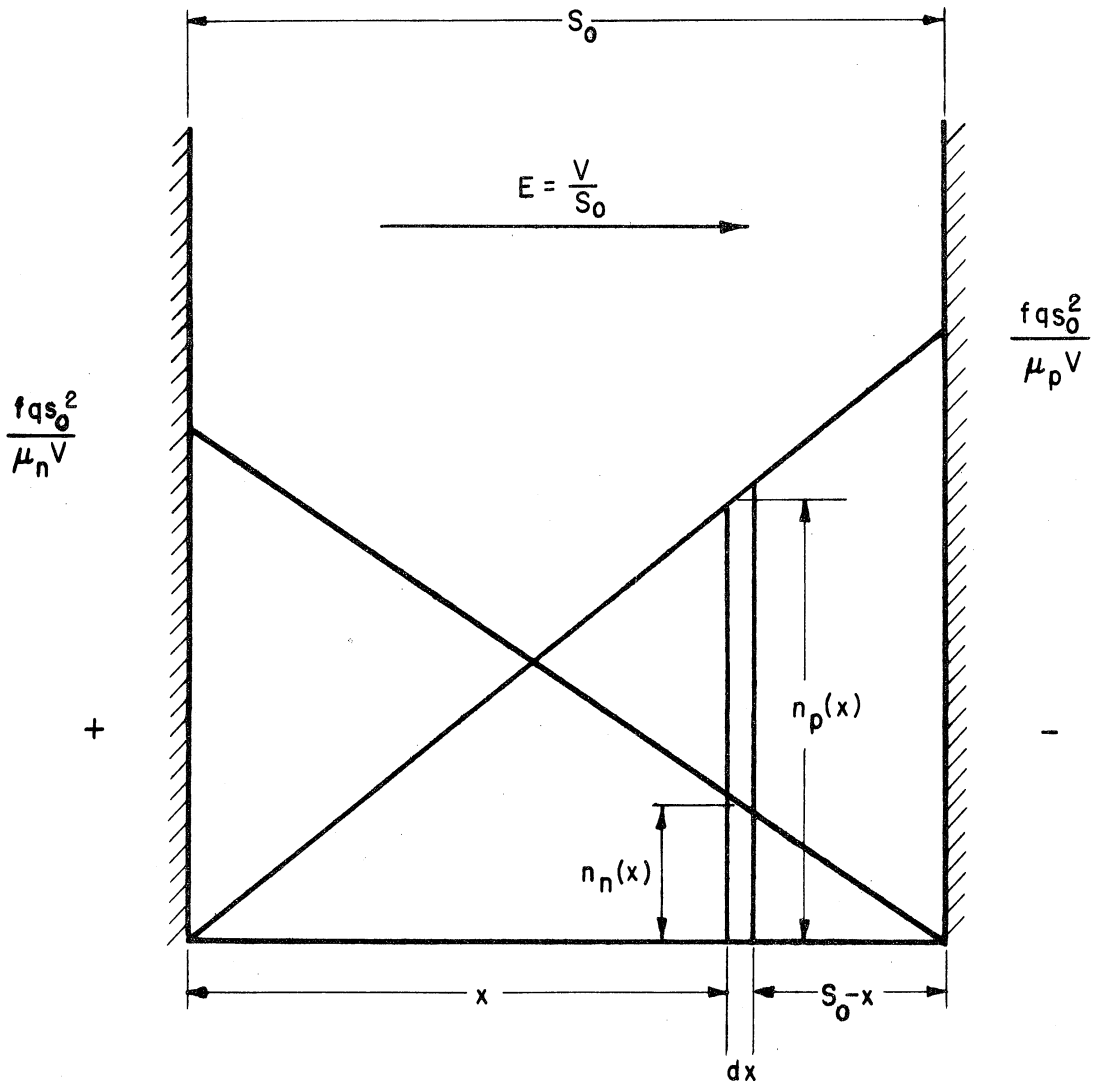

Fig. 3.1. Ionic density distribution between the two parallel plates—simple theory.

gx ions per second. Thus the positive ion density, n_p, at any point in the field is given by

$$n_p = \frac{gx}{\mu E_o} \quad . \tag{3.2}$$

Therefore, the positive-ion density varies linearly from 0, at the positive plate, to $(gs_o)/(\mu E_o)$ at the negative plate. Similarly, the negative ion density, n_n, at a point x, is

$$n_n = \frac{g(s_o-x)}{\mu E_o} \quad . \tag{3.3}$$

The saturation current, J_m, in this case will be

$$J_m = q_e\, gs_o \quad , \tag{3.4}$$

where q_e is the unit ionic charge. If the collection efficiency, f, is less than unity due to loss of ions by recombination, the current density, J, reaching each plate becomes

$$J = f\, q_e\, gs_o = f\, J_m \quad . \tag{3.5}$$

To determine the effect of recombination on the distribution of ions between the plates, one may proceed as follows. Since the positive and negative ions are assumed to have the same value of mobility, the distribution of one type of ions will be the image of the other. This can be expressed by

$$n_n(x) = N(x) \tag{3.6}$$

and

$$n_p(x) = N(s_o-x) \quad , \tag{3.7}$$

where $N(x)$ or $N(s_o-x)$ is a general function, the form of which will be determined for the particular conditions imposed by this problem.

As a result of the continuity of flow, the current density should be the same throughout the gap. Therefore, the collected current at any time is

$$J = q_e E_o \mu [N(x) + N(s_o-x)] \tag{3.8}$$

which could be written as

$$\frac{J}{q_e E_o \mu} = N(x) + N(s_o-x) \quad . \tag{3.9}$$

According to Eq. (3.9), the sum of the negative and positive ion densities is always constant at any point. This condition, together with the requirement that both densities be zero at one or the other electrode, is satisfied if and only if the function $N(x)$ is linearly proportional to x, i.e.,

$$n_n = N(x) = Kx \tag{3.10}$$

and

$$n_p = N(s_o-x) = K(s_o-x) \quad , \tag{3.11}$$

where K is the constant of proportionality, which from (3.2) and (3.3) has the value $g/\mu E_o$. Therefore, one can assume triangular distribution of ion density, varying linearly from 0 to $(fgs_o)/\mu E_o$, for the approximate case now being considered. This can be confirmed by a mechanistic analysis using an integration of the introduction and loss terms.

The number of ions lost by recombination in a unit volume per second is

$$\rho\, n_n\, n_p = \rho\, \frac{f^2 g^2 x(s_o - x)}{\mu^2\, E_o^2}$$

$$= \frac{\rho\, f^2 g^2 s_o^2}{\mu^2\, V^2}\,(s_o - x)x \quad .$$

Therefore, the total number lost throughout the space per unit area is

$$R = \int_o^{s_o} \rho\, n_n\, n_p\, dx \qquad (3.12)$$

$$= \frac{\rho s_o}{6}\left(\frac{f g s_o^2}{\mu V}\right)^2 \text{ ion-pairs per second.}$$

The total number of ion-pairs produced per second in the same space above is gs_o. Therefore, the collection efficiency is given by

$$f = 1 - \frac{R}{gs_o} \quad . \qquad (3.13)$$

Substituting for R and reducing, we get

$$f = 1 - \xi f^2 \quad , \qquad (3.14)$$

where

$$\xi = \frac{\rho g}{\mu^2}\left(\frac{s_o^4}{6V^2}\right) \quad .$$

Solving for f, we thus get

$$f = -\frac{1}{2\xi} \pm \sqrt{(1/2\xi)^2 + (1/\xi)} \quad .$$

Only the + sign is true, since f must be a positive real quantity. The above solution could be written as[40]

$$f = \frac{J}{J_m} = \frac{2}{1 + \sqrt{1 + 4\xi}} \quad . \qquad (3.15)$$

This equation defines a generalized saturation curve, as illustrated in

Fig. 3.2, for plane-parallel geometry. The dimensionless quantity, ξ, consists of two parameters: $(\rho g/\mu^2)$ is a characteristic of the gas at given temperature and pressure, whereas $(s_o^4/6V^2)$ is dependent on the external conditions such as the geometry of the chamber and the voltage applied to the electrodes. The latter parameter naturally varies for different geometries. For cylindrical chambers, for example, ξ becomes[41]

$$\xi_{cyl.} = \left(\frac{g\rho}{\mu^2}\right)\left[\frac{(r_1-r_2)^4}{6V^2}\right]\cdot\left[\frac{r_1+r_2}{2(r_1-r_2)}\ln\frac{r_1}{r_2}\right]^2 , \qquad (3.16)$$

where r_1 and r_2 are the radii of the cylinder whose outer electrode is at a potential +V with respect to the inner one.

The output current as calculated on the basis of (3.15) for the planar geometry is shown in Fig. 3.3, for different plate voltages. An approximate picture of the general behavior of the gauge could be determined by computing the proper values of ξ in each case. Such detailed study, however, will be postponed to the next section when a more exact treatment is considered. In the forthcoming solution, the modification of the electric field intensity near the electrodes, as a result of the nonlinear distribution of ion densities, will be taken into account.

3.3. GENERAL METHOD

The basic relations which are required to study the conduction of electricity through gases under the most general conditions are the equation of continuity and the field equation. The field equation, known as Poisson's equation, may be written in the following form

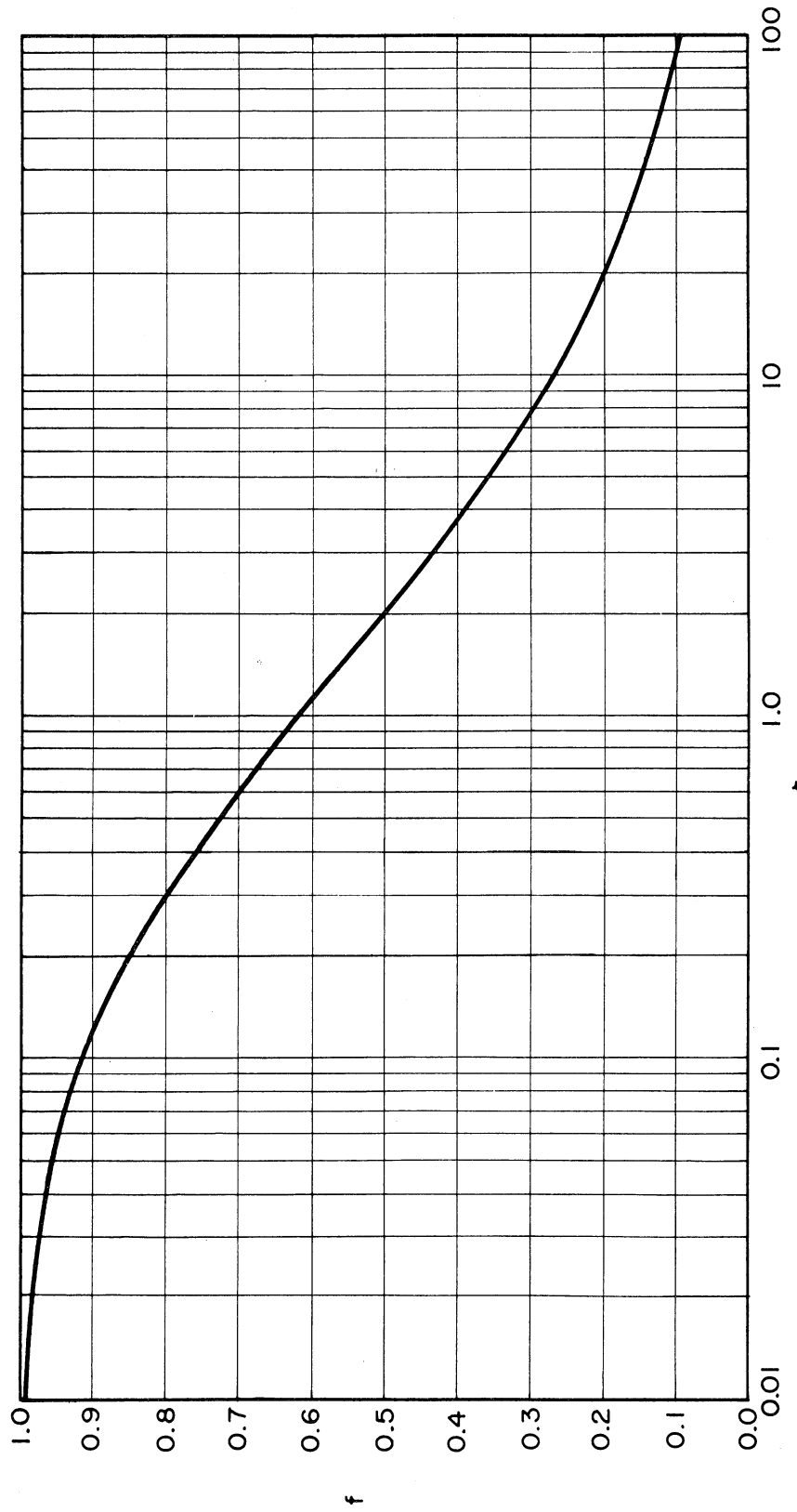

Fig. 3.2. Generalized saturation curve—simple theory.

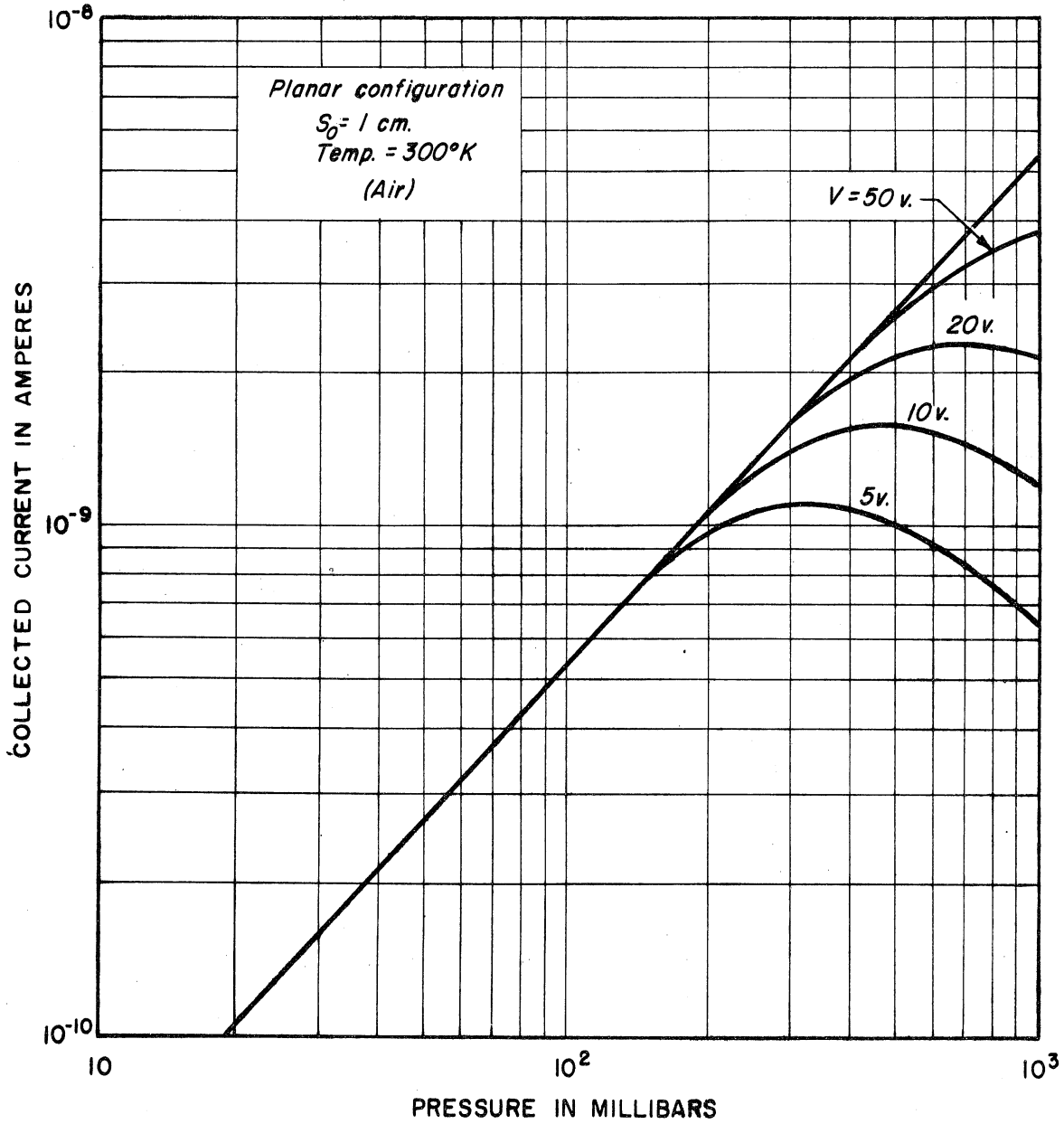

Fig. 3.3. The effect of plate voltage on the i-P characteristic—simple theory.

$$\text{div } \vec{E} = \frac{q_e}{\epsilon_o} (n_p - n_n - n_e) , \qquad (3.17)$$

where

$\vec{E}$ = the electric field intensity at any point, volt per meter, a vector quantity,

n_p = number density of positive ions per m^3,

n_n = number density of negative ions per m^3,

n_e = number density of electrons per m^3,

q_e = the electronic charge, value 1.6×10^{-19} coulomb, and

ϵ_o = permittivity of vacuum, value $10^{-9}/36\pi$ farad per meter.

On the other hand, the equation of continuity is, in fact, a mathematical statement of the principle of conservation of charge. The derivation of this equation for the positive ions in a radioactive ionization gauge is as follows.

Consider a small region in space, dx dy dz, centered at x, y, z. The rate of change of positive ions is

$$\frac{\partial n_p}{\partial t} \text{ dx dy dz} \quad . \qquad (3.18)$$

These ions arise from the excess of production over recombination in the volume and from a net flow across the surfaces. The former contribution is represented by

$$(g - r_i - r_e) \text{ dx dy dz} \quad , \qquad (3.19)$$

where g is the average rate of production of positive ions per unit volume per second, r_i, the rate of decay by recombination with negative ions,

and r_e, the rate of decay by recombination with electrons.

The second process contributing to the rate of change in ion density is the net flow of the respective ions across the boundaries of volume under consideration. Let $J_{px}(x,y,z)$ be the current density due to the flow of positive ions in the x-direction at the center of elemental volume dx dy dz. Then the corresponding current density in the x-direction at the midpoint of the dy dz face located at $[x - (dx/2)]$ is

$$J_{px}(xyz) - \frac{\partial}{\partial x} J_{px}(xyz) \frac{dx}{2} \quad .$$

This midpoint value will be the average value for the face so that the positive-ion flow across the face <u>into</u> dx dy dz will be

$$\frac{1}{q_e}\left[J_{px} - \frac{\partial J_{px}}{\partial x} \frac{dx}{2}\right] dy\ dz \quad .$$

Similarly, the flow <u>out of</u> dx dy dz across the face at $[x + (dx/2)]$ is

$$\frac{1}{q_e}\left[J_{px} + \frac{\partial J_{px}}{\partial x} \frac{dx}{2}\right] dy\ dz \quad .$$

Then the net flow across the dy dz pair of faces into dx dy dz is

$$- \frac{1}{q_e} \frac{\partial J_{px}}{\partial x} dx\ dy\ dz \quad .$$

Proceeding in a similar manner for the faces dx dy and dx dz leads to a total net flow into dx dy dz of

$$- \frac{1}{q_e} \operatorname{div} \vec{J}_p\ dx\ dy\ dz \quad . \qquad (3.20)$$

Equating the net rate of change inside dx dy dz to the sum of expressions (3.19) and (3.20), one gets

$$\frac{\partial n_p}{\partial t}\,dx\,dy\,dz = (g-r_i-r_e)\,dx\,dy\,dz - \frac{1}{q_e}\,\mathrm{div}\,\vec{J}_p\,dx\,dy\,dz \quad .$$

Dividing through by dx dy dz gives

$$\frac{\partial n_p}{\partial t} = (g-r_i-r_e) - \frac{1}{q_e}\,\mathrm{div}\,\vec{J}_p \quad , \tag{3.21}$$

which is the continuity equation for the positive ions. The corresponding equations for electrons and negative ions differ only in the first term of the right-hand side of the equation. Thus for electrons it becomes

$$\frac{\partial n_e}{\partial t} = (g-a-r_e) + \frac{1}{q_e}\,\mathrm{div}\,\vec{J}_e \quad , \tag{3.22}$$

where a is the rate of decay of electrons as a result of attachment to neutral atoms or molecules forming negative ions. Also, for negative ions, the continuity equation is

$$\frac{\partial n_n}{\partial t} = (a-r_i) + \frac{1}{q_e}\,\mathrm{div}\,\vec{J}_n \quad . \tag{3.23}$$

We can suppose that the motion of each charge carrier is governed, independently of all others, by the random diffusive action provoked by thermal agitation as well as the systematic drift produced by the electric field. We shall also suppose that the electric field is small enough so that it does not appreciably disturb the equilibrium distribution of velocities of carriers and thus their drift velocity is directly proportional to the electric field.[24] Under these conditions it is justifiable to consider the current of different carriers as the resultant of densities of a conduction and a diffusion current. The latter is directly proportional

to the gradient of carrier concentration, grad n. Thus we can write for the different current densities

$$\vec{J}_p = q_e \mu_p n_p \vec{E} - q_e D_p \text{ grad } n_p \quad , \tag{3.24}$$

$$\vec{J}_e = q_e \mu_e n_e \vec{E} + q_e D_e \text{ grad } n_e \quad , \tag{3.25}$$

$$\vec{J}_n = q_e \mu_n n_n \vec{E} + q_e D_n \text{ grad } n_n \quad , \tag{3.26}$$

where μ is the mobility of the respective carrier, and D the corresponding diffusion coefficient. The diffusion coefficient D is related to the mobility μ by Einstein's relation[27]

$$D = \mu V_T \quad , \tag{3.27}$$

where V_T is the voltage equivalent of the temperature T, also called the kinetic temperature. It is defined by the relation $V_T = kT/q_e$, where k is Boltzmann's constant, value 1.38×10^{-23} joules per degree Kelvin, and q_e the electronic charge, 1.6×10^{-19} coulombs. The total current density, $\vec{J}$, is the sum of all ionic and electronic current densities. Thus

$$\vec{J} = \vec{J}_p + \vec{J}_n + \vec{J}_e \quad . \tag{3.28}$$

The rate of electron-ion recombination, r_e, as used in Eqs. (3.21) and (3.22), is proportional to the probability of encounters with oppositely charged carriers, as mentioned in Chapter II. Therefore, the rate at which electrons disappear by recombination is

$$r_e = \rho_e n_e n_p \quad , \tag{3.29}$$

where ρ_e is the coefficient of electron-ion recombination. Similarly, the rate of recombination of negative and positive ions is given by

$$r_i = \rho_i n_n n_p \quad , \tag{3.30}$$

where ρ_i is the coefficient of volume ion-ion recombination. Substituting the above expressions in Eqs. (3.21), (3.22), and (3.23), one can summarize the relations governing electrical conduction in gases as follows:

$$\text{div } \vec{E} = \frac{q_e}{\epsilon_o} (n_p - n_n - n_e) \qquad \left[\text{Field Equation}\right]$$

$$\left.\begin{aligned}
\frac{\partial n_p}{\partial t} &= (g - \rho_i n_p n_n - \rho_e n_p n_e) - \frac{1}{q_e} \text{div } \vec{J}_p \\
\frac{\partial n_n}{\partial t} &= (a - \rho_i n_n n_p) + \frac{1}{q_e} \text{div } \vec{J}_n \\
\frac{\partial n_e}{\partial t} &= (g - a - \rho_e n_e n_p) + \frac{1}{q_e} \text{div } \vec{J}_e
\end{aligned}\right\} \left[\text{Continuity Equations}\right]$$

$$\vec{J} = \vec{J}_p + \vec{J}_n + \vec{J}_e$$

$$\left.\begin{aligned}
\vec{J}_p &= q_e \mu_p (n_p \vec{E} - V_T \text{ grad } n_p) \\
\vec{J}_n &= q_e \mu_n (n_n \vec{E} + V_T \text{ grad } n_n) \\
\vec{J}_e &= q_e \mu_e (n_e \vec{E} + V_T \text{ grad } n_e)
\end{aligned}\right\} \qquad \left[\text{Flow Equations}\right]$$

Inspection of the above relations readily shows that they form a system of simultaneous nonlinear partial differential equations. The mathematical problem in finding a general solution is rather involved. However, the problem becomes easy to handle in the case of certain simple geometries or when the density of ionization is sufficiently small so that it will not appreciably affect the field strength and therefore the drift velocities.

3.4. THEORY OF PLANAR GAUGE—COMPLETE ATTACHMENT

3.4.1. Statement of Assumptions and Basic Equations.—In this section, the relationship between the collected ion current and the pressure of the irradiated gas is developed for a cylindrical volume of unit cross section between two infinite plates. It is assumed that the electric field intensity is not strong enough to cause any ionization by collision; the field is, however, sufficient to render any contribution due to diffusion current negligible. It is also assumed that all electrons are attached to neutral gas molecules, forming negative ions and leaving them as the sole carriers of negative charges.

Let the gas in the active volume between two parallel plates be uniformly irradiated by a source of ionization of constant intensity, and let g be the number of ion-pairs produced per second in a unit volume. Let us also assume that the collecting electrode is surrounded by an appropriate guard electrode so that the electric field is practically uniform up to the boundary of the sensitive volume. Take as a frame of reference a Cartesian coordinate system with its origin on the positive electrode and its x-axis in the direction of the electric field (Fig. 3.4). Under equilibrium conditions the number densities of the ions, n_p and n_n, are independent of time at any given distance, and therefore a function of position, x, only.

As mentioned earlier, unless the electric field is very weak the motion of ions by diffusion is insignificant compared to that under the influence of the electric field. This can be easily illustrated by the fol-

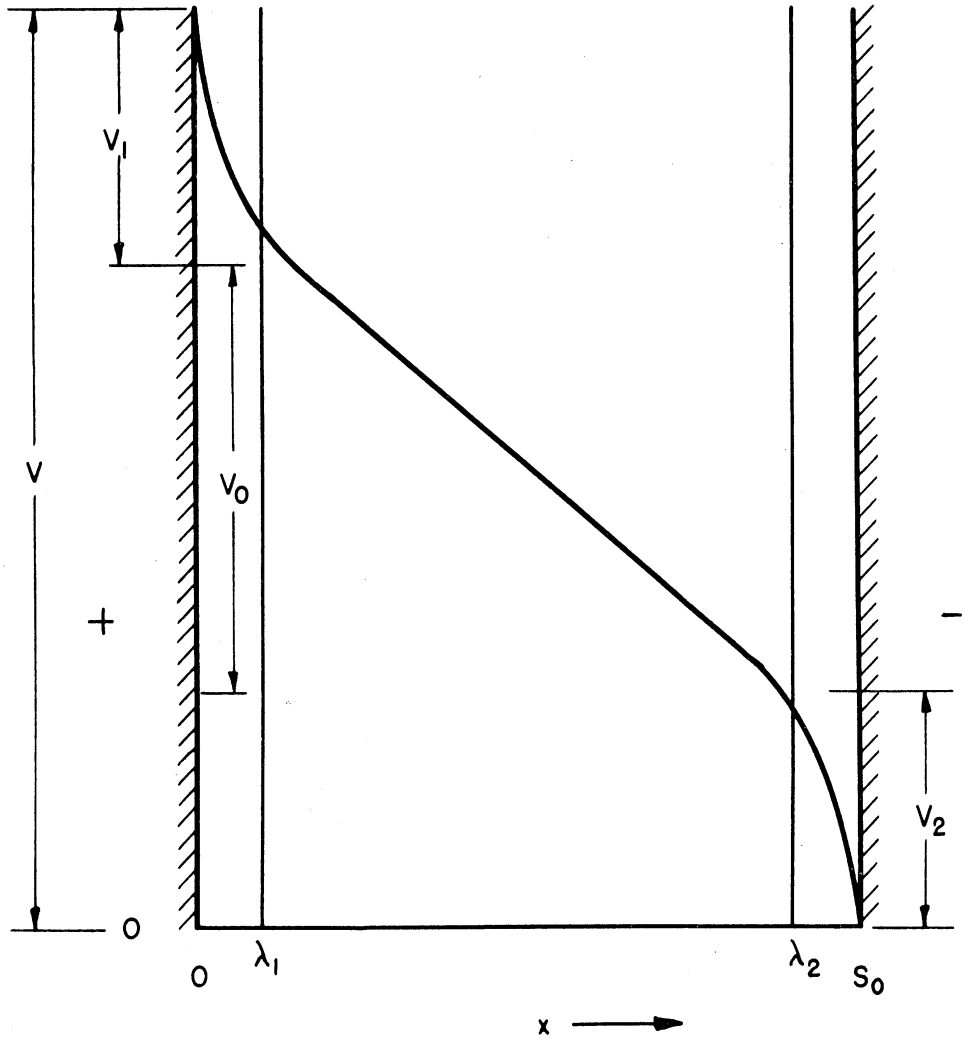

Fig. 3.4. The potential distribution in planar configuration.

lowing example. Consider the positive ions in a planar configuration in which the total current density is given by

$$J_p = q_e \mu_p \left[n_p E_x - V_T \frac{dn_p}{dx} \right] , \qquad (3.31)$$

where E_x is the electric field component in the x direction, which equals $(- dV/dx)$. As a first approximation one can put $E_x = - V_o/s_o$ and dn_p/dx as $(n_p)_o/s_o$, where s_o and V_o are the distance and potential difference between the plates, respectively, and $(n_p)_o$ the maximum number density of positive ions near the negative plate. Substituting this in the above formula gives

$$J_p \cong q_e \mu_p (n_p)_o \frac{V_o - V_T}{s_o} . \qquad (3.32)$$

The kinetic temperature, V_T, at normal temperatures is of the order of 10^{-2} volt, whereas the potential difference, V_o, in typical gauges is usually higher than 30 volts. Therefore it is clear that the diffusive contribution can be omitted with no appreciable error in the current which becomes almost completely due to conduction contribution.

Since complete attachment is assumed, all electrons cling to neutral molecules immediately after their generation and thus the rate of attachment will be equal to that of ion production, i.e., a = g. Hence, under equilibrium conditions, the gaseous conduction in a planar gauge is governed by the following basic equations:

$$\frac{dE_x}{dx} = \frac{q_e}{\epsilon_o} (n_p - n_n) , \qquad (3.33)$$

$$\mu_p \frac{dn_p E_x}{dx} = g - \rho_i n_p n_n \quad , \tag{3.34}$$

$$-\mu_n \frac{dn_n E_x}{dx} = g - \rho_i n_n n_p \quad , \tag{3.35}$$

$$J = q_e E_x (\mu_p n_p + \mu_n n_n) \quad , \tag{3.36}$$

where the ionic mobilities, μ_p and μ_n, are considered constant at all points of the field.

3.4.2. Derivation of Current-Pressure Relation.—In the derivation of the current-pressure characteristic for a planar radioactive ionization gauge, one needs first to determine the electric field distribution in the ionized gas between the two parallel electrodes. Subsequently, an expression for the current will be developed from the equation of the total voltage resulting from the integration of electric field across the distance between the plates. Thus to determine the distribution of electric field inside the gap one proceeds as follows. From Eqs. (3.33) and (3.36), one gets

$$q_e n_p = \frac{1}{\mu_p + \mu_n} \left[\frac{J}{E_x} + \epsilon_o \mu_n \frac{dE_x}{dx} \right] \quad , \tag{3.37}$$

and

$$q_e n_n = \frac{1}{\mu_p + \mu_n} \left[\frac{J}{E_x} - \epsilon_o \mu_p \frac{dE_x}{dx} \right] \quad . \tag{3.38}$$

Multiplying Eq. (3.33) by E_x and substituting in the sum of Eqs. (3.34) and (3.35), the following differential equation is obtained, governing the process:

$$\frac{d^2 E_x^2}{dx^2} = \frac{2q_e}{\epsilon_o} [g - \rho_i n_p n_n] \left(\frac{1}{\mu_p} + \frac{1}{\mu_n} \right) \quad . \tag{3.39}$$

From this equation, $(d^2E_x^2)/dx^2$ always has the same sign as $(g - \rho_i n_p n_n)$, since the mobilities are always positive quantities. Inserting into Eq. (3.39) the values of n_p and n_n given by (3.37) and (3.38) yields[42,43]

$$\frac{d^2E_x^2}{dx^2} = \frac{2q_e}{\epsilon_o}\left(\frac{1}{\mu_p} + \frac{1}{\mu_n}\right)\left[g - \frac{\rho_i}{q^2(\mu_p+\mu_n)^2E_x^2}\left(J + \frac{\mu_p\epsilon_o}{2}\frac{dE_x^2}{dx}\right)\left(J - \frac{\mu_n\epsilon_o}{2}\frac{dE_x^2}{dx}\right)\right] . \tag{3.40}$$

As yet no general solution of this differential equation has been obtained except when g is constant and $\mu_p = \mu_n$. Particular solutions, however, have been worked out under special conditions[44,45] such as in the study of currents near saturation assuming equal mobilities, $\mu_p = \mu_n = \mu$, and under particular values of pressure, chosen to make $(\rho_i\epsilon_o)/q_e\mu$ have special values.

For constant values of g and equal ionic mobilities, $\mu_p = \mu_n = \mu$, Eq. (3.40) has a general solution which can be found by changing variables. Putting $E_x^2 = y$ and $dy/dx = W$, in Eq. (3.40), one gets

$$W\frac{dW}{dy} = \frac{4q_e}{\epsilon_o\mu}\left\{g - \frac{\rho_i}{4q_e^2\mu^2 y}\left(J^2 - \frac{\mu^2\epsilon_o^2}{4}W^2\right)\right\} . \tag{3.41}$$

Integrating this gives

$$\frac{\mu^2\epsilon_o^2}{4}W^2 - J^2 = \frac{2q_e g \mu \epsilon_o}{1 - \frac{\rho\epsilon_o}{2q_e\mu}}y + C\,y^{\frac{\rho\epsilon_o}{2q_e\mu}} , \tag{3.42}$$

where C is a constant of integration.

From this relation one can determine the ratio of the electric field intensity midway between the plates, E_o, to the field intensity near the plates, E. Since $\mu_p = \mu_n$, the field is symmetrical and midway between the

plates $dE/dx = W = 0$ (Fig. 3.5). If the net charge between the electrodes is zero in the center, d^2E/dx^2 will vanish there too. Hence from (3.41) and (3.42),

$$E_o^2 = \frac{\rho J^2}{4q_e^2 g \mu^2} \tag{3.43}$$

and

$$-E_o^2 \frac{4q_e^2 g \mu^2}{\rho} = \left(1 - \frac{\rho\epsilon_o}{2q_e \mu}\right) C E_o^{\frac{\rho\epsilon_o}{q_e\mu}} \tag{3.44}$$

At the positive plate, $n_p = 0$, as ions are repelled from it and none is created beyond its boundary to replace those that move away. For similar reasons $n_n = 0$ at the negative plate. Hence at either plate $n_p n_n = 0$, and recombination does not occur. But, in general, the solution gives

$$n_p n_n = \frac{1}{4q_e^2 \mu^2 E_x^2}\left(J^2 - \frac{\mu^2\epsilon_o^2}{4} W^2\right) ; \tag{3.45}$$

hence if E_1 is the field strength at either plate, we have

$$-E_1 (2q_e g \mu \epsilon_o) = \left(1 - \frac{\rho \epsilon_o}{2q_e\mu}\right) C E_1^{\frac{\rho\epsilon_o}{q_e\mu}} . \tag{3.46}$$

Hence from Eqs. (3.44) and (3.46) and after rearranging,

$$\left(\frac{E_1}{E_o}\right)^2 = \beta_o^{\frac{\beta_o}{\beta_o - 1}} , \tag{3.47}$$

where $\beta_o = (2q_e\mu)/(\rho\epsilon_o)$, a dimensionless parameter. One notices from this equation that E_o is never greater than E_1, for $\beta_o^{\beta_o/(1-\beta_o)}$ diminishes from unity to zero as β_o increases from zero to infinity. Again, since β_o depends on μ/ρ and is independent of either g or J, the ratio of the electric intensities does not depend on either the intensity of ionization or the current between the electrodes. At low pressures

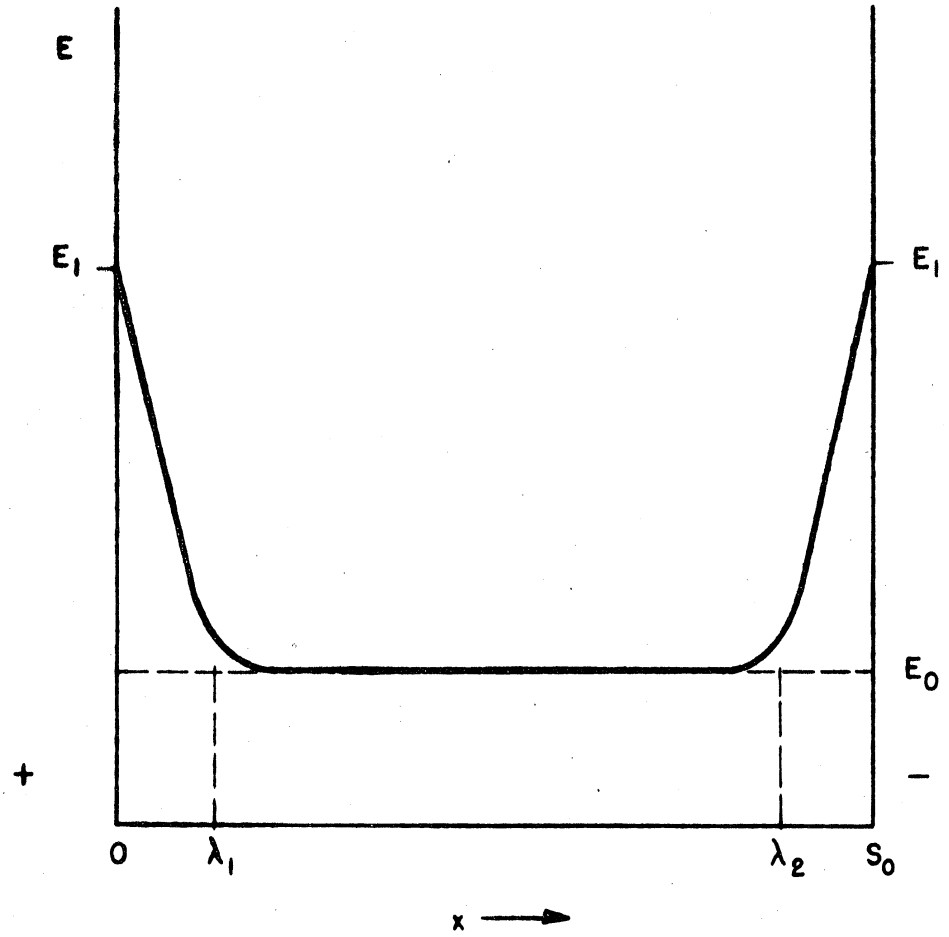

Fig. 3.5. Variation of the electric field E across the gap as modified by space-charge effects near the plates.

β_0 becomes large and under such conditions $E_1/E_0 = \sqrt{\beta_0}$, approximately.

Experiments on the distribution of electric field between the electrodes showed that, when the current is small, the regions where E_1 differs appreciably from E_0 are confined to two layers near the plates of thicknesses λ_1 and λ_2. Variation of the field E between the electrodes is illustrated in Fig. 3.5, where the negative and positive ions have the same mobility. The values of λ can be roughly evaluated in the following manner. At the coundary of the layer next to the electrode there are as many positive as negative ions per unit volume, and since the velocities of the ions are the same, half the current must be carried by the positive and half by the negative ions. Thus if J is the total current density and q_e the charge on an ion, $J/(2q_e)$ positive ions must cross the area of a plane through the boundary point in unit time, and these can only come from the quantity g created in the volume of unit area and λ meters long. This makes $g\lambda = J/(2q_e)$, so that

$$\lambda = \frac{J}{2q_e g} \quad . \tag{3.48}$$

Since at the electrodes, $n_p n_n = 0$, the volume ion-ion recombination is negligible, and the field E_1 is therefore produced by the space charge of positive ions at the cathode and of negative ions at the anode. The corresponding potential distribution is shown in Fig. 3.4, where V_1 and V_2 are the potential drops near the anode and cathode, respectively, V_0, the uniform potential drop in the central portion of the gap, and V is the anode potential above the cathode at ground. In the middle region,

between λ_1 and λ_2, where the field is uniform, E_o, $n_p n_n$ has a significant value, and recombination is occurring, presumably at a rate just to compensate for g, so that the density remains constant and n_p equals n_n. Thus in the central portion of the gap

$$n_p = n_n = n_o = \sqrt{g/\rho} \tag{3.49}$$

and

$$E_o = \frac{J}{2q_e\mu}\sqrt{\rho/g} \quad . \tag{3.50}$$

Let us now determine the total current density between the electrodes. First consider the state of things near the positive electrode between x = 0 and x = λ, where $\lambda = J/(2q_e g)$. Since there is no recombination in this region, Eqs. (3.33), (3.34), and (3.35) become

$$\frac{dE_x}{dx} = \frac{q_e}{\epsilon_o}(n_p - n_n) \quad , \tag{3.51}$$

$$\mu \frac{d}{dx}(n_p E_x) = g \quad , \tag{3.52}$$

$$-\mu \frac{d}{dx}(n_n E_x) = g \quad . \tag{3.53}$$

If g is uniform and assuming no positive ions near the anode, i.e., n_p = 0 when x = 0, then integration gives

$$\mu\, n_p\, E_x = gx \quad , \tag{3.54}$$

and

$$\mu\, n_n\, E_x = \frac{J}{q_e} - gx \quad . \tag{3.55}$$

Substituting these values for n_p, n_n in Poisson's equation,

$$E_x \frac{dE_x}{dx} = \frac{q_e}{\mu\epsilon_o}\left[2gx - \frac{J}{q_e}\right]$$

or

$$E_x^2 = \frac{2q_e}{\mu\epsilon_o}\left[gx^2 - \frac{J}{q_e}x\right] + C_1 \quad , \tag{3.56}$$

where C_1 is a constant to be determined from the condition that when $x = \lambda = J/(2q_e g)$, $E_x = E_o$, where

$$E_o^2 = -\frac{J^2}{4q_e^2\mu^2} \quad . \tag{3.57}$$

Substitution in Eq. (3.56)

$$C_1 = E_o^2 (1 + \beta_o)$$

where

$$\beta_o = \frac{2q_e\mu}{\rho\,\epsilon_o}$$

as before.

The fall of potential across the layer next to the positive electrode is

$$V_p = -\int_o^\lambda E_x\, dx \quad . \tag{3.58}$$

Substituting the value of E_x given by Eq. (3.56) and integrating,

$$V_p = \frac{E_o\lambda}{2}\left\{\sqrt{1+\beta_o} + \frac{1}{\sqrt{\beta_o}} \ln\left(\sqrt{\beta_o} + \sqrt{1+\beta_o}\right)\right\} \quad . \tag{3.59}$$

Also, the potential rise next to the negative electrode is

$$V_n = \frac{E_o\lambda}{2}\left\{\sqrt{1+\beta_o} + \frac{1}{\sqrt{\beta_o}} \ln\left(\sqrt{\beta_o} + \sqrt{1+\beta_o}\right)\right\} \quad . \tag{3.60}$$

The potential drop due to the uniform field in the space between the layers is

$$V_o = E_o\,(s_o - 2\lambda) \quad , \tag{3.61}$$

where s_o is distance between the two electrodes. The total voltage drop, V, between the electrodes is made up of the sum of the three already determined expressions (3.59-3.61). Adding all three expressions yields

$$V = E_o\lambda\left\{\sqrt{1+\beta_o} + \frac{1}{\sqrt{\beta_o}} \ln\left(\sqrt{\beta_o} + \sqrt{1+\beta_o}\right)\right\} + E_o(s_o - 2\lambda) \quad . \quad (3.62)$$

Substituting for E_o and λ their values, and rearranging,

$$V = AJ^2 + BJ \quad , \quad (3.63)$$

where

$$A = \sqrt{\rho/g}\, \frac{1}{4q_e^2 g\mu}\, \Psi(\beta_o) \quad ,$$

$$B = \sqrt{\rho/g}\, \frac{s_o}{2q_e\mu} \quad ,$$

$$\Psi(\beta_o) = \sqrt{1+\beta_o} + \frac{1}{\sqrt{\beta_o}} \ln\left(\sqrt{\beta_o} + \sqrt{1+\beta_o}\right) - 2 \quad .$$

The solution of Eq. (3.63) is given by

$$J = \left[\left(\frac{B}{2A}\right)^2 + \frac{V}{A}\right]^{1/2} - \frac{B}{2A} \quad . \quad (3.64)$$

On substituting the values of B/2A and V/A in Eq. (3.64), one finds

$$J = \frac{b\, J_m}{1 + \sqrt{1 + b\Psi(\beta_o)}} \quad , \quad (3.65)$$

where J_m = saturation current density = $q_e g s_o$, and

$$b = \frac{4\mu V}{s_o^2 \sqrt{\rho g}} \quad .$$

As seen from Eq. (3.65) above, the expression for the current density in the ionized gas between the two electrodes involves a host of different parameters. Some of these are characteristic of the gas involved, such

as the rate of ion production, g, the coefficient of recombination, ρ, or the mobility μ. Others are function of the geometry, and external agents such as the applied voltage.

3.5. COMPUTATION OF CURRENT-PRESSURE CHARACTERISTICS

For the sake of comparison of the theoretical results with the corresponding experimental results later, it is necessary to evaluate the collected ion current, J, as given by Eq. (3.65). One has first to determine the numerical expressions for the saturation current, J_m, and the dimensionless parameters b and β_o.

The saturation current, J_m, is directly proportional to the gas density and the effective ionized volume of the gauge; in the case of the planar gauge, $J_m = q_e g s_o$. The number of ion pairs produced in a unit volume per second, g, was obtained by measuring the saturation current experimentally and use of the above expression. This gave

$$g = 10^{16} \frac{P}{T} \text{ ion pairs per } m^3 \text{ per sec} \quad , \tag{3.66}$$

where P is the pressure in millibars and T, the temperature in degrees Kelvin. Consequently the saturation current density is determined by

$$J_m = q_e g s_o = 1.6 \times 10^{-3} \frac{P s_o}{T} \text{ amp/m}^2 \quad , \tag{3.67}$$

where s_o is the distance between the electrodes in meters.

The ionic mobility in air, according to Langevin (see Chapter II), can be put in the form

$$\mu = 9.35 \times 10^{-4} \frac{T}{P} \frac{(\text{meters})^2}{\text{volt-second}} \quad . \tag{3.68}$$

Also, the recombination coefficient of ions in air in the pressure range of interest can be expressed as

$$\rho = 4.6 \times 10^{-12}\left(\frac{273}{T}\right)^{3/2} w(z) \qquad (3.69)$$

where

$$w(z) = 2w_o - w_o^2$$

$$w_o = 1 - \frac{2}{z}\left[1 - e^{-z}(z+1)\right]$$

and

$$z = \frac{2d_o}{\ell g}$$

$$= 9.47 \times 10^{-4}\left(1 + \frac{111.3}{T}\right)\left(\frac{273}{T}\right)^2 P \quad .$$

Hence the dimensionless parameters β_o and b can be determined by substituting the above values of μ and/or ρ in the following expressions:

$$\beta_o = 3.618 \times 10^{-8}\,\frac{\mu}{\rho}$$

and

$$b = 3.74 \times 10^{-11}\,\frac{V}{s_o^2\sqrt{\rho}}\left(\frac{T}{P}\right)^{3/2} \quad .$$

Knowing the values of β_o and b, one can readily compute any i-P curves for different temperatures, plate voltages, or spacings as illustrated below.

3.5.1. Variation of Output Current with Plate Voltage.—Figure 3.6 shows a set of calculated curves relating the output currents to pressure in a planar gauge, at room temperature, taken as 300°K, with g given the value 10^{16} P/T. These curves were calculated for different plate voltages; meanwhile the distance between the plates was held at $s_o = 1$ cm. By inspec-

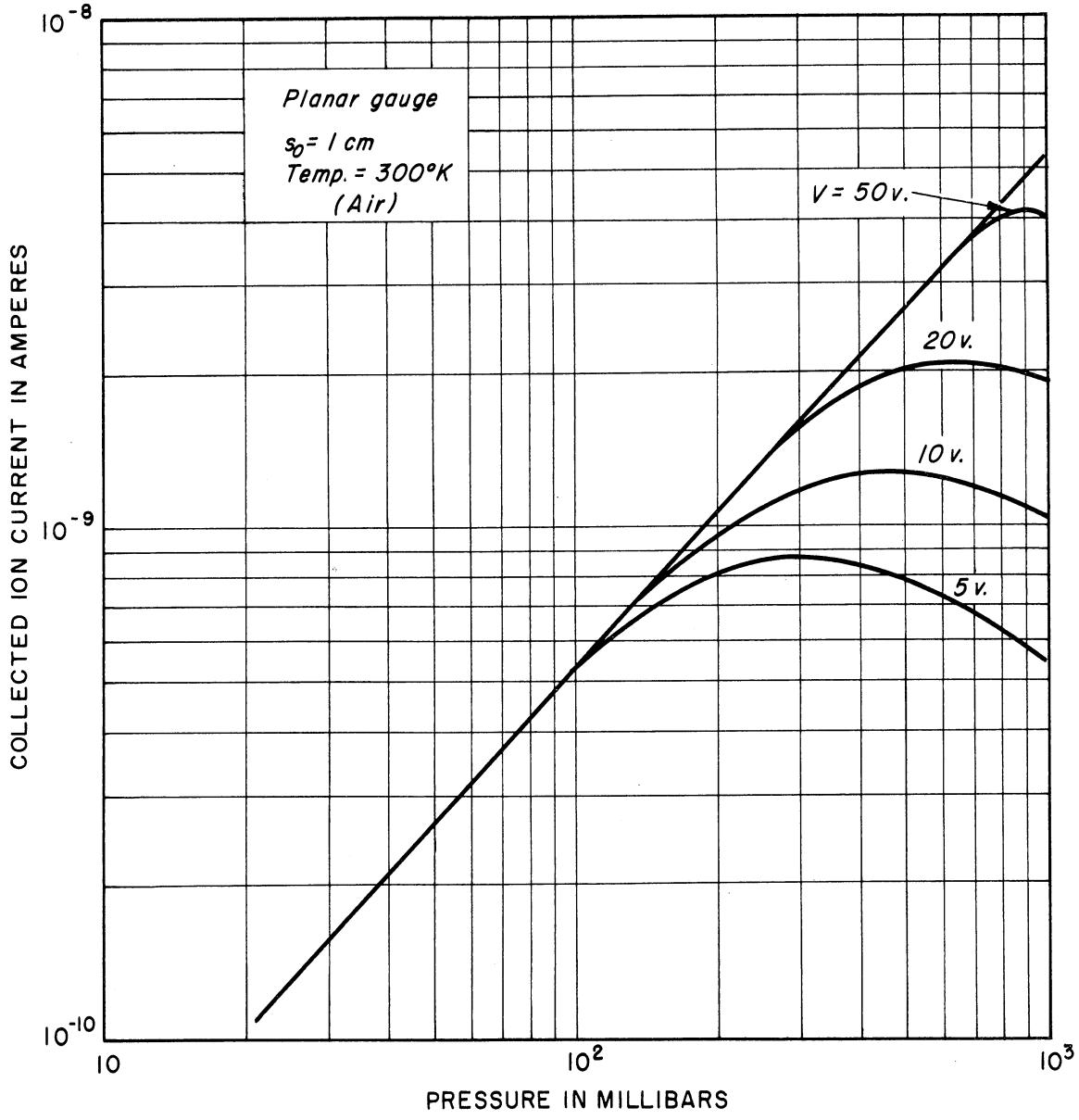

Fig. 3.6. Calculated current-pressure characteristics for different plate voltages—modified theory.

tion, one can generally divide each output characteristic into two distinct portions; a linear part in which almost all ionization products are collected, known as the saturation region, and a nonlinear portion where some of the ions are neutralized by recombination, resulting in a decrease of the net output current. The output increases and approaches the saturation value as the voltage is raised. From Figs. 3.6 and 3.7 one observes the similarity in shape of the calculated i-P curves and the experimentally observed curves; in both cases the linear part of the characteristic is readily extended to higher-pressure regions at higher plate voltages. As the applied voltage is increased, the sweeping of ions becomes more effective, thus lowering the chance of recombination between them, and hence producing more output current.

3.5.2. Effect of Temperature on the Gauge Output.—Figure 3.8 shows the output-pressure characteristic as computed for several temperatures, with the voltage and spacing between the plates kept unchanged. It is clear from the curves that in the linear region the output current is inversely proportional to temperature. This follows from the fact that the saturation current is directly proportional to the rate of ionization, g, which was given as*

$$g = \text{constant } (P/T) \quad . \tag{3.70}$$

*Experimental verifications indicated a slight deviation from the above relation which was based on the assumption that the ionization density is a function of the gas density alone. However, a better approximation for the rate of ionization may be given by $g = \text{constant } (P/T^n)$, where n is slightly higher than 1.

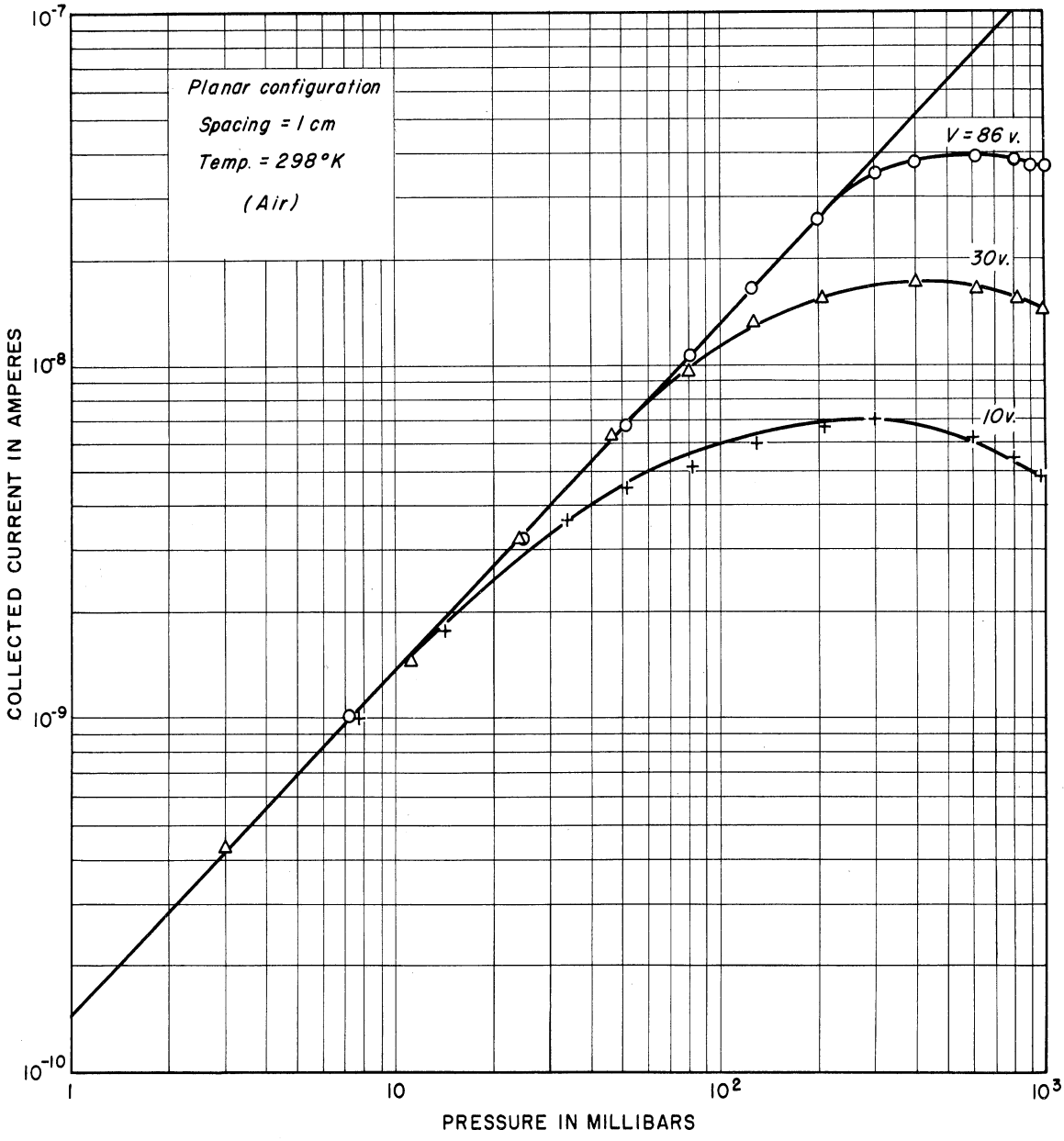

Fig. 3.7. Variation of i-P characteristics with plate voltage for an experimental planar gauge.

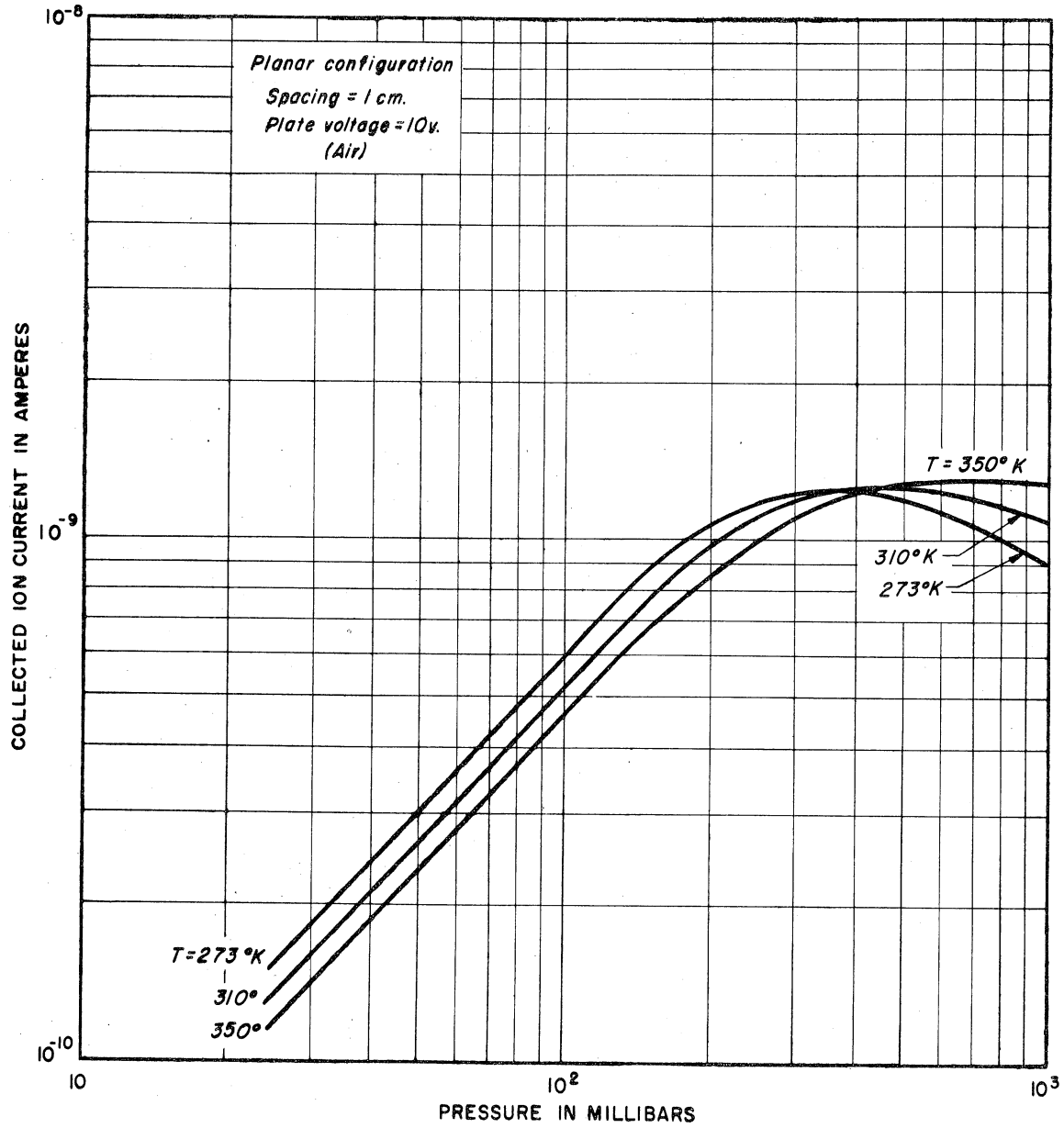

Fig. 3.8. Calculated i-P characteristics for different gas temperatures—modified theory.

On the other hand, the output current in the nonlinear zone increases with temperature for the same pressure. Such an increase results from the collection of more ions escaping recombination. The ions attain higher mobilities at higher temperatures, thus reducing the probability of recombination, and more ions are collected and therefore more output current is obtained.

3.5.3. The Effective Volume and Output Current.—The current output in a device of the kind here considered usually varies between 10^{-12} - 10^{-9} amp for a pressure range of from 10^{-1} to 100 mb. Because of the relative difficulty of handling such small currents, it is highly desirable to find some means by which one can achieve greater currents. One way to do so is to ionize larger volumes of gas. However, this method does not always increase the current output. This is illustrated by the computed examples shown in Fig. 3.9. In this case the ionized volume is changed by varying the distance, s_o, between the parallel plates. The proportionality of output current relative to volume is valid only when saturation currents are collected, that is, where the current-pressure characteristic is linear. The degree of proportionality diminishes, however, as the characteristic falls in the nonlinear portion, and it may even be reversed at the higher end of the pressure range. These analytical results are fairly analogous to the experimental observations, as seen in Fig. 3.10.

3.5.4. Correlation of Theoretical and Some of the Experimental Results.—In Fig. 3.11, the experimental results are compared to the corresponding computed curve for a particular case where the distance between

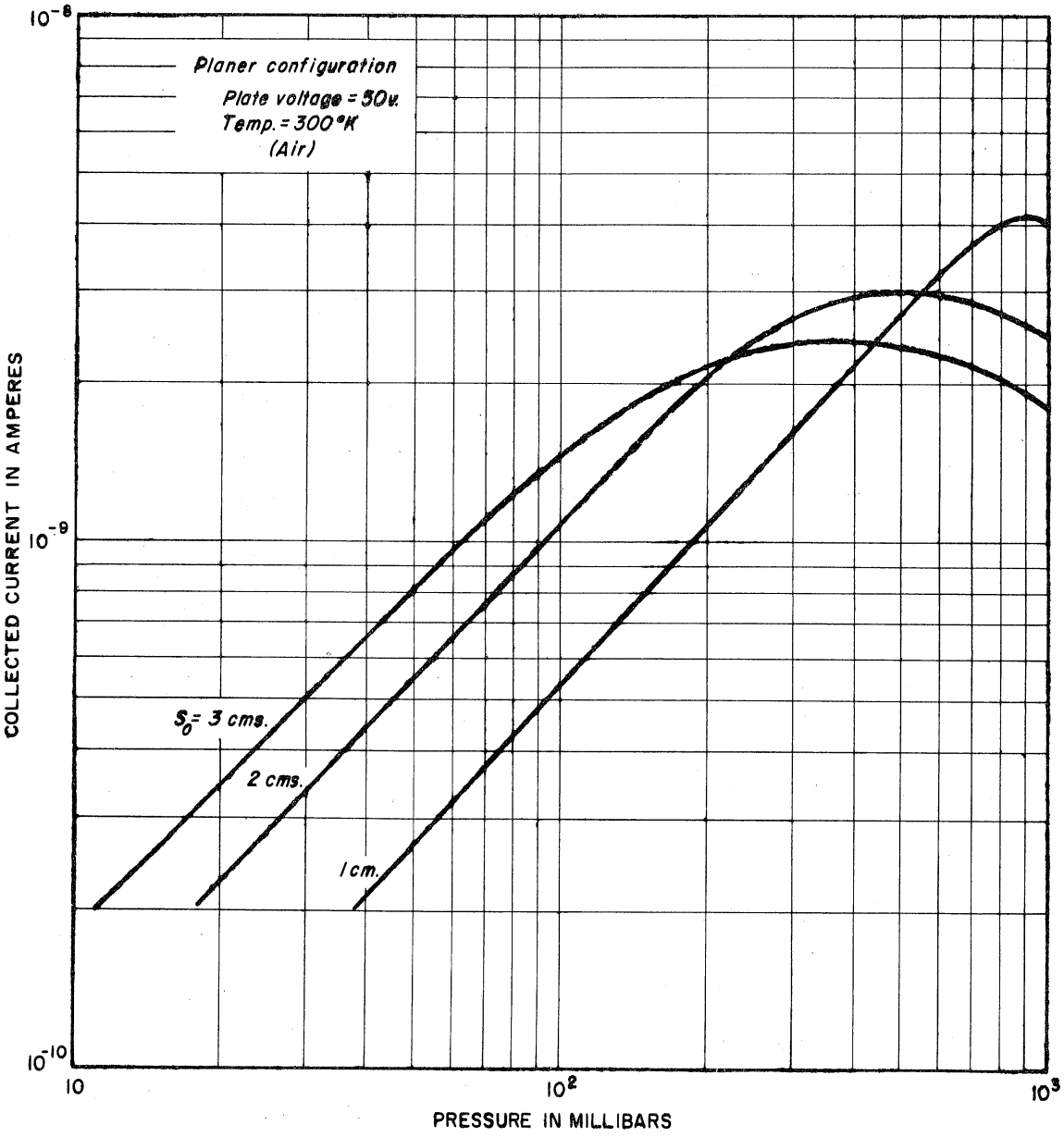

Fig. 3.9. Calculated i-P characteristics for different ionization volumes—modified theory.

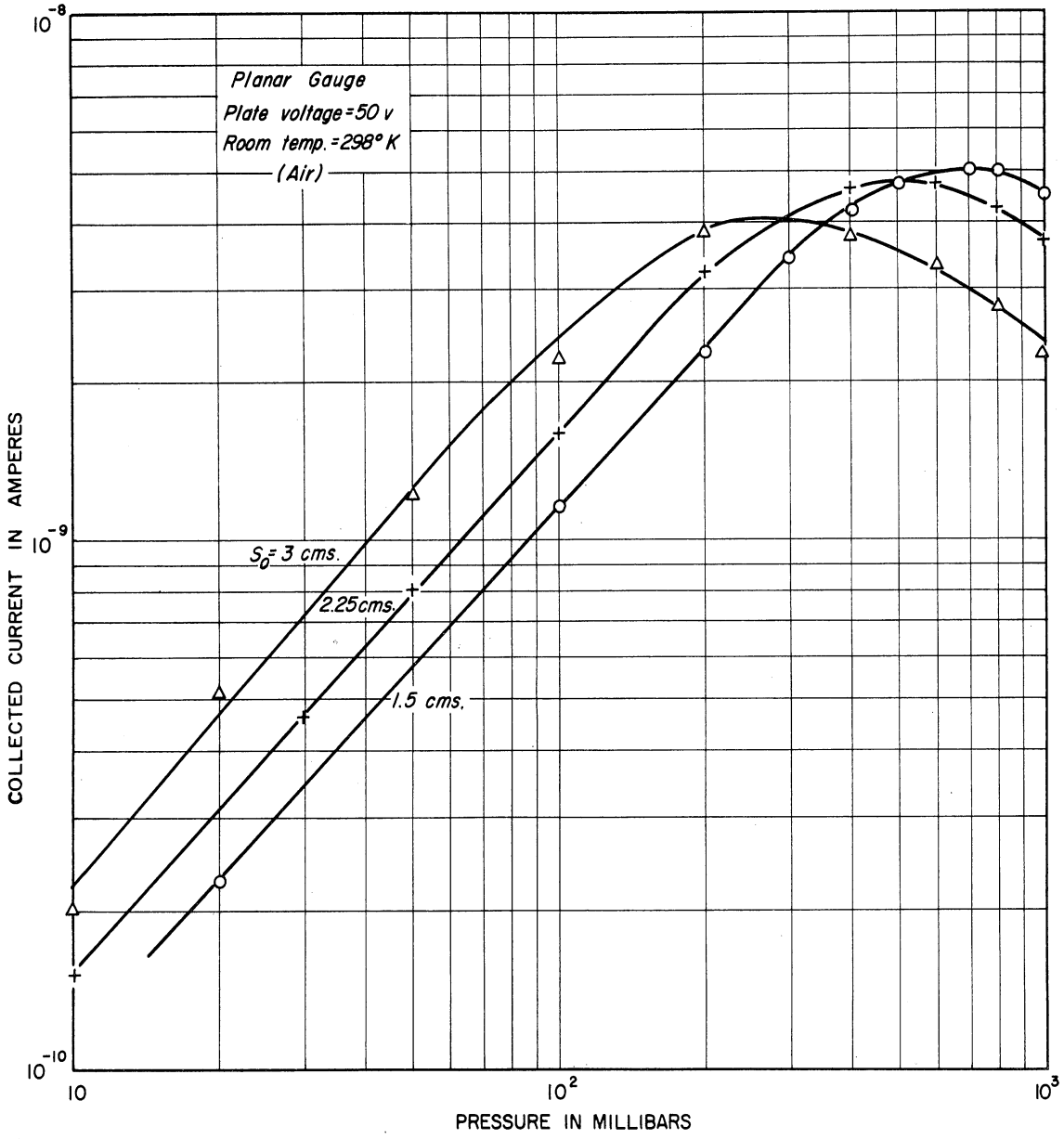

Fig. 3.10. Experimental i-P characteristics of a planar gauge using different plate spacings.

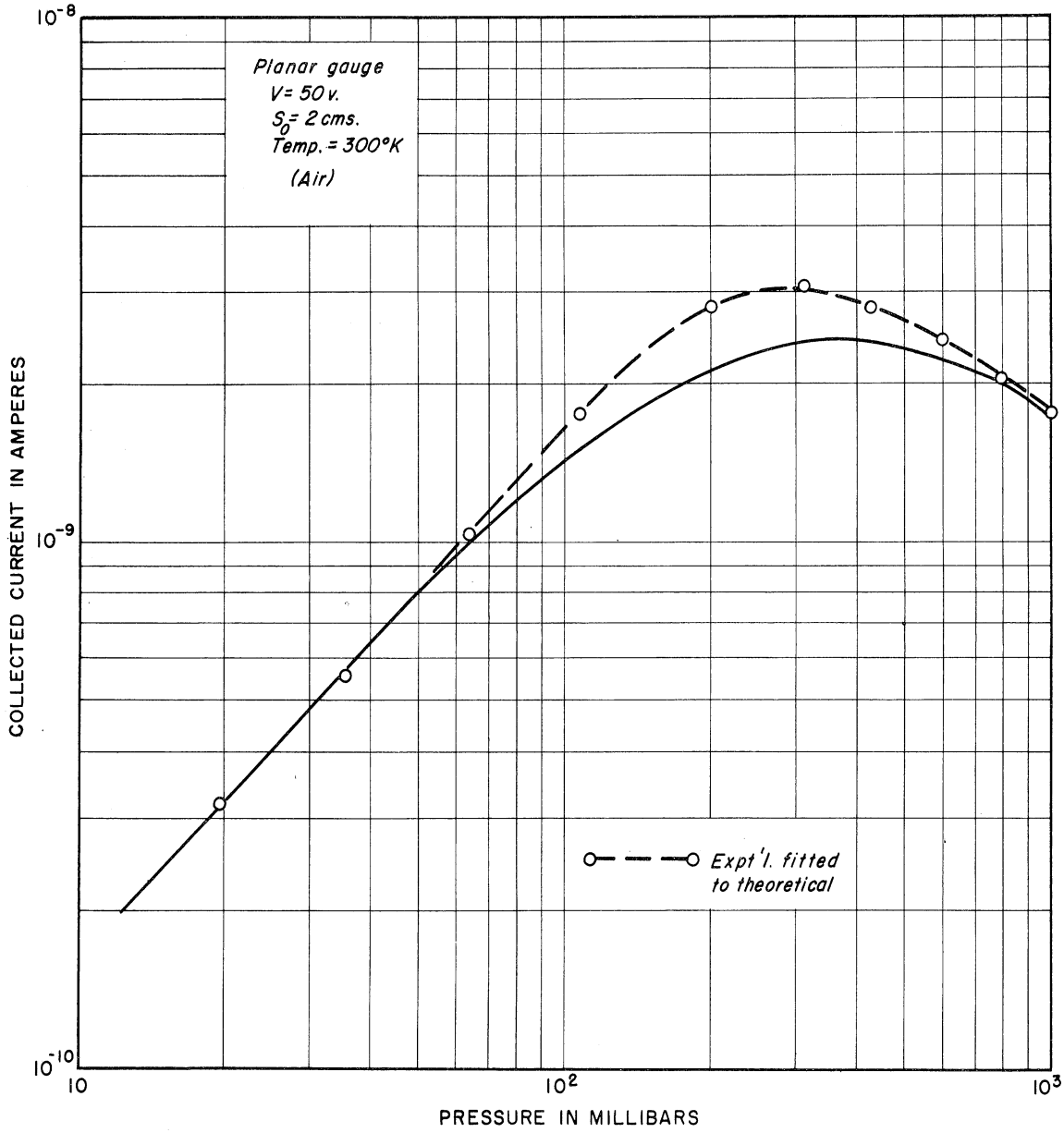

Fig. 3.11. Correlation between experimental and theoretical i-P curves. The experimental curve is adjusted to yield agreement in the linear portion—saturation current.

the plates was 3 cm, and a potential difference of 50 volts. The broken line represents the experimental curve adjusted for purposes of comparison to the theoretical curve such that both the experimental and calculated lines coincide in the linear region, where saturation prevails and presumably all ionization products are collected. In the nonlinear portion, we notice that, as the pressure goes up, the experimental characteristic departs from the theoretical, reaches a maximum, and then gradually drops until they meet at the higher end of pressure range. This departure may be explained in the following manner: the theoretical calculations were based on the assumption that both types of charge carriers were ions, i.e., complete attachment throughout the pressure range. This is not always true, since the negative charge carriers are, in fact, a mixture of free and attached electrons. The proportion of the attached electrons usually diminishes as the pressure decreases. But the major loss of charge is caused by ion-ion recombination; thus one expects a reduction in this loss when the pressure is decreased. As a consequence of this reduction in recombination, more charges will reach the electrodes and this is indicated by the increase in the output current. A modified solution considering the effect of electron attachment on the conduction current will be considered in the following section.

3.6. PLANAR-GAUGE THEORY—VARIABLE ATTACHMENT

3.6.1. Assumptions.—It was stated in Section 2.6 that certain molecules and atoms have the property of forming stable negative ions by the

capture of an additional electron. Thus it is highly improbable that a purely electronic current will pass through a gas composed of such molecules and atoms, and the entirely different properties of negative ions and electrons as current carriers make the attachment process of great importance in determining the conduction characteristics of the gas.

Therefore, in determining a current-pressure curve, one can assume that: (1) the mobilities of both negative and positive ions have the same value, (2) the negative charge carriers are both electrons and molecular or atomic ions; their proportion is a function of pressure, electric field and type of gas, (3) the electric field is sufficiently large for the diffusion currents to be negligible, (4) at either plate carriers with similar charges are repelled, and thus in the vicinity of either plate there is no recombination, and (5) electron-ion recombination is negligible.

Here again, following the same line adopted in the case of complete attachment, only the planar configuration will be considered.

3.6.2. Derivation of i-P Relation.—Proceeding in a manner similar to that of Section 3.4 in finding an i-P relation, the general equations governing the conduction in a planar ionization gauge are:

$$\frac{d}{dx}(\mu n_p E_x) = g - \rho\, n_n\, n_p \quad , \tag{3.71}$$

$$\frac{d}{dx}(\mu n_n E_x) = a - \rho\, n_n\, n_p \quad , \tag{3.72}$$

$$\frac{dE_x}{dx} = \frac{q}{\epsilon_o}(n_p - n_n - n_e) \quad . \tag{3.73}$$

with

a = the net rate of negative-ion formation and

n_e = the electronic density averaged throughout the volume.

Subtracting Eq. (3.72) from (3.71) and then integrating the result gives the total current density, J, due to flow of both ions and electrons:

$$J = J_e + q_e \mu E_x (n_p + n_n) \quad , \tag{3.74}$$

where J_e is the average electron-borne current density, $\cong q_e(g-a)s_o$, with s_o denoting the distance between the two plates. Thus the current due to the flow of ions alone is

$$J' = J - J_e = q_e \mu E_x (n_p + n_n) \quad . \tag{3.75}$$

The field is minimum, E'_{x_o}, at some point between the plates where

$$(n_p)_o = (n_n)_o + (n_e)_o \quad . \tag{3.76}$$

Due to the comparatively very high mobility of electrons, their concentration $(n_e)_o$ will be considerably smaller than that of negative ions, $(n_n)_o$. Thus one can again assume that at the minimum field point

$$(n_p)_o \cong (n_n)_o = n_o \quad . \tag{3.77}$$

Also at that point

$$\left(\frac{dn_p}{dx}\right)_o \cong \left(\frac{dn_n}{dx}\right)_o \quad . \tag{3.78}$$

Substituting these values in the continuity equations, one can get from the positive ion equation

$$\mu E_x \frac{dn_p}{dx} + \mu n_p \frac{dE_x}{dx} = g - \rho\, n_n\, n_p \quad ,$$

which becomes

$$\mu E'_{x_o} \left(\frac{dn_p}{dx}\right)_o = g - \rho\, n_o^2 \quad . \tag{3.79}$$

Similarly for the negative ions,

$$-\mu E'_{x_o} \left(\frac{dn_n}{dx}\right)_o = a - \rho\, n_o^2 \quad . \tag{3.80}$$

Adding Eqs. (3.79) and (3.80), and by the aid of Eq. (3.78), one gets

$$0 = (g+a) - 2\,\rho\, n_o^2$$

or

$$g' = \frac{g}{2}(1+\eta) = \rho\, n_o^2 \quad , \tag{3.81}$$

where g' is the average rate of negative-ion production and $\eta = a/g$, the negative-ion-formation factor.

The net ion-current density, J', is thus given by

$$J' = 2q_e\, \mu\, E'_{x_o}\, \eta_o \quad , \tag{3.82}$$

from which the minimum field is

$$E'_{x_o} = \frac{J'}{2q_e \mu n_o} \quad . \tag{3.83}$$

With Eq. (3.81), this could be written as

$$E'_{x_o} = \frac{J'}{2q_e \mu} \sqrt{\rho/g'} \quad . \tag{3.84}$$

The above equation has the same form as the corresponding one, (3.57), with J' and g' replacing J and g, respectively.

As in Section 3.4, it is assumed that there is no recombination in a layer of thickness λ_1 from the positive plate and one of λ_2 from the

negative plate (Fig. 3.12). Then the number of positive ions leaving the layer λ_1 per unit area per second is $J'/2q_e$. But the region furnishes a maximum number of positive ions $g\lambda_1$ per unit area in one second; thus

$$\lambda_1 = \frac{J'}{2q_e g} \quad . \tag{3.85}$$

In this region Eqs. (3.71), (3.72), and (3.73) become

$$\frac{dE_x}{dx} = \frac{q_e}{\epsilon_o}(n_p - n_n - n_e) \tag{3.86}$$

$$\frac{d}{dx}(\mu n_p E_x) = g \tag{3.87}$$

$$-\frac{d}{dx}(\mu n_n E_x) = a \tag{3.88}$$

Since g and a are constant under steady-state conditions, integration of Eq. (3.87) with $n_p = 0$ and $x = 0$, gives

$$\mu n_p E_x = gx \quad . \tag{3.89}$$

Similarly, for negative ions,

$$\mu n_n E_x = \frac{J'}{q_e} - ax \quad . \tag{3.90}$$

From Eqs. (3.86), (3.87), and (3.88), one gets:

$$\frac{dE_x^2}{dx} = \frac{2q_e}{\epsilon_o}\left[\frac{2g'x}{\mu} - \frac{J'}{q_e \mu}\right] . \tag{3.91}$$

Integration gives

$$E_x^2 = \frac{2q_e}{\epsilon_o \mu}\left[g'x^2 - \frac{J'x}{q_e}\right] + C_2 \quad , \tag{3.92}$$

where C_2 is a constant of integration whose value is determined by the

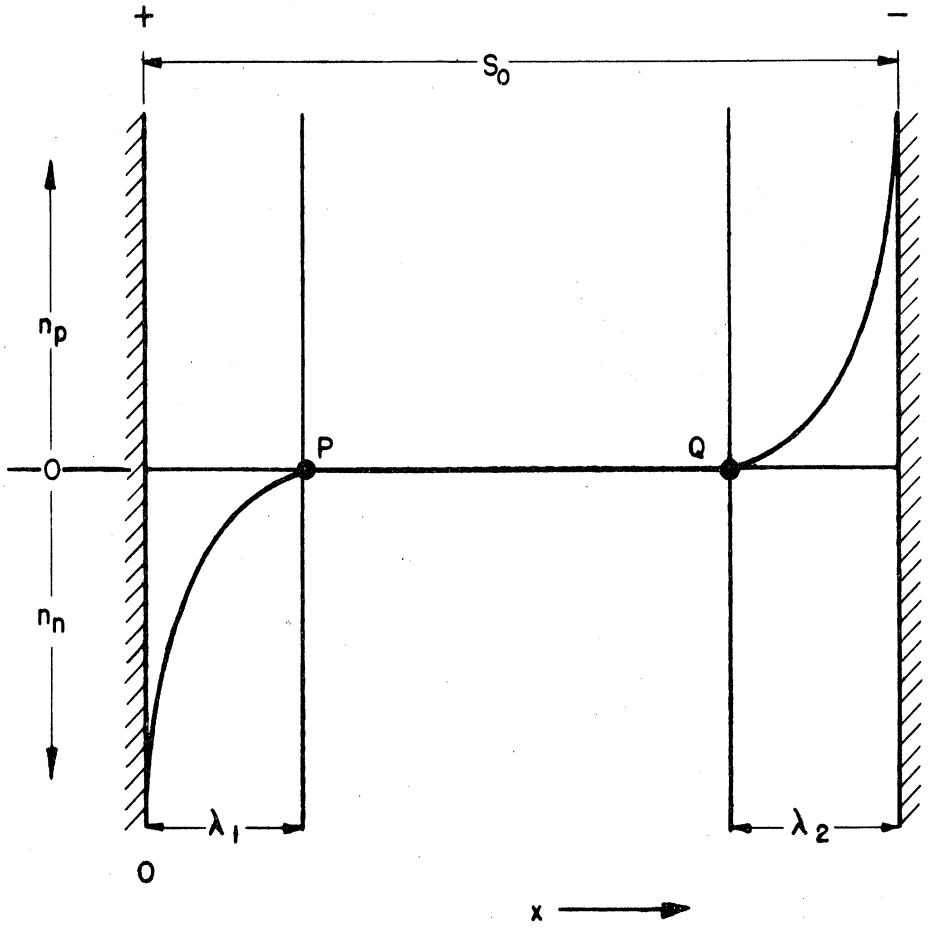

Fig. 3.12. Distribution of net ion density in a planar gauge.

boundary conditions when $x = \lambda_1 = J'/(2q_e g')$, the field $E_x = E'_{x_o}$. Thus

$$C_2 = E'^2_{x_o} (1+\beta_1) \quad ,$$

where

$$\beta_1 = \frac{\beta_o}{4} (1+\eta) (3-\eta) \quad ,$$

with

$$\beta_o = \frac{2q_e \mu}{\epsilon_o \rho}$$

as before.

Let us now consider the situation at the negative plate, i.e., between $x = s_o - \lambda_2$ and $x = s_o$, with $\lambda_2 = J'/2qa$. Here again recombination is negligible; therefore Eqs. (3.86), (3.87), and (3.88) are valid in this region. Since the negative ion density vanishes due to repulsion at the negative plate, $n_n = 0$ at $x = s_o$. Thus integration of Eq. (3.88) gives, for negative ions,

$$\mu n_n E_x = - a(x-s_o) \quad . \tag{3.93}$$

Similarly, for positive ions

$$\mu n_p E_x = g(x-s_o) + \frac{J'}{q_e} \quad . \tag{3.94}$$

Substituting in (3.86), and integrating,

$$E_x^2 = \frac{2q_e}{\epsilon_o \mu} \left[g'(x-s_o)^2 + \frac{J'}{q_e} (x-s_o) \right] + C_3 \quad , \tag{3.95}$$

where C_3 is to be determined from the condition that $E_x = E'_{x_o}$ at $x = s_o - \lambda_2$. Thus

$$C_3 = E'^2_{x_o} (1+\beta_2) \quad ,$$

where

$$\beta_2 = \frac{\beta_o}{4} (1 + 1/\eta) (3 - 1/\eta) \quad .$$

The voltage drop across the layer next to the positive electrode is

$$V_1 = - \int_o^{\lambda_1} E_x \, dx \quad . \tag{3.96}$$

Substituting the value of E_x given by (3.95),

$$V_1 = - \int_o^{\lambda_1} \sqrt{a_1 x^2 + b_1 x + c_1} \, dx \quad , \tag{3.97}$$

where

$$a_1 = \frac{q_e}{\epsilon_o \mu} (1+\eta)$$

$$b_1 = - \frac{2J'}{\epsilon_o \mu}$$

and

$$c_1 = E'^2_{x_o} (1+\beta_1) \quad .$$

Using Dwight's Tables of Integrals,[46] one can write the value of the voltage drop in this layer as

$$V_1 = \frac{1}{4a_1} \left[E_{x_1} \left(\frac{dE_x^2}{dx} \right)_o - E'_{x_o} \left(\frac{dE_x^2}{dx} \right)_{\lambda_1} \right] + \frac{4a_1 c_1 - b_1^2}{8a_1 \sqrt{a_1}} \ln \left| \frac{2E'_{x_o} \sqrt{a_1} + \left(\frac{dE_x^2}{dx} \right)_{\lambda_1}}{2E_{x_1} \sqrt{a_1} + \left(\frac{dE_x^2}{dx} \right)_o} \right| \quad , \tag{3.98}$$

where

$$\lambda_1 = \frac{J'}{2q_e g}$$

$$E'_{x_o} = \frac{J'}{q_e \mu} \sqrt{\frac{\rho}{2g(1+\eta)}}$$

$$E_{x_1} = E'_{x_o} \sqrt{1+\beta_1}$$

and from (3.91)

$$\left(\frac{dE_x^2}{dx}\right)_{x=o} = -\frac{2J'}{\epsilon_o \mu}$$

and

$$\left(\frac{dE_x^2}{dx}\right)_{x=\lambda_1} = -\frac{J'}{\epsilon_o \mu}(1-\eta) \quad .$$

Substitution of these values in the above expression for V_1 and then reducing gives

$$V_1 = \frac{E'_{x_o}\lambda_1}{1+\eta}\left[\sqrt{1+\beta_1} - \frac{1}{2}(1-\eta) + \frac{1 - \frac{\beta_o}{4}(1-\eta)^2}{\sqrt{\beta_o}} \ln \frac{1 - (1-\eta)\frac{\sqrt{\beta_o}}{2}}{\sqrt{1+\beta_1} - \sqrt{\beta_o}}\right] . \tag{3.99}$$

It may be interesting to note that when $\eta = 1$, β_1 becomes β_o, and thus Eq. (3.99) reduces to Eq. (3.59), the corresponding one for the case where complete attachment was assumed, viz., $\eta = 1$.

Similarly, the voltage drop in the layer next to the negative plate could be written in the form

$$V_2 = \frac{E'_{x_o}\lambda_2}{1+\frac{1}{\eta}}\left[\sqrt{1+\beta_2} - \frac{1-\frac{1}{\eta}}{2} + \frac{1 - \frac{\beta_o}{4}\left(1-\frac{1}{\eta}\right)^2}{\sqrt{\beta_o}} \ln \frac{1 - \left(1-\frac{1}{\eta}\right)\frac{\sqrt{\beta_o}}{2}}{\sqrt{1+\beta_2} - \sqrt{\beta_o}}\right] \tag{3.100}$$

This again reduces to (3.60) when $\eta = 1$. The potential drop in the middle region is determined by

$$V_o = -\int_{\lambda_1}^{s_o-\lambda_2} E_x \, dx \quad ,$$

which gives

$$V_o = E'_{x_o} (s_o-\lambda_1-\lambda_2) \quad . \tag{3.101}$$

The total voltage drop between the two plates is simply the sum of all three expressions above. Therefore, adding them up and simplifying, one gets

$$V = A'J'^2 + B'J' \tag{3.102}$$

where

$$A' = \frac{B'}{J_m(1+\eta)} \Psi(\beta_o,\eta)$$

$$B' = \frac{s_o}{2q_e\mu} \sqrt{\frac{2\rho}{g(1+\eta)}}$$

$$J_m = q_e g s_o \quad , \text{ saturation current density,}$$

and

$$\Psi(\beta_o,\eta) = \frac{1}{2}\left\{ \sqrt{1+\beta_1} + \sqrt{1+\beta_2} - \frac{\eta + 1/\eta}{2} - 3 \right.$$
$$+ \frac{1 - \frac{\beta_o}{4}(1-\eta)^2}{\sqrt{\beta_o}} \ln \frac{1 - (1-\eta)\frac{\sqrt{\beta_o}}{2}}{\sqrt{1+\beta_1} - \sqrt{\beta_o}}$$
$$\left. + \frac{1 - \frac{\beta_o}{4}\left(1 - \frac{1}{\eta}\right)^2}{\sqrt{\beta_o}} \ln \frac{1 - \left(1 - \frac{1}{\eta}\right)\frac{\sqrt{\beta_o}}{2}}{\sqrt{1+\beta_2} - \sqrt{\beta_o}} \right\} .$$

Solving Eq. (3.102) for the ionic current density, J', gives

$$J' = -\frac{B'}{2A'} + \sqrt{\left(\frac{B'}{2A'}\right)^2 + \frac{V}{A'}} \quad . \tag{3.103}$$

But

$$\frac{B'}{2A'} = \frac{J_m(1+\eta)}{2\Psi(\beta_o,\eta)}$$

$$\frac{V}{A'} = \frac{bJ_m^2}{4} \frac{(1+\eta)\sqrt{2(1+\eta)}}{\Psi(\beta_o,\eta)}$$

and

$$b = \frac{4\mu V}{s_o^2\sqrt{\rho g}} .$$

Substituting in (3.103) for B'/2A' and V/A' gives

$$J' = \frac{J_m(1+\eta)}{2\Psi(\beta_o,\eta)}\left[\sqrt{1 + \frac{2b\Psi(\beta_o,\eta)}{\sqrt{2(1+\eta)}}} - 1\right]$$

This could also be written

$$J' = \frac{bJ_m\sqrt{(1/2)(1+\eta)}}{1 + \sqrt{1 + b\Psi(\beta_o,\eta)\sqrt{2/(1+\eta)}}} . \qquad (3.104)$$

But

$$J' = J - J_e$$

$$= J - J_m(1-\eta) .$$

Hence the total output current will be:

$$J = J_m\left[\frac{b\sqrt{(1/2)(1+\eta)}}{1 + \sqrt{1 + b\Psi(\beta_o,\eta)\sqrt{2/(1+\eta)}}} + (1-\eta)\right] . \qquad (3.105)$$

Inspection of the above equation reveals its similarity to the corresponding one, Eq. (3.65), Section 3.4.2, for complete attachment, although the former is modified by the presence of the negative-ion-formation factor, η. Assuming different values of η will naturally produce different char-

acteristics; this is shown in Fig. 3.13, where the characteristic curve is calculated for air assuming complete attachment (the solid line), and partial attachment (the broken line) (see next section); the corresponding experimental curve is also shown.

3.6.3. Determination of the Negative-Ion-Formation Factor.—It is necessary to find a means to evaluate η. As stated in Section 3.3, the electron density, n_e, is governed by the continuity equation (3.22), viz.,

$$\frac{\partial n_e}{\partial t} = (g\text{-}a\text{-}r_e) + \frac{1}{q_e} \operatorname{div} \vec{J}_e \quad .$$

Under the same conditions assumed there, the above equation for a planar configuration becomes

$$\mu_e E_o \frac{dn_e}{dx} + (g\text{-}a) = 0 \qquad (3.106)$$

where E_o is the average electric field intensity, value V/s_o, with s_o and V as the distance and voltage applied between the two plates, respectively.

The rate of electron attachment, a, depends on the collision frequency between electrons and neutral gas molecules, z_e, the electron number density, n_e, and the probability of attachment, δ_e. Thus the negative ions are formed at the rate of

$$a = \delta_e z_e n_e \quad , \qquad (3.107)$$

where

$$z_e = \frac{\bar{c}_e}{\ell_e} = \frac{3q_e}{4m_e\mu_e} \quad .$$

On substituting in Eq. (3.106), one can determine the distribution of electron density by solving the following equation

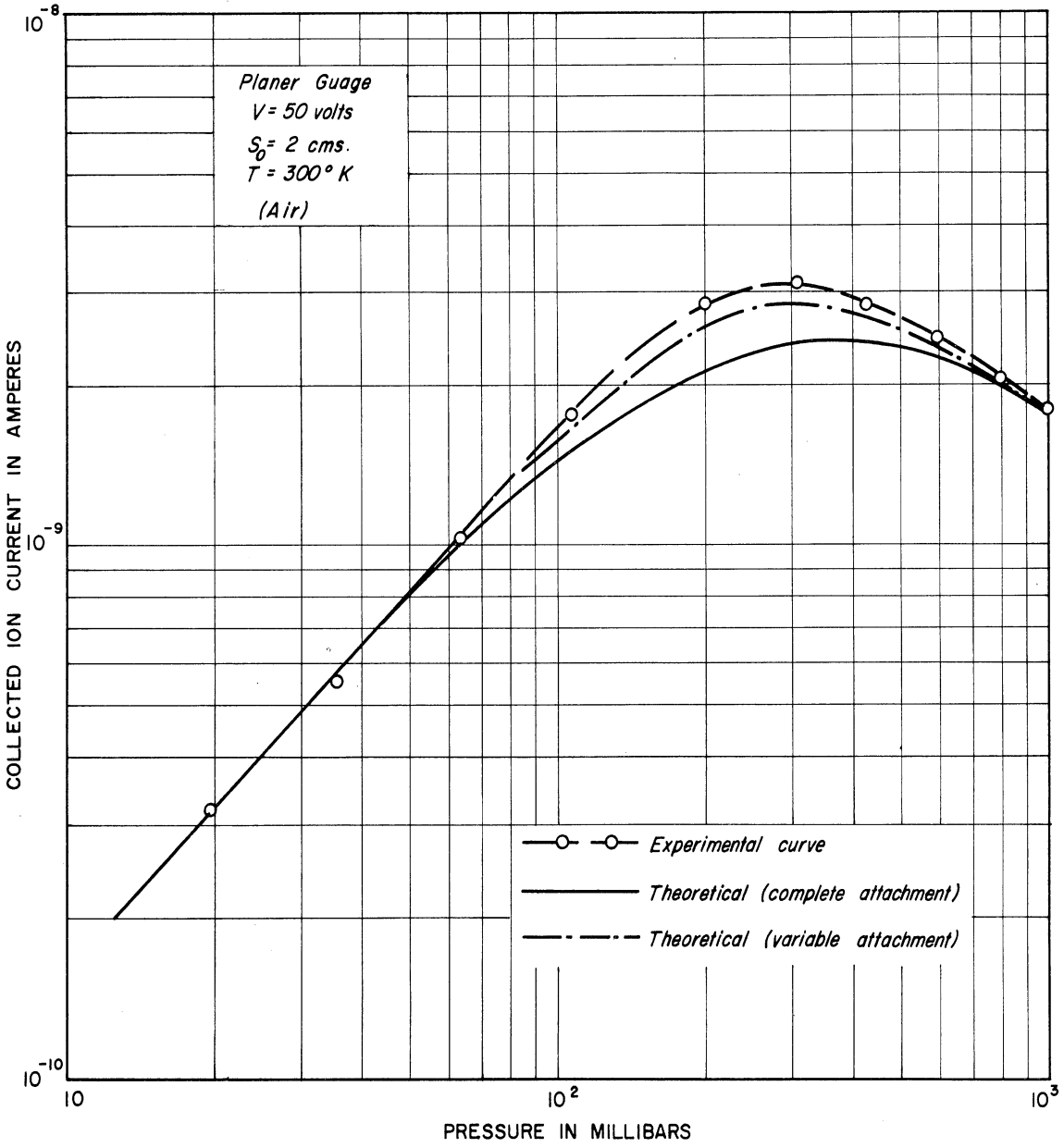

Fig. 3.13. Correlation between experimental and modified theoretical curves, assuming variable electron attachment.

$$\frac{dn_e}{dx} - \gamma' n + \frac{gs_o}{\mu_e V} = 0 \quad , \tag{3.108}$$

where

$$\gamma' = \frac{s_o z_e \delta_e}{\mu_e V} \quad .$$

If g is uniform and assuming no electrons near the cathode, i.e., $n_e = 0$ when $x = s_o$, then integration of Eq. (3.108) gives

$$n_e = \frac{gs_o}{\mu_e V \gamma'} \left[1 - e^{-\gamma'(s_o - x)} \right] \quad . \tag{3.109}$$

The average electron density, $\bar{n}_e$, is

$$\bar{n}_e = \frac{gs_o}{\mu_e V \gamma'} \left[1 - \frac{1}{\gamma' s_o} (1 - e^{-\gamma' s_o}) \right] \quad . \tag{3.110}$$

Substituting in Eq. (3.107) gives the average rate of negative ion formation

$$a = g \left[1 - \frac{1}{\gamma' s_o} (1 - e^{-\gamma' s_o}) \right] \quad . \tag{3.111}$$

Therefore, the attachment factor, $\eta = a/g$, will be given by

$$\eta = 1 - \frac{1}{\gamma} (1 - e^{-\gamma}) \quad , \tag{3.112}$$

where

$$\gamma = \frac{3q_e}{4m_e} \frac{\delta_e}{\mu_e^2} \frac{s_o^2}{V} \quad . \tag{3.113}$$

For reasons that will be discussed in Section 4.5.6 of the next chapter, Bloch and Bradbury's theoretical values of δ_e were utilized in evaluating γ above. The electron mobility, μ_e, was computed from the approximate relation, Eq. (2.16), based on Compton's derivation.

3.6.4. Interpretation of Some Numerical Examples.—In calculating

the i-P curves, as determined by Eq. (3.105), a method parallel to that adopted in Section 3.5 will be followed. Some of the parameters can be used here with the same values as employed there; then the earlier values are re-usable in Eq. (3.105). On the other hand, the negative-ion-formation factor, η, is a dimensionless parameter depending on two new quantities: the probability of attachment, δ_e, and the electronic mobility, μ_e. Both δ_e and μ_e are functions of the ratio of the field strength and pressure, E/P. Neither are the rate of ionization, g, and consequently the saturation current, $J_m = q_e g s_o$, the same as before, because in a mixture of gases the effective rate of ionization is the sum of the partial ionizations of the component gases, i.e.,

$$g_{mix} = \sum_{k}^{N} g_k f_k \quad , \tag{3.114}$$

where g_k and f_k are, respectively, the rate of ionization and molar fraction of the kth gas present in a mixture of N gases.

Let us first consider a mixture of nitrogen and oxygen. The average probability of attachment becomes

$$\bar{\delta}_e = \frac{\left(\delta_e \frac{f}{\ell_e}\right)_{O_2}}{\left(\frac{f}{\ell_e}\right)_{O_2} + \left(\frac{f}{\ell_e}\right)_{N_2}} \quad , \tag{3.115}$$

where $(f/\ell_e)_{O_2}$ is the molar fraction of oxygen divided by the corresponding electron mean free path and $(f/\ell_e)_{N_2}$ is the same quantity for nitrogen. But $(f)_{O_2} + (f)_{N_2} = 1$; hence the above attachment probability can be expressed by

$$\bar{\delta}_e = (\delta_e)_{O_2} \frac{1 - (f)_{N_2}}{1 - (f)_{N_2}\left[1 - \frac{(\ell_e)_{O_2}}{(\ell_e)_{N_2}}\right]} \quad . \qquad (3.116)$$

The experimental values for $(\delta_e)_{O_2}$ are given in Bradbury's[36] data for oxygen as a function of E/P (Fig. 2.12). The molar fraction, $(f)_{N_2}$, is considered constant for a given mixture throughout the pressure range.

Similarly, the effective rate of ionization is given by

$$g_{mix} = (gf)_{N_2} + (gf)_{O_2} \quad ,$$

which can be written

$$g_{mix} = (g)_{N_2}\left\{\frac{(g)_{O_2}}{(g)_{N_2}} + (f)_{N_2}\left[1 - \frac{(g)_{O_2}}{(g)_{N_2}}\right]\right\} . \qquad (3.117)$$

The above relation is empirically modified by Bortner and Hurst[47] in terms of the energy required to produce an ion pair, W_i, in the ith component gas. It can be written for a gas mixture as:

$$g_{mix} = A\left[\frac{1}{W_{O_2}} + F_{N_2}\left(\frac{1}{W_{N_2}} - \frac{1}{W_{O_2}}\right)\right] \quad , \qquad (3.118)$$

where A is a constant whose value depends on the temperature and density of the gas used as well as on the type and the average energy of the ionizing particles; W_{O_2} and W_{N_2} are the energies required to produce an ion pair in pure oxygen and nitrogen, respectively;

$$F_{N_2} = \frac{P_{N_2}}{P_{N_2} + a\, P_{O_2}}$$

is the effective molar fraction of nitrogen, with P_{N_2} and P_{O_2} as the partial pressures of nitrogen and oxygen, whereas a is a constant related to

the stopping powers of the gases present; it has been determined experimentally for different gas mixtures.[47] It has the value 1.06 for N_2 - O_2 mixtures.

Using the above relations in conjunction with Eq. (3.105), it was possible to determine the i-P curves for any mixture of oxygen and nitrogen. Some calculated examples are shown in Fig. 3.14. Striking new results appearing in this theoretical prediction are that:

(a) only one part in a hundred of oxygen is sufficient to upset the linearity of the i-P relation at high pressures;

(b) as the oxygen content is increased in proportion, the non-linear portion sinks rapidly until it reaches a minimum value at which the trend is reversed and a gradual increase in output sets in with higher oxygen proportions; and

(c) in the linear portion where saturation prevails, the current always increases with increasing proportions of oxygen.

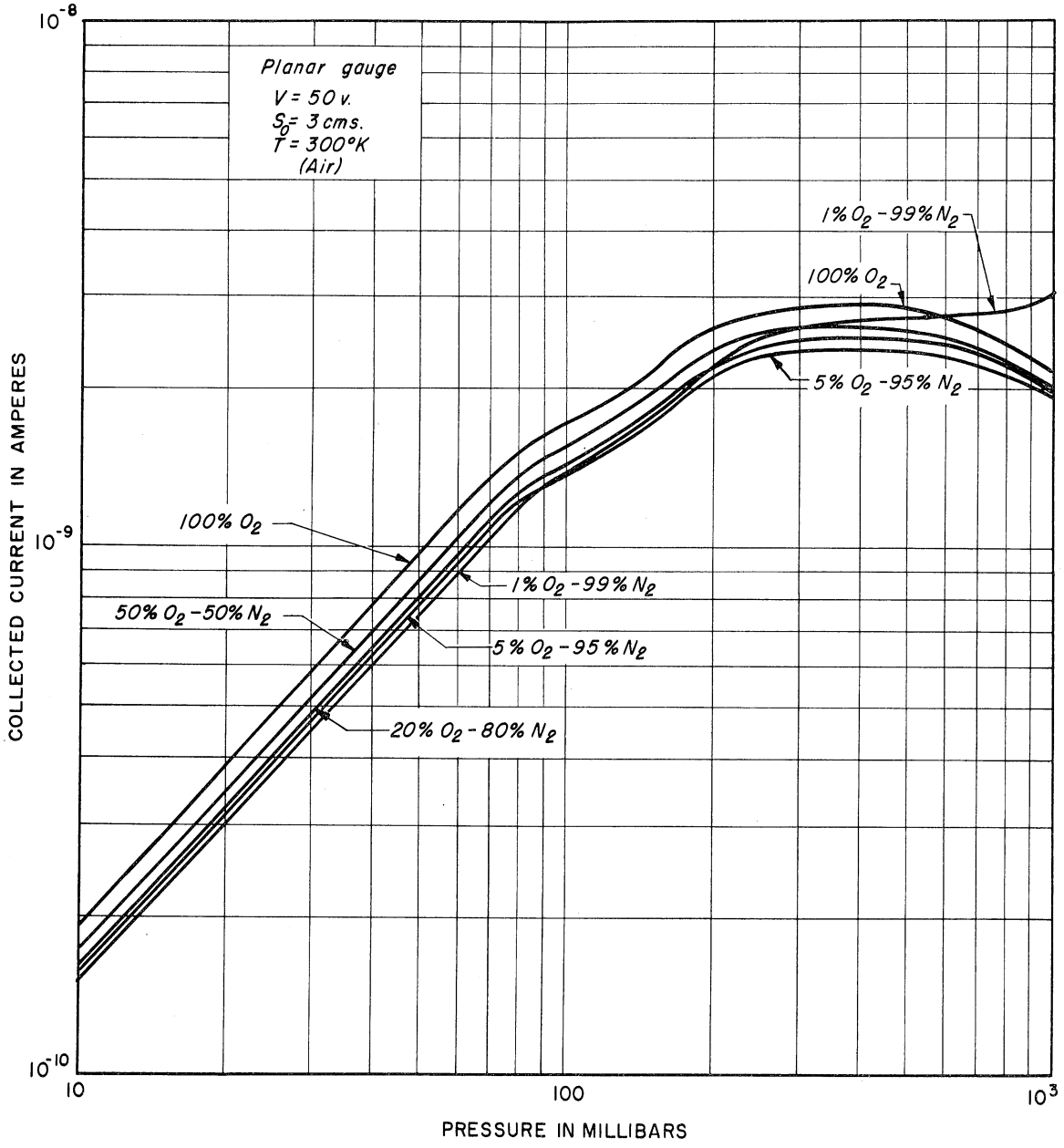

Fig. 3.14. Theoretical i-P curves for several mixtures of nitrogen and oxygen—variable attachment.

CHAPTER IV

EXPERIMENTAL CONSIDERATIONS

4.1. INTRODUCTION

The scope of experimental work which might be carried out on radioactive ionization gauges is almost unlimited. Examples of the many areas in which laboratory investigations could be made are:

1. The effect of the different configurations on the gauge characteristics.
2. The size of and the material used in the chamber's environmental envelope and electrodes.
3. The strength and type of the ionizing source.
4. Limitations imposed on the value of collecting voltages.
5. The effect of temperature on the rates of ionization, recombination, or electron attachment.
6. The hysteresis phenomenon, that is, failing of the rising-density curve to follow the immediately preceding falling-density curve.
7. Dark current.

In this work, however, we shall restrict ourselves to the study of only a few of the aspects which appear more important as needed, under the circumstances encountered in the technique of performing pressure measurements at high altitudes.

The construction and characteristics of a commercially known radioactive ionization gauge is briefly described, followed by a short discussion of the dark-current phenomenon. The major part of this chapter is devoted to investigating and comparing with theoretical prediction some of the probable causes of the hysteresis phenomenon. A number of other aspects are also discussed; a specially made planar radioactive ionization gauge was used in this work. Finally, as a result of the experience gained and better understanding of the different ionic processes in radioactive ionization gauges, two different types of gauge designs are described. In one of them, with radium as the ionizing source, the hysteresis is largely eliminated, whereas in the second, with a tritium source, the sensitivty of the gauge at low pressures is considerably increased while the early tendency toward a constant dark current is successfully pushed to a lower density.

4.2. CHARACTERISTICS OF NRC RADIOACTIVE IONIZATION GAUGE

The early work of this investigation was carried out using a NRC type 510 gauge.[5] This radioactive gauge has been known commercially as the "Alphatron,"* since the particles used there for ionization are alphas emitted from a radioactive material. The construction of the chamber of this particular model is schematically shown in Fig. 4.1.** It consists of a radioactive source (B), an ion collector (C), and an ion-

*Copyright, National Research Corporation.
**Courtesy of National Research Corpoation.

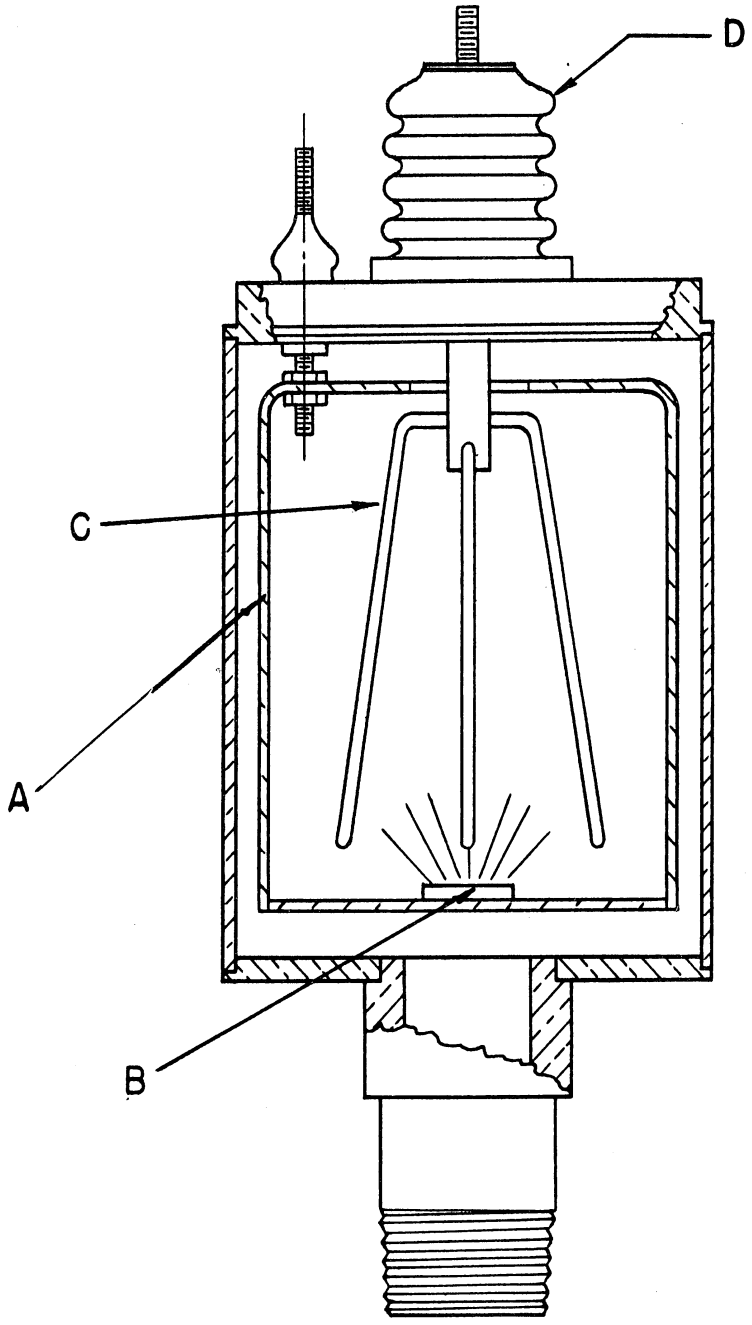

Fig. 4.1. Diagram of NRC Type No. 510 radioactive ionization gauge. (A) electrode, (B) radium source, (C) collector electrode, (D) feed-through insulator.

ization chamber (A) which acts as positive electrode in the polarizing field.

The radioactive source consists of a small plate 1 cm^2, one side of which is the active area made of a gold-radium alloy containing approximately 0.2 mg of radium. The plate is electroplated with a thin film of nickel which acts as a seal and thus enables retention of the first by-product, radon gas, and its subsequent decay products.

The ion collector electrode (C) is supported by the high-leakage-resistance feed-through insulator (D) and is connected to the electrometer tube of a d-c amplifier outside the vacuum chamber. A four-wire construction is used to shorten the ion collection distances and so to prevent excessive ion recombinations and consequent loss of output and linearity at high pressures.

The ionization chamber (A) is a cylinder closed at both ends having holes at each end for gas passage and for introduction of the collector electrode (C). Electrical connection and mechanical support are provided by three metal-to-glass seals soft-soldered to the vacuum-chamber bulkhead. The chamber is maintained at a positive potential to provide an electric field driving positive ions in the direction of electrode (C). A 45-volt battery is used between the electrode (A) and ground to create the necessary electric field for ion collection.

A Kiethley* electrometer was used to measure the output (ionization) current, and a typical i-P characteristic is shown in Fig. 4.2. The re-

*Kiethley electrometer model 200, Kiethley Instruments, Cleveland, Ohio.

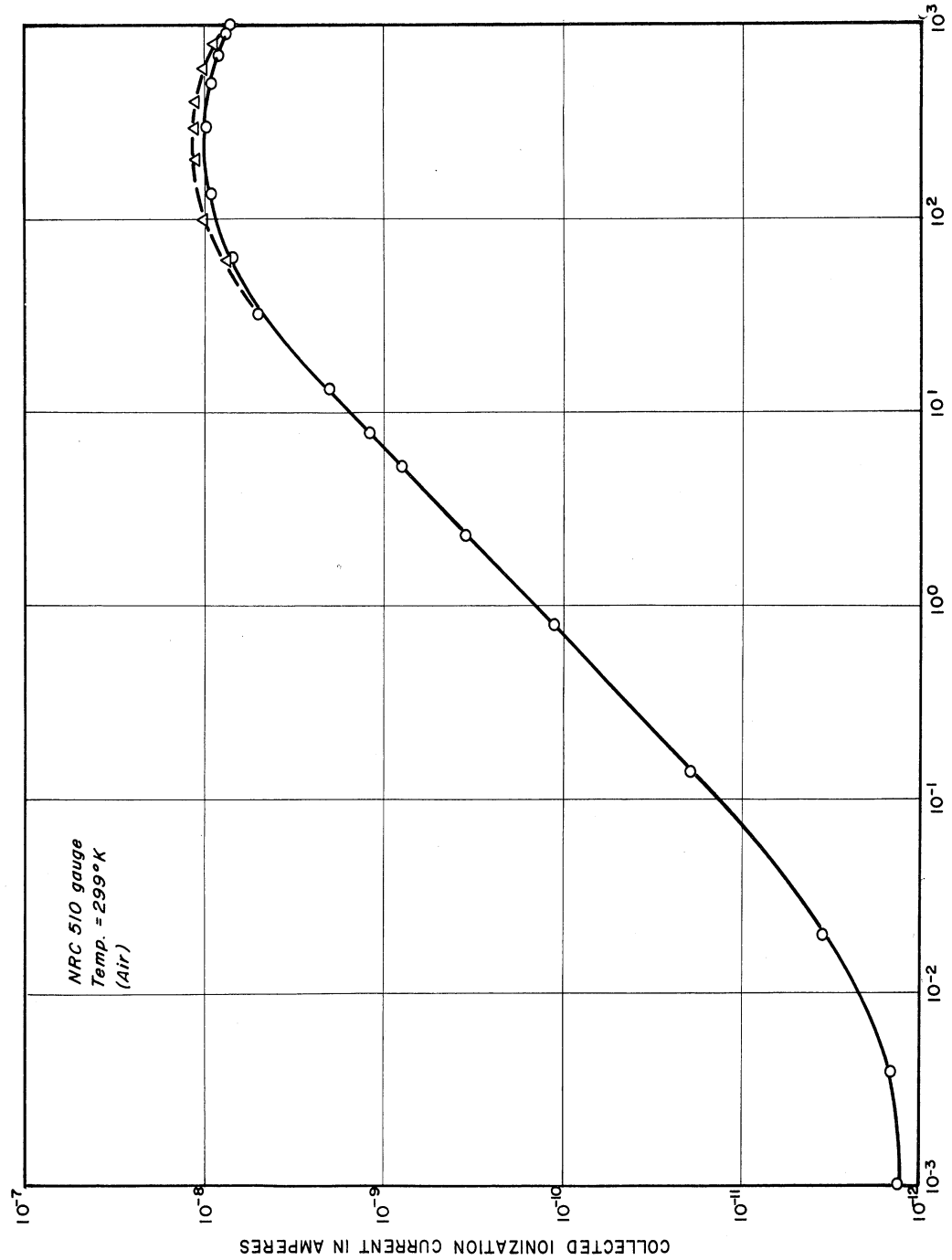

Fig. 4.2. Typical i-P characteristic of NRC No. 510 radioactive ionization gauge—room temperature 27°C.

sults are discussed in the following sections. The significant items are the departure from linearity at low as well as at high densities, and the slow variations, referred to as hysteresis, at high densities.

As shown in Fig. 4.2, the linear range lies between 10^{-2} and about 30 mb. The departure from linearity at the upper end of the pressure range is mainly due to recombination of ions in the fashion explained in Chapters II and III.

The nonlinearity at the low portion of pressures, below 10^{-2} mb, is attributable to secondary electron emission from the collector occurring as a result of the impacts of the high-energy alpha particles and X-ray radiation emitted from the gauge walls, and results in what is called dark current.

4.3. DARK CURRENT

As mentioned above, the current-pressure characteristic of a radioactive ionization gauge levels off at very low pressures, approaching a particular low value known as the dark current. This was illustrated earlier in Fig. 1.4 and is shown in Fig. 4.2.

As the density decreases, the ionization current correspondingly decreases until the dark current becomes a larger and larger fraction of the total current and finally masks the ionization current. This unwanted effect, appearing as a constant current in the gauge output at low pressures, is believed to be due to:

(a) X-rays emitted by the electrodes and the chamber walls as

a result of the impact of alpha or beta particles upon them,

and (b) the considerable number of secondary electrons emitted as a result of bombardment by the source particles of the collecting electrode.

When an alpha or beta particle hits a metal surface, part of its energy is expended in ejecting a few secondary electrons, mostly from the outer regions of the atoms. The balance is absorbed in exciting the electrons of the inner shells, with the subsequent production of X-rays.

It has been found experimentally that the magnitude of the dark current depends upon the intensity of the impinging corpuscular and electromagnetic radiations which undergo no appreciable change under pressures lower than about 10^{-2} mb. In general, the greater the number of particles reaching the positive-ion collector, the greater the magnitude of the dark current. It was thus possible to lower the value of the dark current and consequently to extend the linear portion of the i-P characteristic to lower densities by, in effect, reducing the number of direct impacts of the ionizing particles on the collector. This is illustrated in Fig. 4.3, which shows the i-P characteristics of three gauges, identical in every respect except for the shape of the positive-ion collector, which is a plane disc in one case and a thin wire in the other two. It is interesting to note that the secondary emission exists throughout the pressure range, but is of significance only at low pressures, since at high pressures its value is very small compared to the corre-

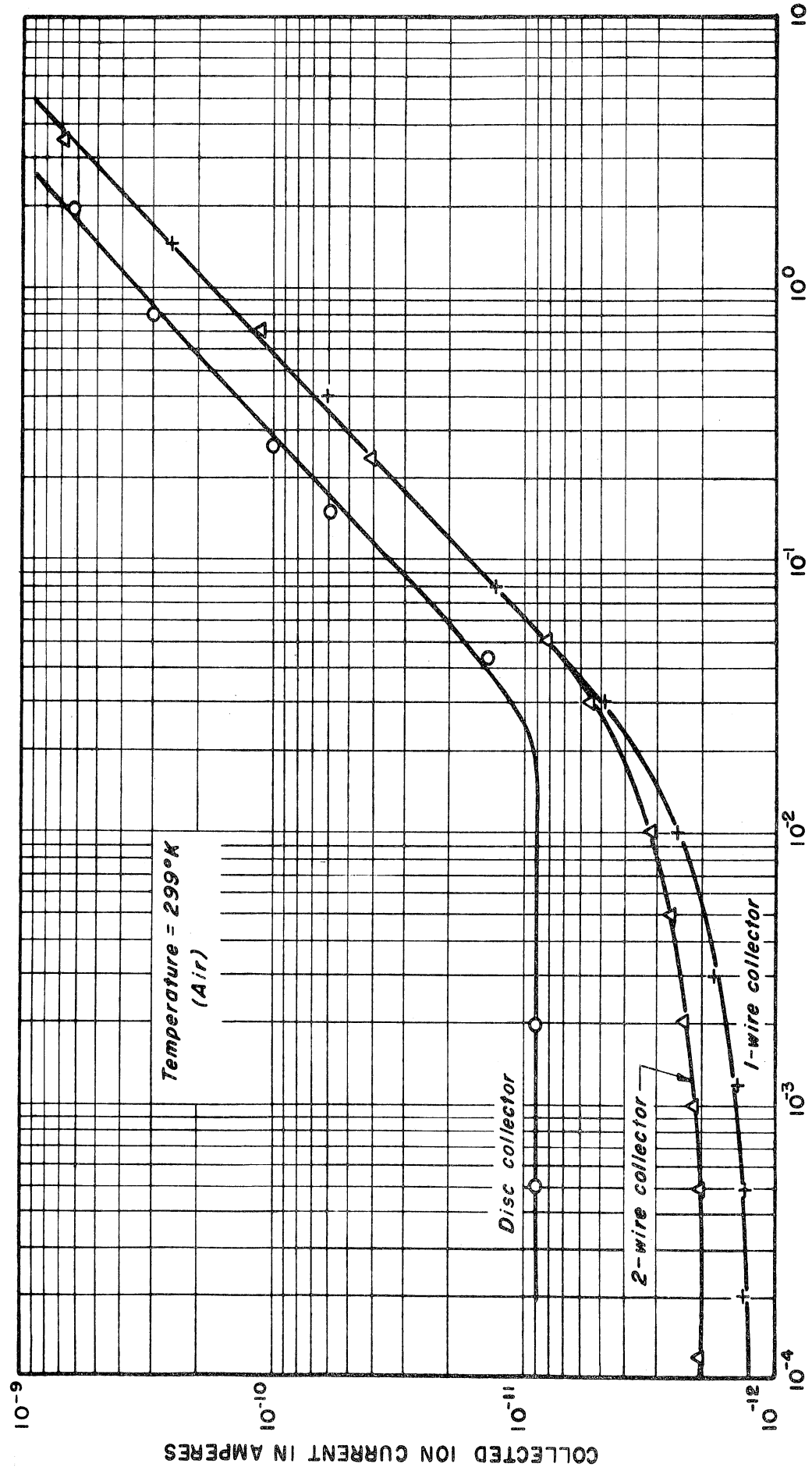

Fig. 4.3. Change of dark current value with collector shape.

sponding ionization current.

4.4. THE HYSTERESIS PHENOMENON

At high density, in addition to departure from linearity, the NRC as well as other radioactive ionization gauges exhibit an undesirable phenomenon: If one observes the current as the pressure is permitted to decrease from relatively high density to some arbitrary value and then permitted to increase to the original pressure, the two current-pressure curves observed may not coincide. This deviation occurs mainly in the nonlinear portion at the high-density end, as illustrated in Fig. 4.2 for the NRC gauge.

4.4.1. Possible Causes of Hysteresis.—The following were considered as the possible major causes of hysteresis:

1. Time variation in source activity.
2. The effect of field configuration.
3. Change in temperature, with resulting variations in the coefficients of the ionization, attachment and recombination processes.
4. Slow change in concentration of one or more of the minor constituents of the gas, having attachment properties different from those of the major constituent.

These factors were investigated, either separately or along with other experiments, through the course of the experimental part of this

research. Various aspects of the results will be discussed in turn.

4.4.2. Verification of the Constancy of Source Activity.—To examine the constancy of the source activity, the pressure inside the gauge was maintained at about 10^{-4} mb for about 72 hours and then abruptly increased to about 1000 mb; concurrently, the collected current was observed until it attained a steady value. This procedure was repeated for different final pressures, all lower than atmospheric. Typical results of this experiment are shown in Fig. 4.4. From these curves one notices that the current first decreases until it reaches a minimum after about an hour, and then slowly increases to reach a final value only slightly higher than the minimum. It should be noted that the greatest dip in current happened at a pressure roughly equivalent to the pressure at which the peak of the i-P characteristic occurs. It was then speculated that the variation of current under the above conditions could be attributed to some kind of instability of the source activity. For example, the radium source might not remain in a state of equilibrium with the other decay products as a result of escape of radon gas, and hence the subsequent radioactive daughter-products.

A mathematical analysis of the source strength as an alpha emitter was then developed, taking into account the various levels of alpha particle energy involved and assuming an exponential leak (see Appendix). Although the general shape of the calculated curves bears some similarity to the experimental ones (Fig. A.2), the relative dip in the calculated ones is comparatively much smaller and sometimes negligible, indicating

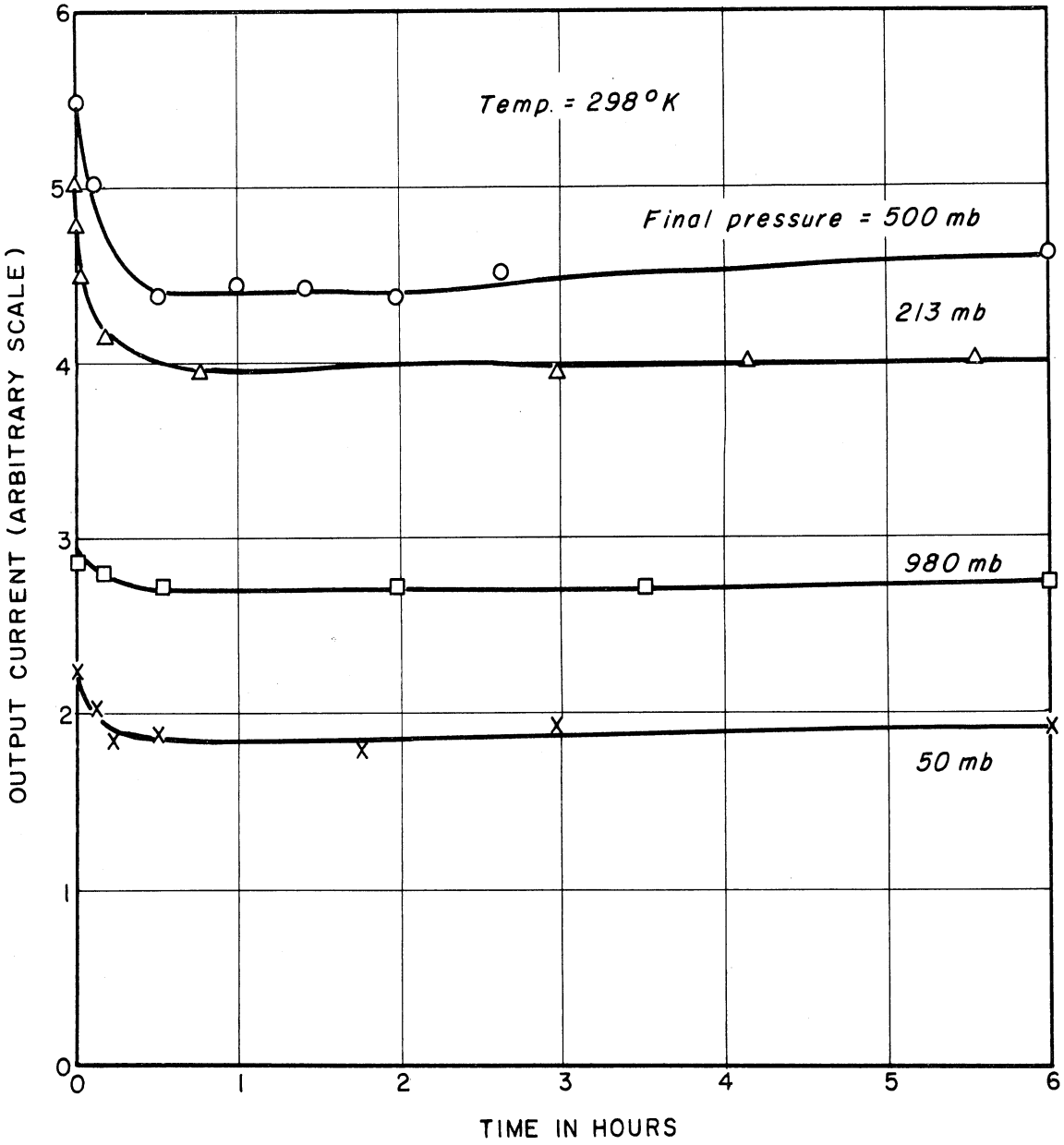

Fig. 4.4. Variation of output current with time at given constant pressure and temperature. Before zero time, the pressure was 10^{-4} mb; after zero time, the final pressure was as indicated.

fair constancy of the source activity.

Another indication of constancy of source activity was obtained by means of a specially built scintillation apparatus. The source and main components of the device are shown in Fig. 4.5. The radium source was mounted on a monel frame inside a glass tube facing a mica window (about 2.0 mg/cm^2), which served as a vacuum-tight seal, while being sufficiently transparent for most alpha particles to pass. The external side of the mica seal faced the window of a DuMont 6467 photomultiplier tube.

An appropriate layer of ZnS:Ag phosphor (about 8 mg/cm^2) was deposited on the outer surface of the photocathode according to the following procedure. The activated zinc sulphide powder was dispersed in distilled water and poured into a settling chamber made from a piece of glass tubing fitted over the face of the photomultiplier with a rubber gasket to prevent leakage. Suitable amounts of barium acetate and potassium silicate were also added to give an evenly dispersed and highly adherent film. The phosphor was allowed to settle; then most of the water and unused potassium silicate solution were slowly removed with a pipette, and the remainer was permitted to evaporate into the atmosphere.

The minimum practical distance between the source and the phosphor film was determined (a) to protect the phosphor film from destruction by the high-energy-particle bombardment, and (b) to minimize dispersion of the alpha particles.

The glass tube and the photomultiplier were enclosed in a light-tight magnetic shield. The required voltages at the phototube dynodes were so

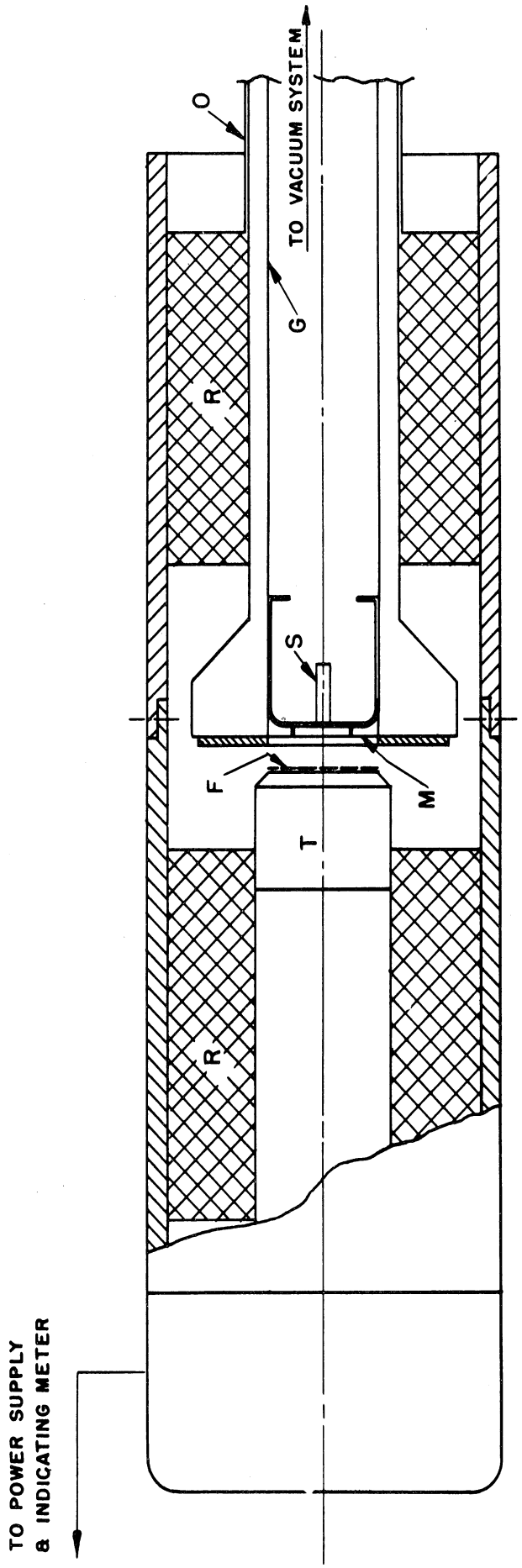

S - RADIOACTIVE SOURCE
M - MICA WINDOW (2.0 mg/cm^2)
F - PHOSPHOR FILM (8.0 mg/cm^2)
T - PHOTOMULTIPLIER (DU MONT 6467)
G - GLASS TUBING
R - BLACK FOAM RUBBER
O - OPAQUE COATING

Fig. 4.5. Scintillation apparatus.

adjusted that the average anode output current was limited to about 60 μamp, a value which is far below the maximum rating of the phototube (5 ma). This low value is advisable to assure adequate stability conditions in the performance of the phototube as far as multiplication factor is concerned. The dynode voltages were supplied by a convenient power supply, illustrated in Fig. 4.6, from which voltages up to 2400 volts were available.

Owing to the fluorescent property of ZnS:Ag material, some of the energy absorbed from the incident particles, alphas in this case, is re-emitted as faint bluish light (scintillations) quantitatively proportional to the energy lost by the incident radiation, i.e., proportional to the number of incident particles.

The section containing the radium source was connected to the vacuum system to determine any variation with pressure of the activity of the source as an alpha emitter. The system was pumped out to about 10^{-3} mb, then maintained at this pressure for about 72 hours during which the activity, as indicated by the scintillation apparatus, was checked and recorded. Air was then admitted into the system, increasing the pressure abruptly to about 400 mb, or atmospheric pressure (1013 mb), where it was held constant for about eight hours. The source activity was again recorded every fifteen monutes. This procedure was repeated several times while keeping the source for longer and longer periods under vacuum.

A summary of the results obtained is shown in Fig. 4.7. It is

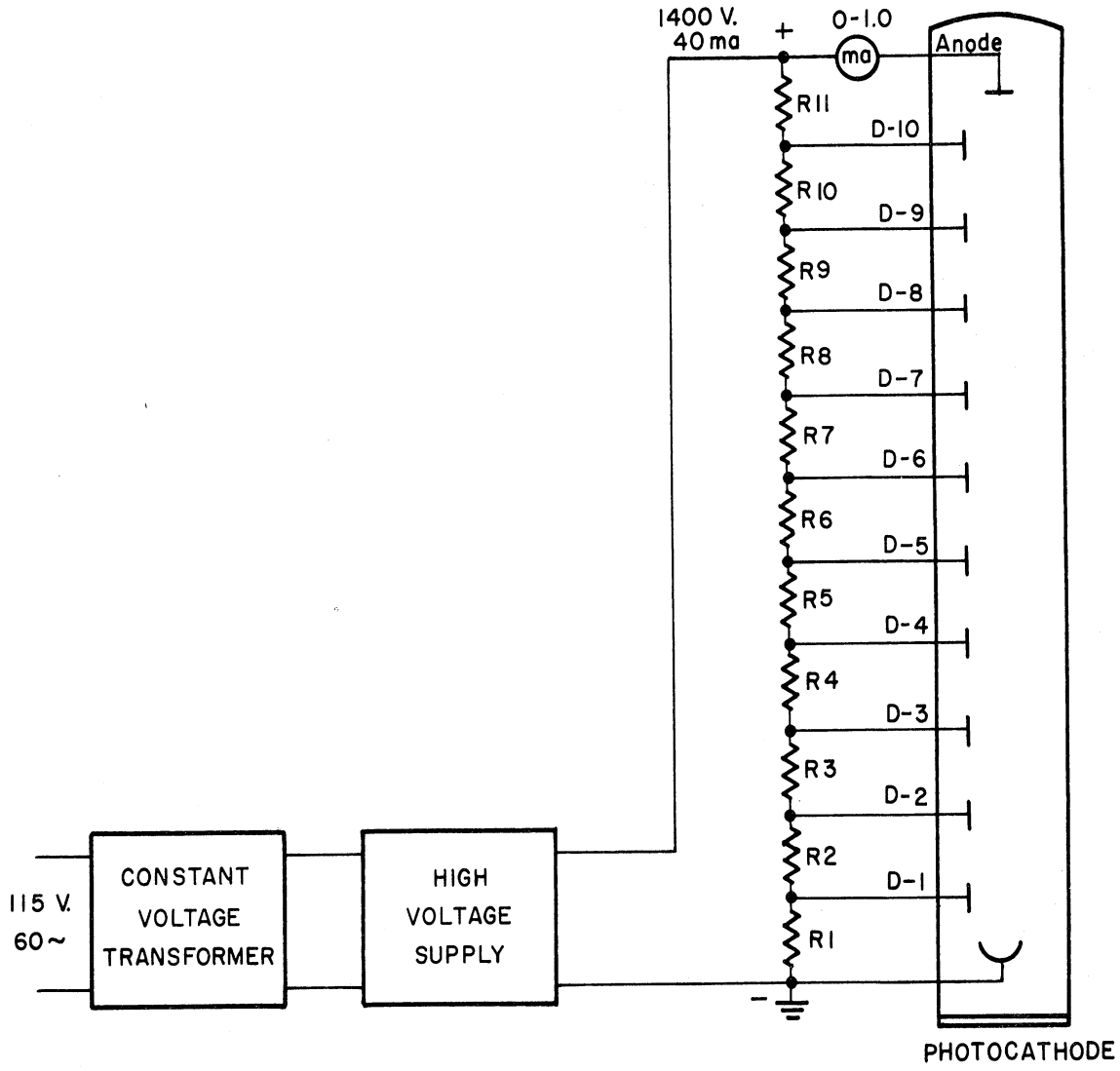

R1 - 6000 ohms, 20 watts

R2 -R11 — 3000 ohms, 10 watts

Fig. 4.6. Photomultiplier circuit diagram.

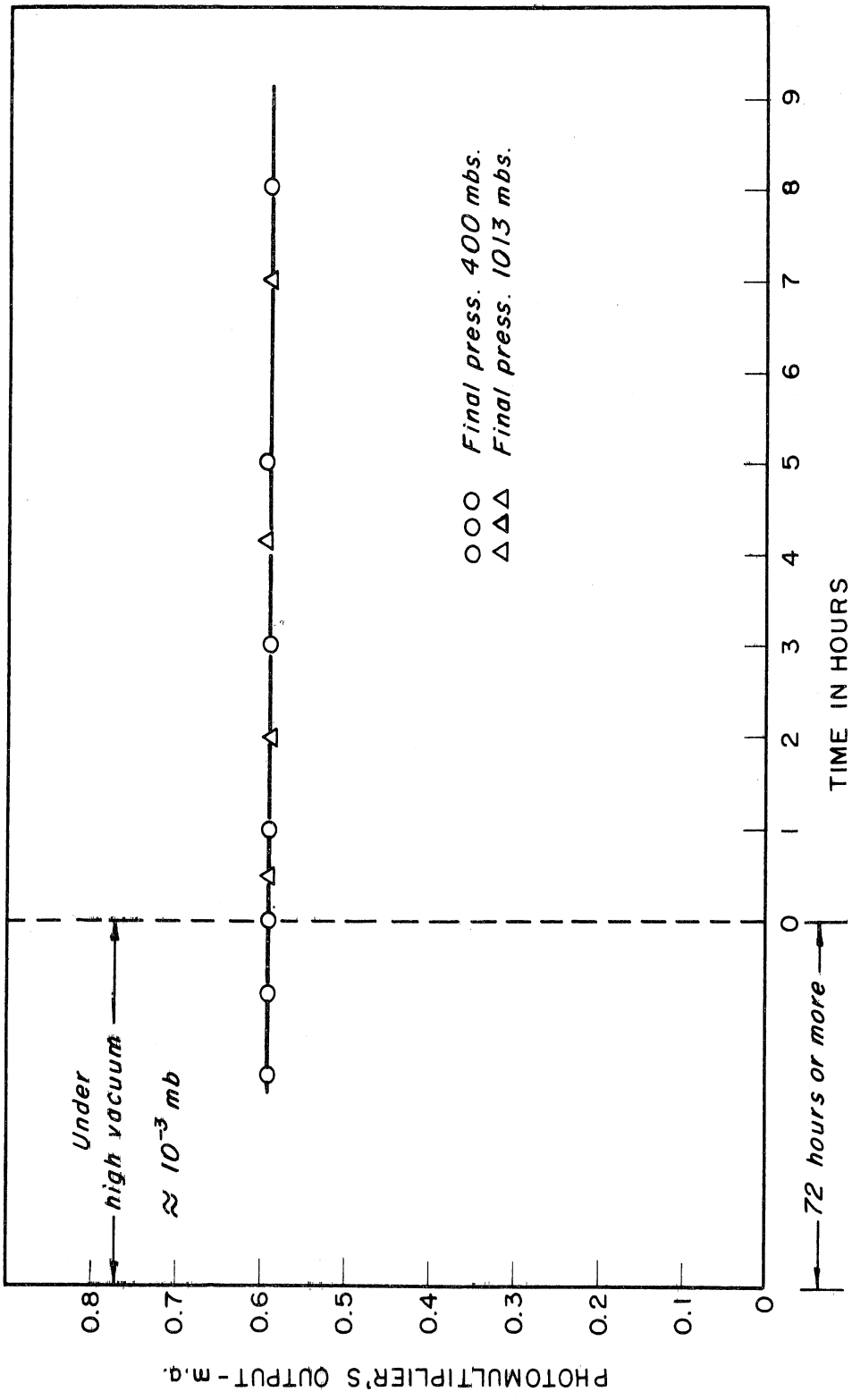

Fig. 4.7. Observed scintillation data for radium source activity.

clear from these data that there was no appreciable change in the source activity with pressure as indicated by the constancy of the anode current of the photomultiplier tube. Thus it was concluded that the hysteresis in the i-P curves at high densities was not due to a change in the source intensity.

4.4.3. Effect of Electric Field on Hysteresis.—Interesting conclusions were drawn from consideration of the distribution of the electric field inside the NRC model 510 radioactive ionization gauge. The field between the positive-ion collector and the wall is quite nonuniform (see Fig. 4.8*). The effective collection of positive ions is confined largely to the small volumes around the four collectors, outside the dashed circle where the field intensity is appreciable. On the other hand, the bulk of the ionization chamber lies in a region of considerably lower intensity (Fig. 4.9*). Thus it is very hard to attain saturation current collection under the normal operating conditions where the potential differences between the positive-ion collectors and the chamber wall is around 40 volts. Electron attachment due to the presence of electronegative impurities and hence ion-ion recombinations are responsible for the deviation from the saturated values of collected currents.

On applying a much higher voltage, about 500 volts for example, the effective collection volume is considerably increased. Though the field

---

*The writer wishes to thank Professor A. D. Moore of the Department of Electrical Engineering of The University of Michigan for his assistance in mapping the above field.

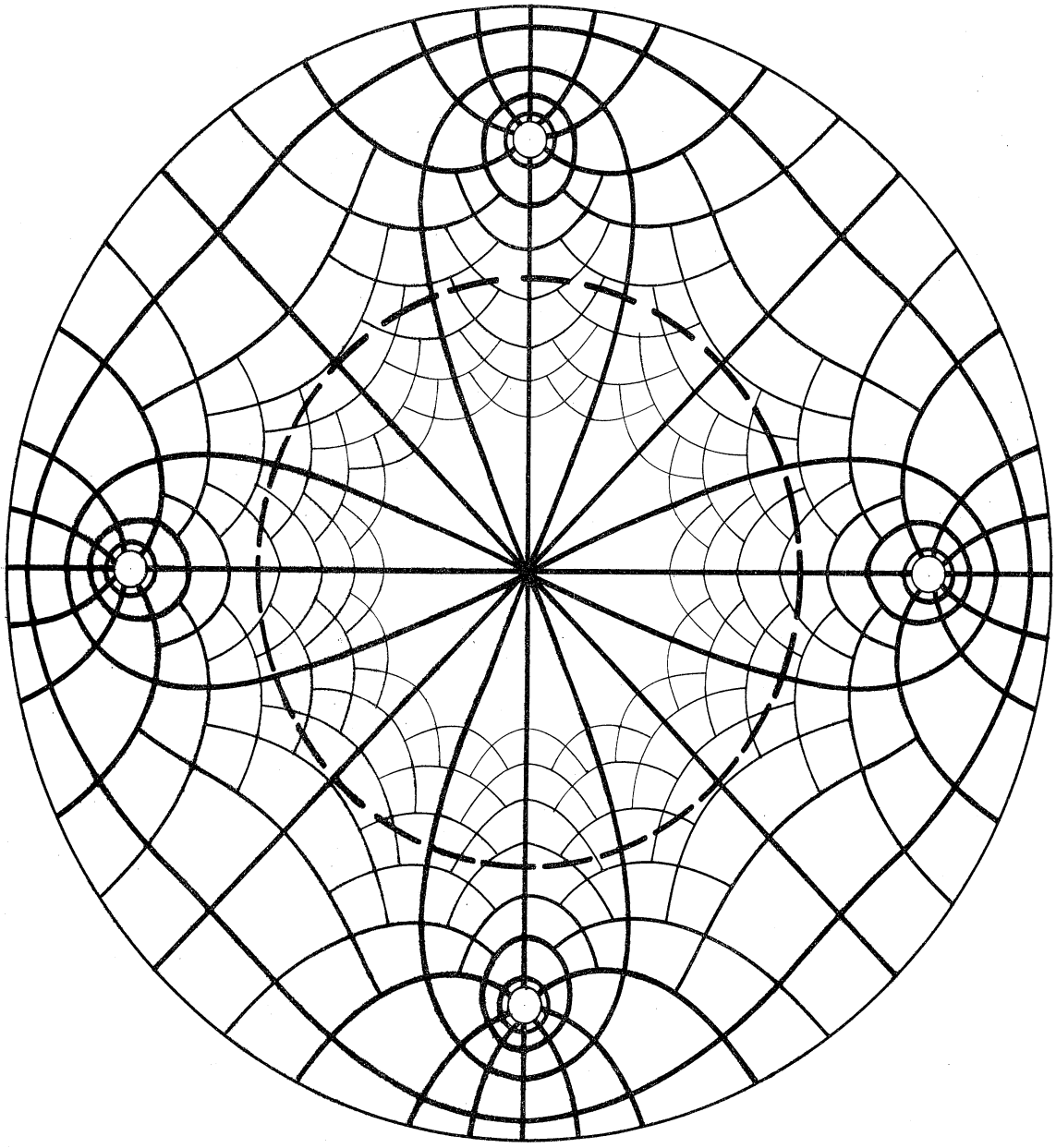

Fig. 4.8. Electric field map of NRC 510 gauge.

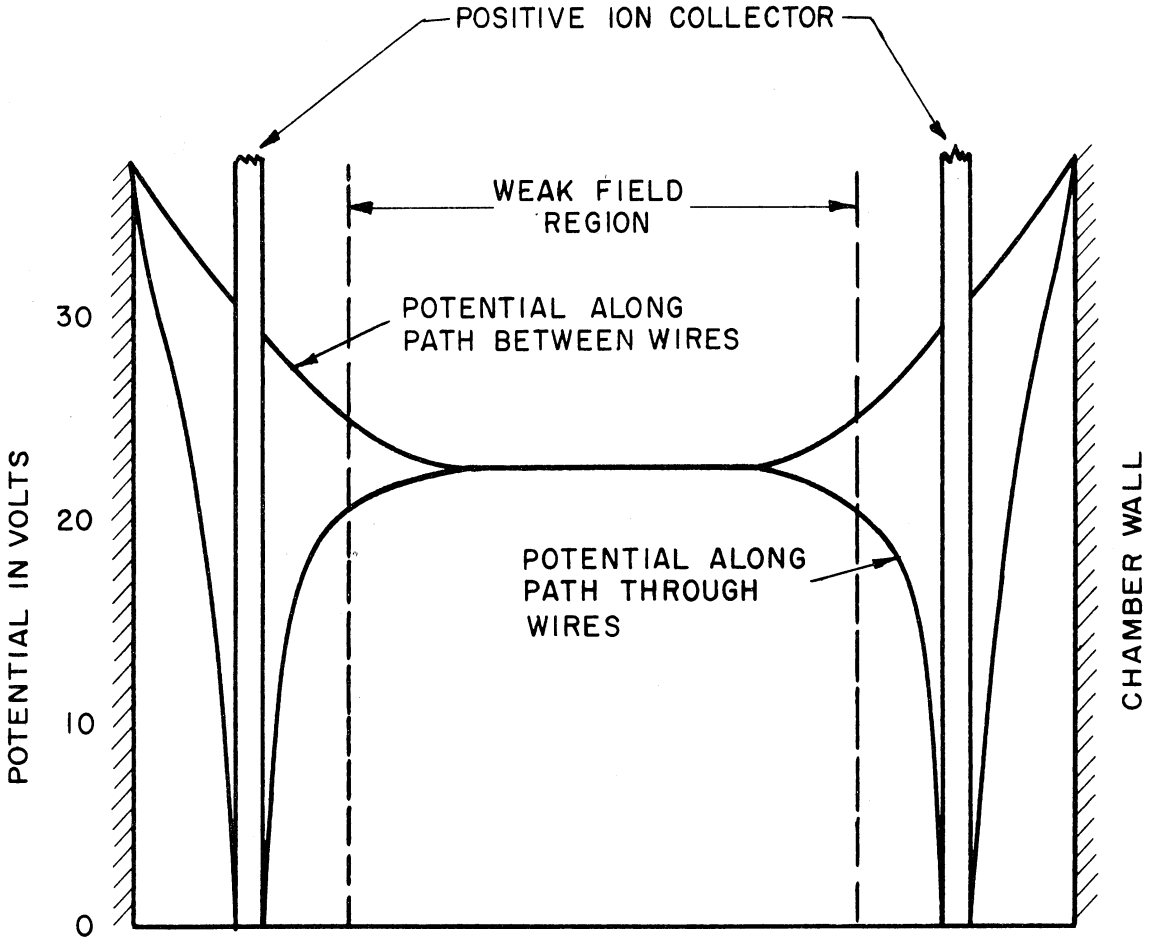

Fig. 4.9. Potential distribution in an NRC 510 gauge.

is still nonuniform, it was possible in this manner to extend the linearity of the i-P characteristic of the NRC gauge up to about 400 mb, i.e., ten times its normal range of pressure measurement. It was also noticed that the new curve became linear and reproducible in a region where nonlinearity and hysteresis once prevailed under lower electrode voltages (see Fig. 4.10). This result leads to the belief that the lack of reproducibility in the upper nonlinear region is due to a variation in the rate of electron attachment.

The other possible causes of the hysteresis in radioactive ionization gauges were studied using a laboratory-built planar gauge and will be explained in the next section.

4.5. EXPERIMENTAL RADIOACTIVE IONIZATION GAUGE

4.5.1. Constructional Details.—The constructional details of the experimental gauge were chosen primarily to permit comparison of its performance with expectations on the basis of the theory presented above. However, some details of the design were chosen partly with a view to other considerations, among them ease of transferring what was learned to an instrument for use in rockets.

The design chosen employed two parallel stainless-steel plates arranged so that the separation between them could be adjusted to any value between 5 and 40 mm in 5-mm steps (see Fig. 4.11). The guard rings were used to obtain an essentially uniform electric field intensity in the central zone which contained the sensitive volume of the gauge. The

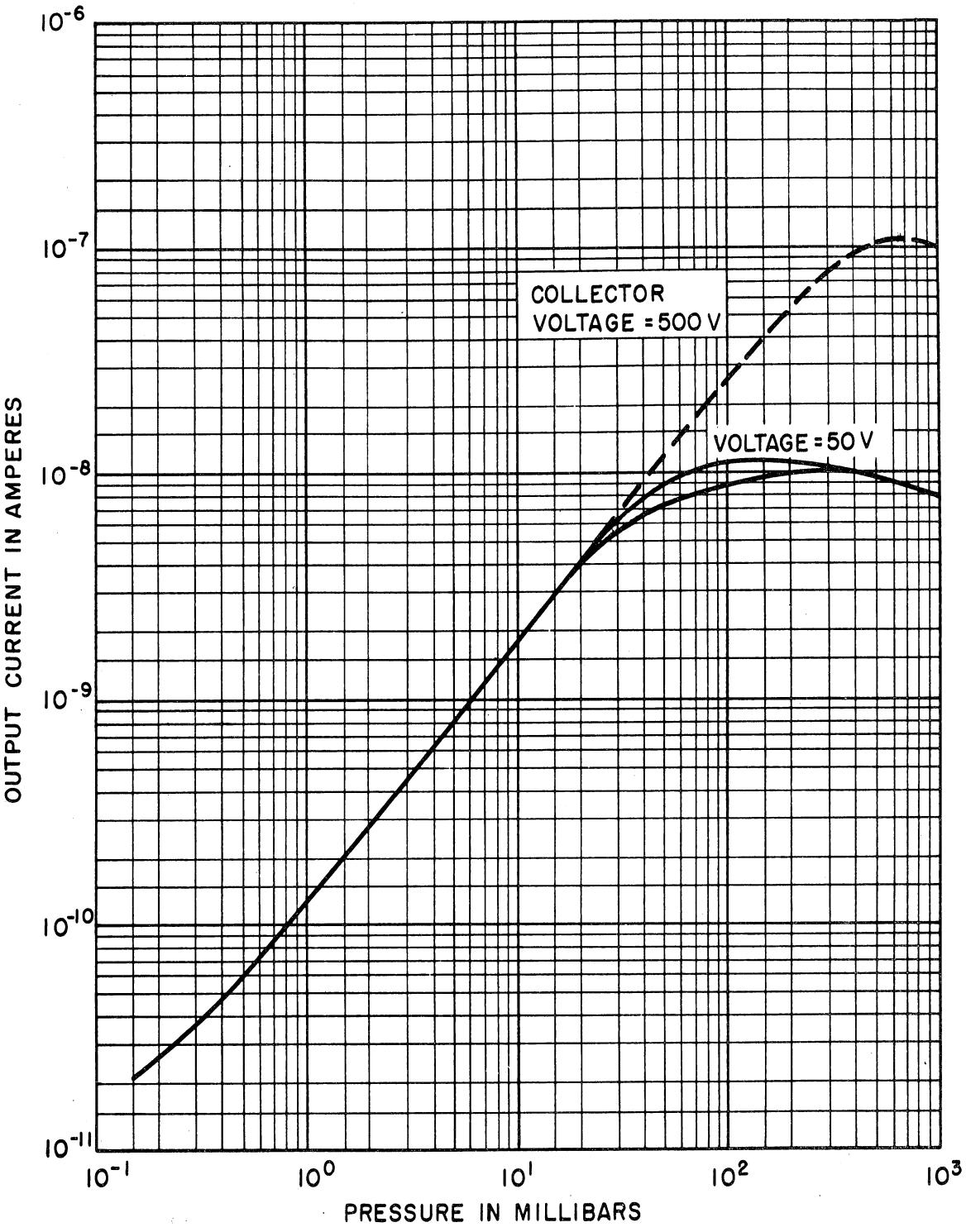

Fig. 4.10. Reduction of recombination loss and hysteresis by using higher collector voltage.

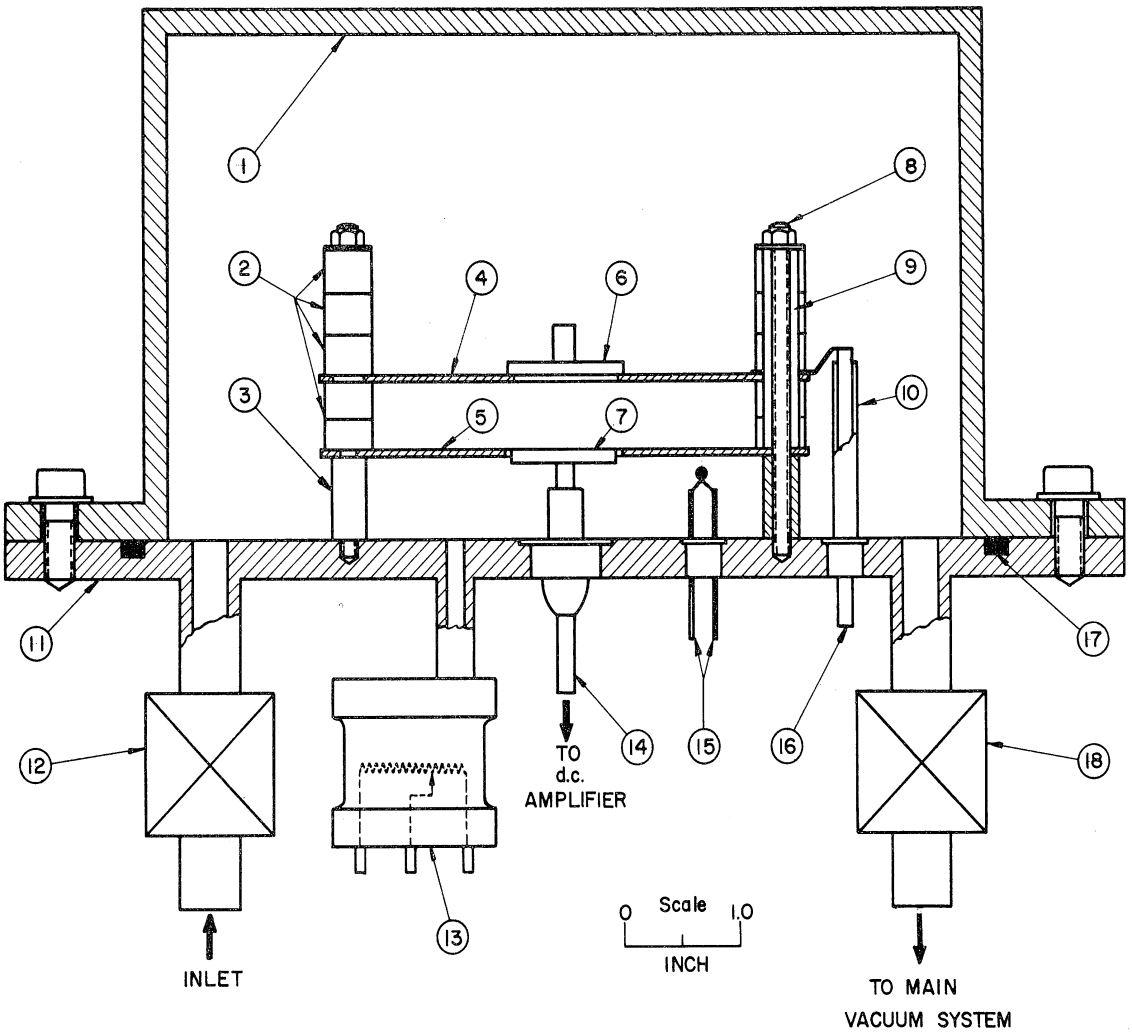

Fig. 4.11. Experimental radioactive ionization pressure gauge. (1) brass bell jar, (2) glass spacers, (3) metal support, (4) high potential electrode, (5) grounded guard electrode, (6) radium source, (7) collecting electrode, (8) supporting rod, (9) and (10) glass-tube insulators, (11) bottom plate, (12) and (18) bellows sealed vacuum valves, (13) Giannini pressure transducer, (14) kovar glass seal, (15) leads to thermistor, (16) lead to high potential electrode, (17) O-ring seal.

gas between the plates was ionized by alpha particles emitted from a radium source of about 166 microgram alpha-equivalent emission (166 microcurie). This source acted as a part of the high potential electrode to collect the electrons or negative ions that reached that plate.

This assembly was housed under a brass bell jar fastened to the base plate and kept vacuum tight by an O-ring gasket. The inlet and outlet parts, in the base plate, were controlled by two sealed-bellow valves. The pressure inside the jar was determined by a calibrated aneroid pressure transducer with a range of from 0-1300 mb. The temperature of the gas between the plates was indicated by a glass-coated-bead thermistor having a relatively short thermal time constant (about two seconds). Two more thermistors, one at the inlet and the other at the outlet, were used to determine the temperatures of the admitted and pumped-out gas, respectively. All the electrical connections to the elements inside the bell jar were made by means of a special commerically available hermetic metal-to-glass multiheader seal.

4.5.2. Effect of Plate Voltages on Output Current.—Figure 4.12 is a chart of a typical set of data taken with the experimental device. The output current in general increases under higher voltages. The rate of increase, however, is seen to vary for the different ranges of pressure.

For the discussion of the results represented in Fig. 4.13, one must consider three different distinct regions on the i-P characteristic. These will be designated by high-, medium-, and low-pressure ranges.

The downward (to the right) bend in the high-pressure region of the

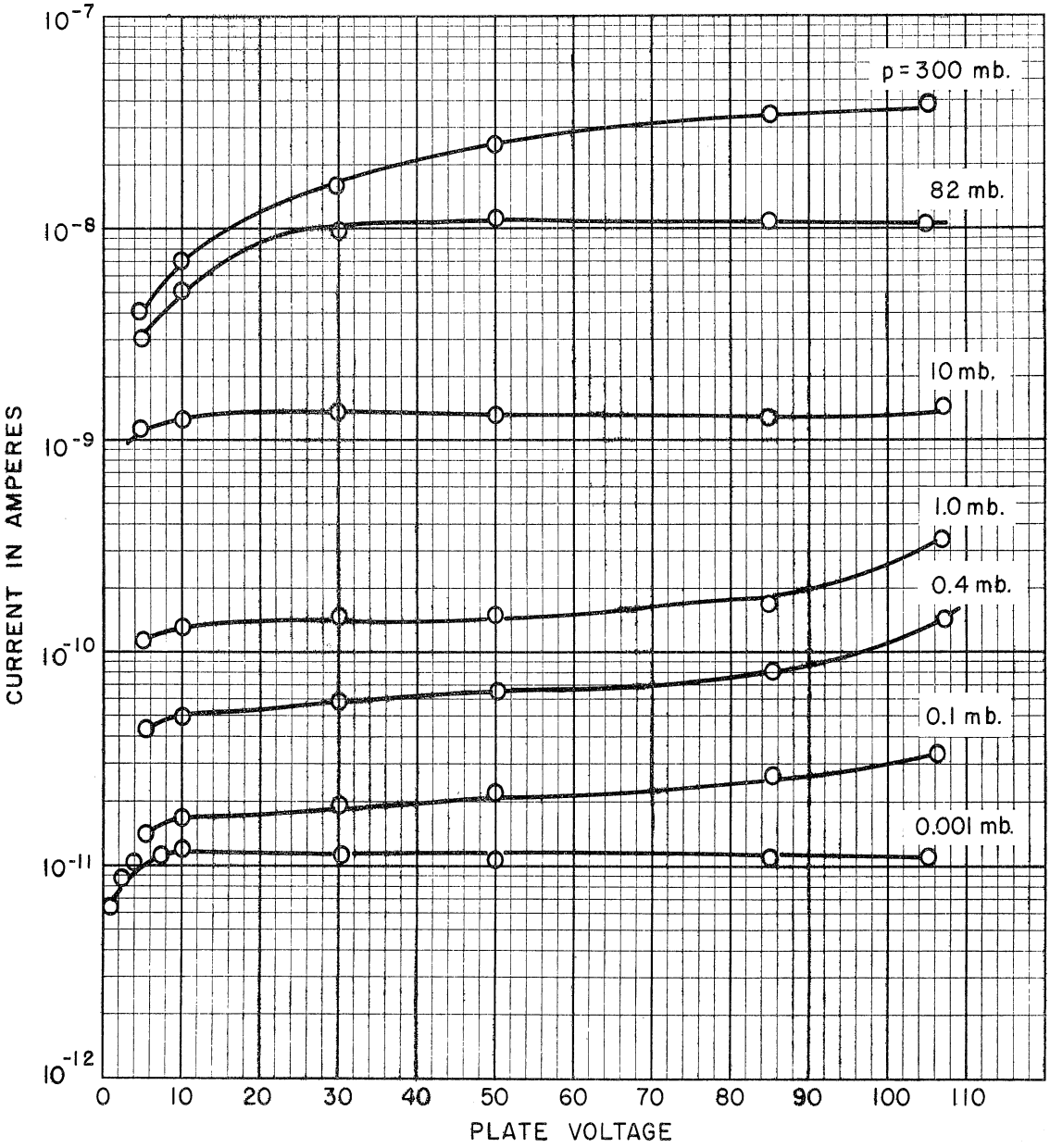

Fig. 4.12. Observed collected currents as function of plate voltage for different constant pressures at room temperature (27°C)—planar gauge.

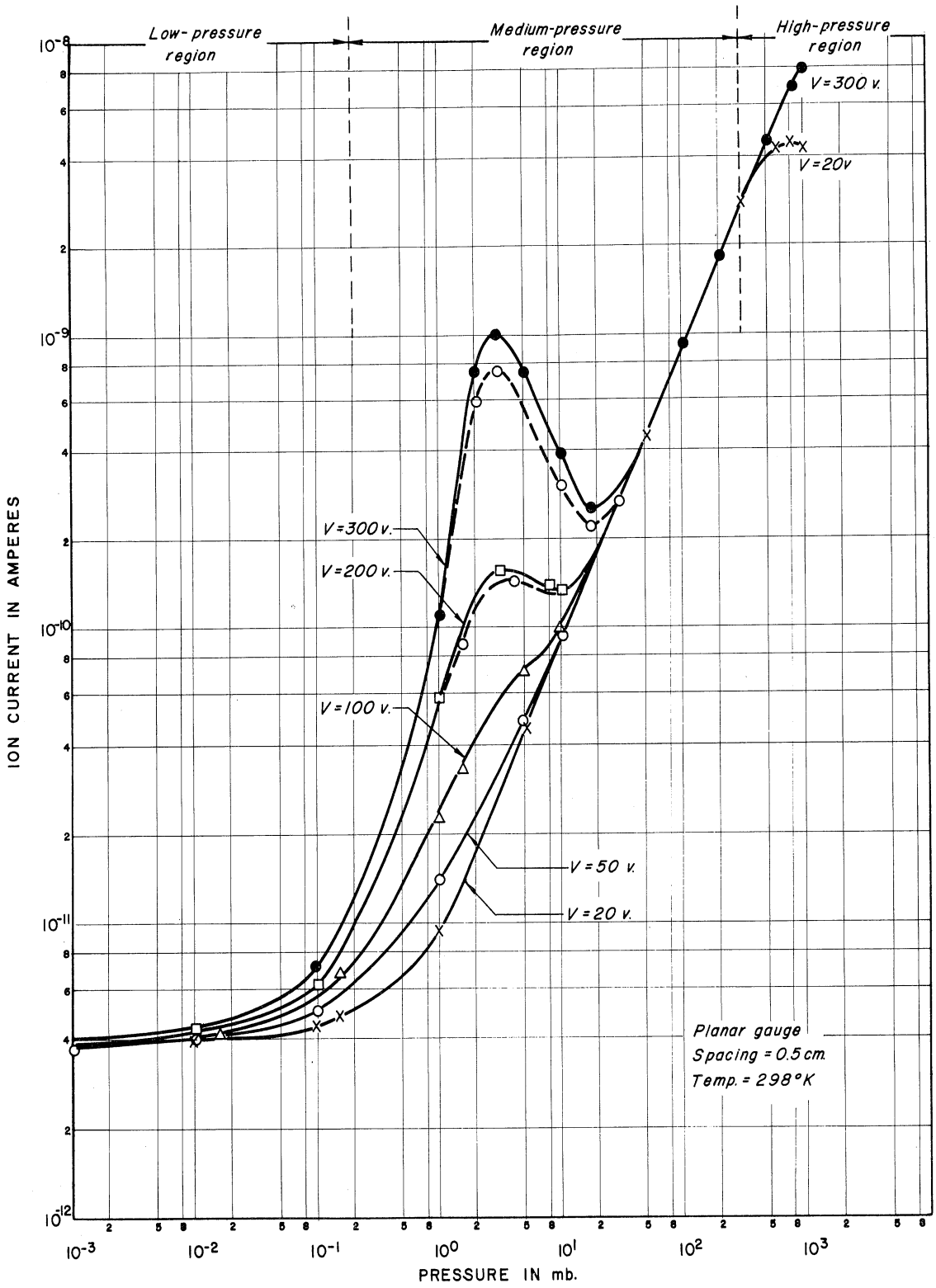

Fig. 4.13. Variation of collected ion current with pressure at room temperature (25°C) for different electrode voltages in a planar radioactive ionization gauge.

i-P characteristic is mainly due to the loss of oppositely charged ions by recombination. The increase in the intensity of the electric field at constant density accelerates the sweeping action of the ions to the electrodes, thus reducing the average transit time of ions between the electrodes. This in turn decreases the duration of encounters between the positive and negative ions while moving in opposite directions, thus reducing the chance of recombination and hence more ion collection as anticipated in Chapter III (Fig. 3.6). Therefore the 300-volt curve remains almost linear in this region, whereas recombination causes the 20-volt curve to bend.

In the medium range the i-P relation is usually linear. In this range the ion density is relatively small, so that recombination effects become unimportant and thus all the ion products are collected. As the pressure goes down, the probability of electron attachment decreases, leaving some of the electrons free, subject to the electric field acceleration. When the kinetic energy gained by such electrons from the field becomes high enough to ionize the gas molecules as a result of inelastic collisions, a considerable increase in the ionization occurs in addition to that due to irradiation by alpha particles. This phenomenon, known as gas amplification, is undesirable for the intended use, and normally is prevented from occurring by maintaining a sufficiently low field strength. This particular type of ionization is observed to increase until it reaches a maximum at a certain lower value of pressure, and then declines as the pressure continues to drop.

It is interesting to note that the i-P characteristic exhibits some hysteresis (in the sense referred to in Section 1.3) under these conditions even after hysteresis is no longer apparent in the linear part of this medium region. This hysteresis is also believed to be a result of the variation in the environmental conditions which results in the attachment of some of the electronic to gas molecules, thus terminating the life of a free electron and consequently its ability to act as an ionizing agent. This change might take the form of the appearance of a small quantity of a kind of gas favorable to electron attachment.

In this gas amplification region, the ratio of the resulting current, i, to the saturation value, i_o, similar to Geballe's equation,[48-50] will be given as

$$\frac{i}{i_o} = \frac{1}{(\alpha-\eta_o)s_o}\left[e^{(\alpha-\eta_o)s_o} - 1\right] . \qquad (4.1)$$

Here α is the first Townsend coefficient which gives the number of new electrons created by a single electron per unit distance of advance in the field direction; η_o, the rate at which an electron may attach to make a negative ion per unit length advance in the field direction; and S_o, the separation between the parallel plates. The saturation current, i_o, is measurable by use of a low-voltage i-P curve. Here α and η_o are functions of the field-to-pressure ratio, E/P, for the kinds of gases involved.

The observations at the lower part of the medium-pressure range

give additional evidence in support of the theory presented in Chapter III, which states that the hysteresis phenomenon in radioactive ionization gages may be attributed to the change in the rate of electron attachment, as a result of alteration of environment. This change may be in the gas composition, as, for example, in forming ozone, a highly electronegative gas, between times of taking the two curves.

If the voltage is continually increased, the number of electrons released by collisions increases as well as their energies until electron avalanches may occur, resulting in a break-down discharge between the plates. This was occasionally observed in the experimentation.

Finally, at the low-pressure range, better known as the dark-current region, the output current levels off and stays constant regardless of any further decrease in pressure. This residual current is found to be a function of the area of the collector and is due to some action taking place at its surface, leading to the emission of electrons from it. The residual current starts off, due to the unbalance in the surface emission, with a negative value and then rises as the field is increased between 0 and 2.5 volts per cm above which the current tends toward a maximum (see Fig. 4.14). One may thus conclude that a substantial part of the dark current is caused by electrons detached from the electrodes or the insulation wall by impact thereon of alpha particles of X-rays in the manner discussed in Section 4.3.

4.5.3. Determination of α/P vs. E/P Curves.—The marked rise of the curves above the saturation value of Fig. 4.13 renders a useful

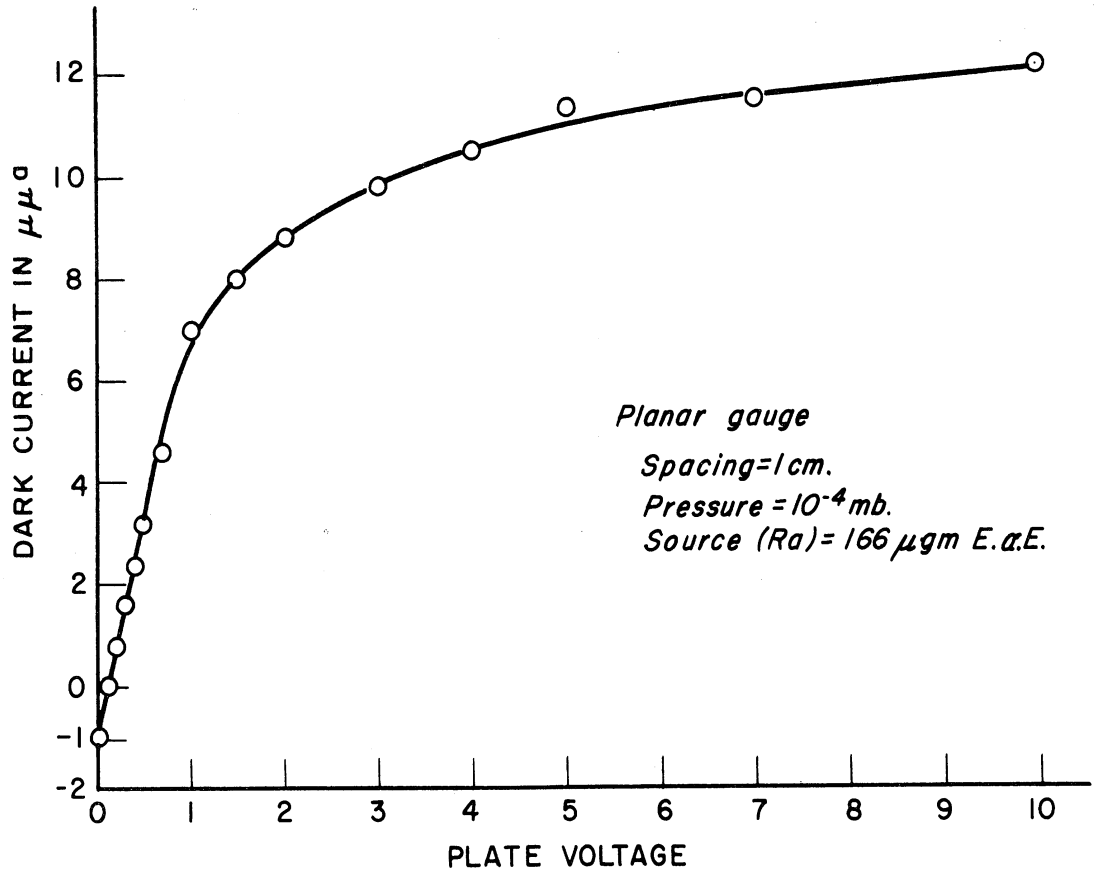

Fig. 4.14. Variation of dark current with plate voltage.

basis for determining one of the most important relations in ionization by collision, viz., the ionization coefficient, α/P, as a function of E/P. Figure 4.15 shows a plot of a typical ionization curve α/P versus E/P, as calculated by means of (4.1) from the experimental results charted in Fig. 4.13, assuming η_o to be negligible. It should be noted here that the above α/P vs. E/P curve satisfies all the points in the ionization-by-collision region regardless of their position with respect to the peak of of the voltage used. The loss of some of the electrons in attachment process, however, results in a reduction on the measured values of the ionization coefficient, α, which assumes a new value $\alpha' = \alpha - \eta_o$, with η_o as the attachment coefficient; this is represented by the broken line in Fig. 4.15.

4.5.4. Effect of Temperature on Gauge Output.—The review in Chapter II covered the main processes that would take place in a radioactive ionization gauge. Among the many important properties discussed there was the temperature dependence of the different processes. Thus one would naturally expect the ion collection currents to vary as a result of temperature variation.

In a vacuum system a momentary rise of drop in the gas temperature occurs adiabatically due to a pressure change. Differences in the gas temperature up to $\pm$ 40°C were observed in many instances when the pressure was suddenly changed. The magnitude of these differences depended on the gauge volume, the initial pressure, and of course on the rate at which the pressure was varied.

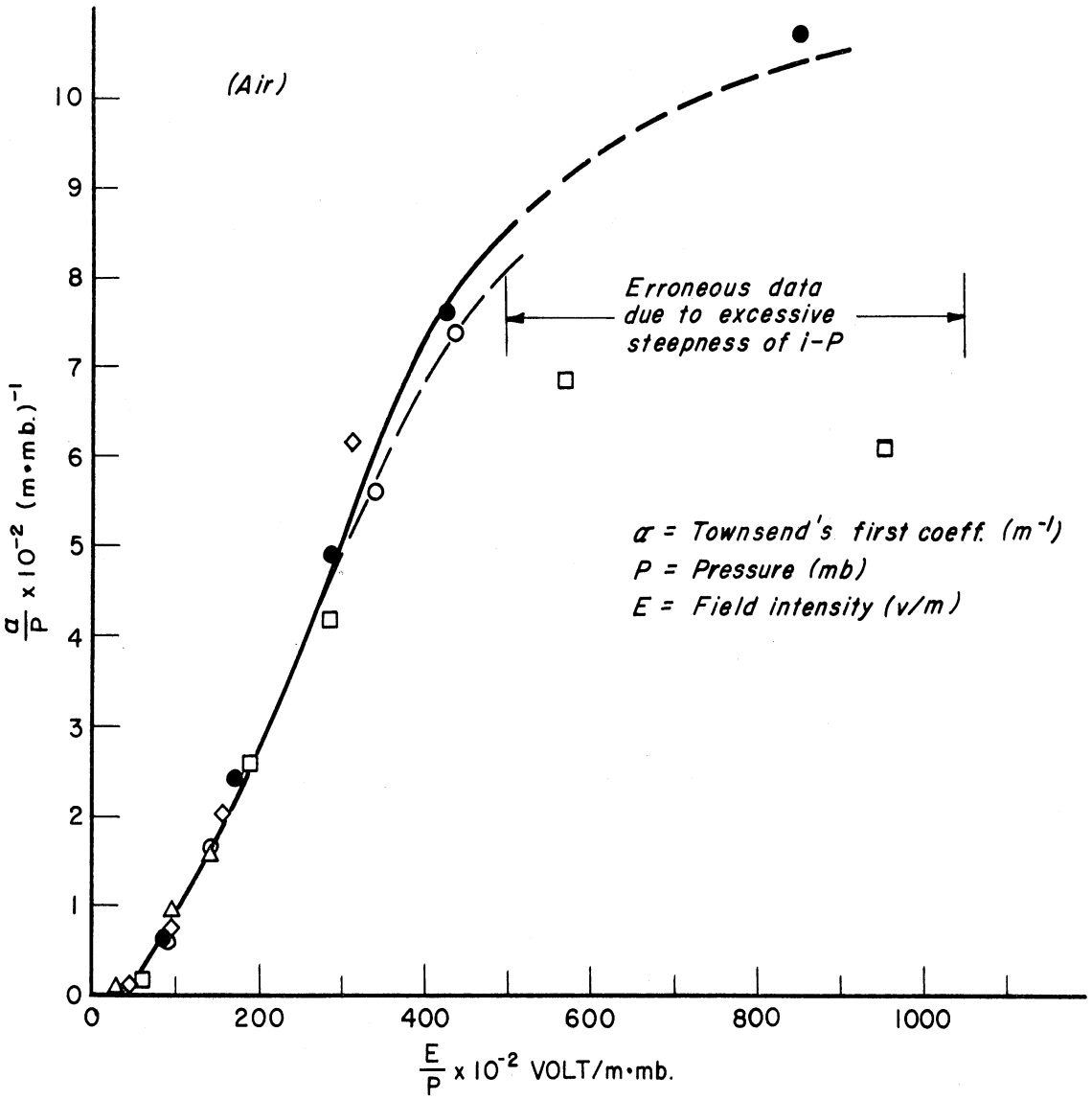

Fig. 4.15. Ionization coefficient (α/P) as a function of the electric field (E/P) in air as derived from Fig. 4.13.

In dynamic tests where the current measurements were made as the pressure was continually changing, the output current was found to respond to the manner in which the pressure was changed in the system. For example, the recombination hump of the i-P characteristic was observed to be high during pump-out period (adiabatic drop in temperature), and vice versa. It was possible then to reduce or even sometimes to eliminate the difference between the two current peaks by reducing the pumping speed and consequently the adiabatic changes in temperature. This is illustrated in Fig. 4.16, where the output current and the corresponding gas temperature were recorded for three different pumping speeds. It can be noticed from these results that the large difference occurred when the temperature change was greatest, and diminished for small temperature variations. The theoretical study of the expected effect of temperature on the electron attachment and ion recombination would, however, lead to results quite contrary to those experimentally observed. Thus for lower temperatures, one expects more electron attachment, and thus more recombination of ions, i.e., less collected ion current. Therefore, the observed change could be explained by assuming that the primary ionization of a particular gas is not only a function of the density but also of the temperature.

The temperature in this test, however, did not stay constant during each cycle of the test. So to examine this unexpected phenomenon, two more experiments were carried out. In the first test sequence, the temperature was held constant while changing the density, whereas in the

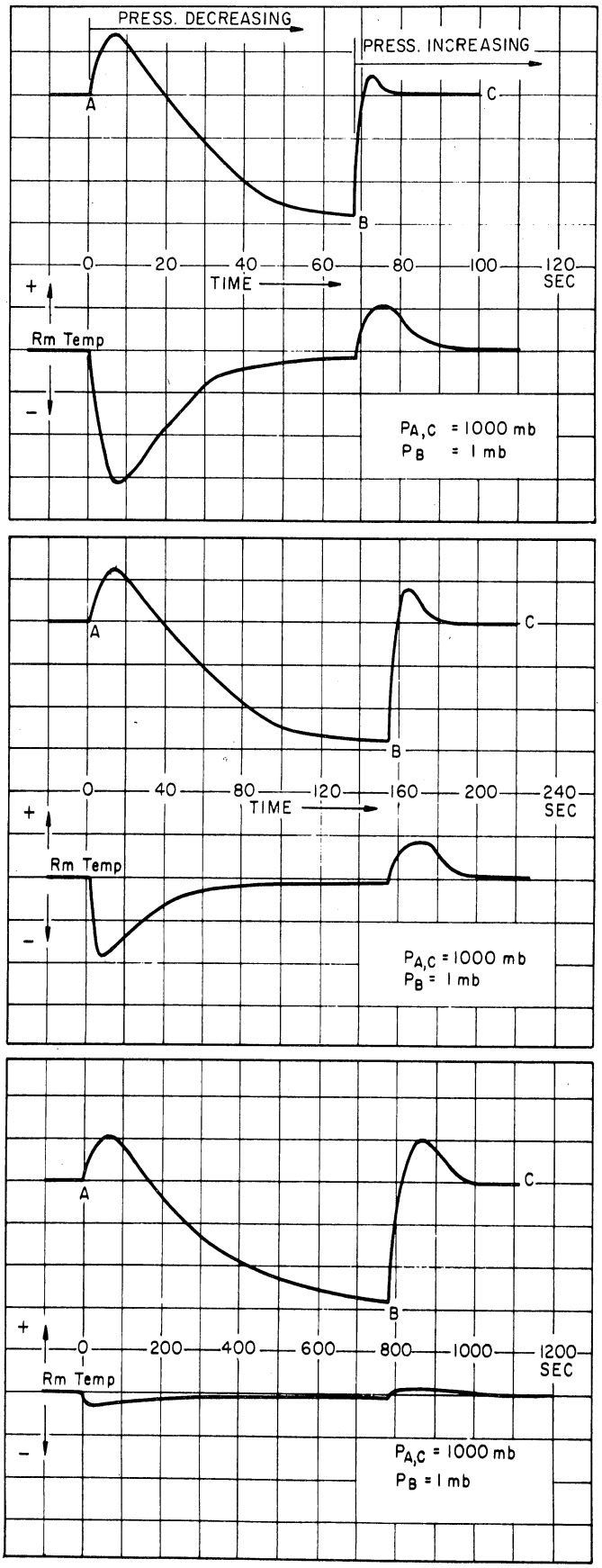

Fig. 4.16. Change of output current and gas temperature with time for various pumping speeds.

second the density was kept constant while varying the temperature.

The results of the first experiment are shown in Fig. 4.17 for two temperatures, 22°C and 52°C, by three pairs of i-P curves for three different plate voltages. Although the curve in the upper nonlinear end tends to straighten upward for higher temperatures in accordance with the theoretical predictions, as shown in Fig. 3.8, yet the i-P curve as a whole shifts downward as the gas temperature is increased. In the linear portion, the output current expectedly falls with increasing temperatures. This drop, however, is found to be more than would account for the corresponding change in gas density at a constant pressure. The additional decrease in the collected saturation ion current is attributed to a variation with temperature of the total ionization. This was shown in an experiment to be described next.

4.5.5. Variation of Primary Ionization with Temperature.—In this experiment the density of the gas was maintained constant by confining the planar gauge in a bell jar whose inside temperature was regulated by heating or cooling the outside walls. The measurements were made at certain points on the linear portion of the i-P curve, where saturation of the collected ion current prevailed. Such a choice insured no detrimental contribution from recombination effects, thus leaving the rate of ion production as the predominant factor in the output. A typical curve, summarizing the experimental results, is shown in Fig. 4.18. It is clear from this curve that the rate of ionization, as determined from the collected saturation ion currents, increases slowly with decreasing temper-

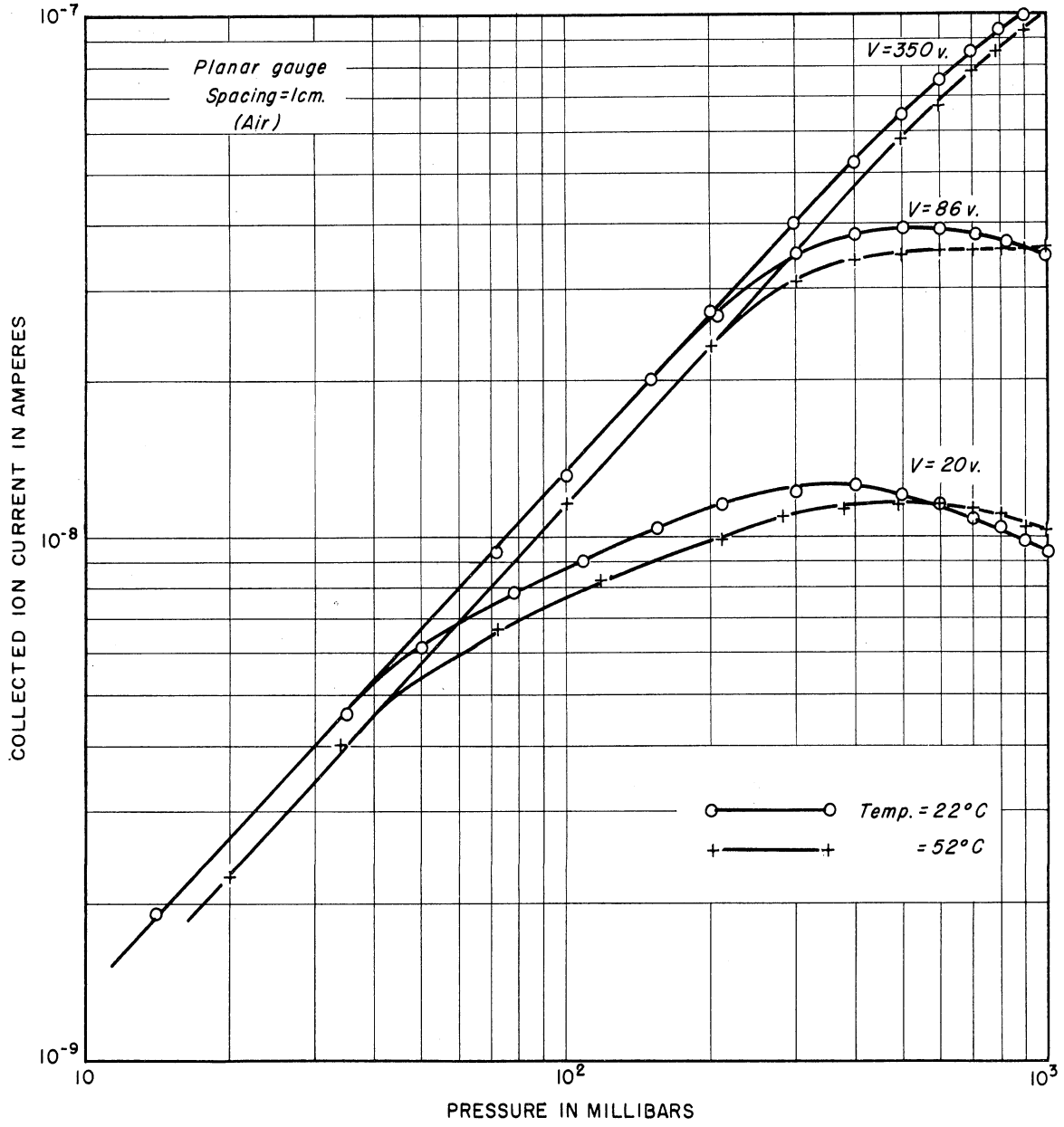

Fig. 4.17. Effect of gas temperature on i-P characteristics under different plate voltages.

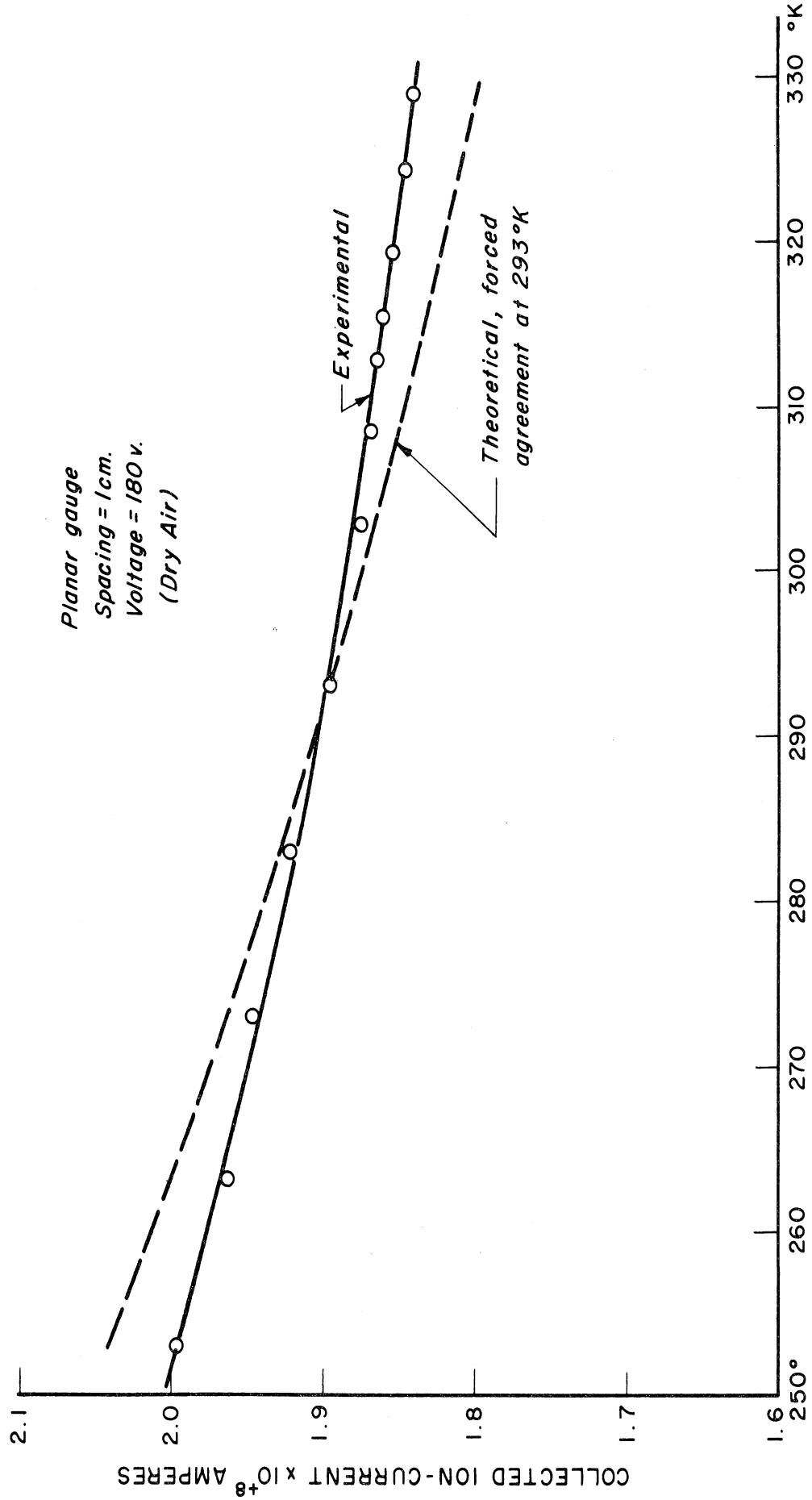

Fig. 4.18. Variation of ionization with temperature under constant density. Theoretical curve (dotted) is fitted with experimental at 293°K.

atures. This is in accord with the observed rise in the peak value of the collected ion current during pump-out period of the previous dynamic test.

In effect, the change of the primary ionization with temperature can be attributed to the influence of thermal agitation on the time of interaction between the ionizing particles and the gas molecules just before producing an ion pair. At constant density, the time of interaction, t, is approximately proportional to $1/c_g$ and hence to $1/\sqrt{T}$, where c_g is the thermal velocity of gas molecules and T, the corresponding temperature. Therefore, the relative change of ionization with temperature is given by

$$\frac{\Delta g}{g} = -\frac{1}{2}\frac{\Delta T}{T} , \qquad (4.2)$$

provided the density of gas is maintained constant. The above relation (shown by a broken line) was found in general agreement with the experimental results (Fig. 4.18). The slight deviation (about in the ratio of 2 to 3) between the slopes of the two lines, however, may be attributed to a probable variation in gas density due to outgassing or adsorption, which may take place, respectively, at high or low temperatures. The important thing is that the experimental curve has the same general shape.

4.5.6. The i-P Characteristic in Mixture of Gases.—It is of interest to compare the theoretical predictions of Section 3.6.4 with some of the experimental results concerning the electric conduction in mixtures of ionized gases. Here, too, only mixtures of nitrogen and oxygen were considered; nitrogen gas was obtained from liquid nitrogen, and tank oxygen was used for the other constituent. This series of experiments was

performed on the previously described planar gauge (Section 4.5.1).

The results obtained by using different proportions of the above two gases are represented in Fig. 4.19. Generally speaking, the experimental curves fall according to the respective gas proportions in the same order as their theoretical counterparts, appearing in Fig. 3.14. However, the all-nitrogen curve shows a major dip in the collected ion current at pressures ranging from about 100 mb to 300 mb at the given electric field intensity. The other curves exhibit the same type of deviation, only to a lesser degree.

A study of the E/P values in this range as represented in Fig. 4.19, or Fig. 4.20 for different plate voltages, revealed some rather striking conclusions. The dip in the collected ion current falls in a range where the field-to-pressure ratios, E/P, have values such that the electron attachment passes through a maximum according to Bloch and Bradbury's theory (see Fig. 2.14). The increase of the attachment rate combined with the low mobility of the resulting ions produce higher negative ion densities. Recombining with the positive ions, which are already there, the negative ions terminate their role as negative charge carriers and thus reduce the collected ion current.

In Fig. 4.21 the corresponding i-P curves were recalculated by using Bradbury's experimental values of δ_e, as given by Fig. 2.12, wherein at low E/P (low electron energies), the extrapolated values of δ_e were used. The new i-P curves fail to show the type of dip being discussed.

Thus these results not only explain the observed dip in the i-P curves,

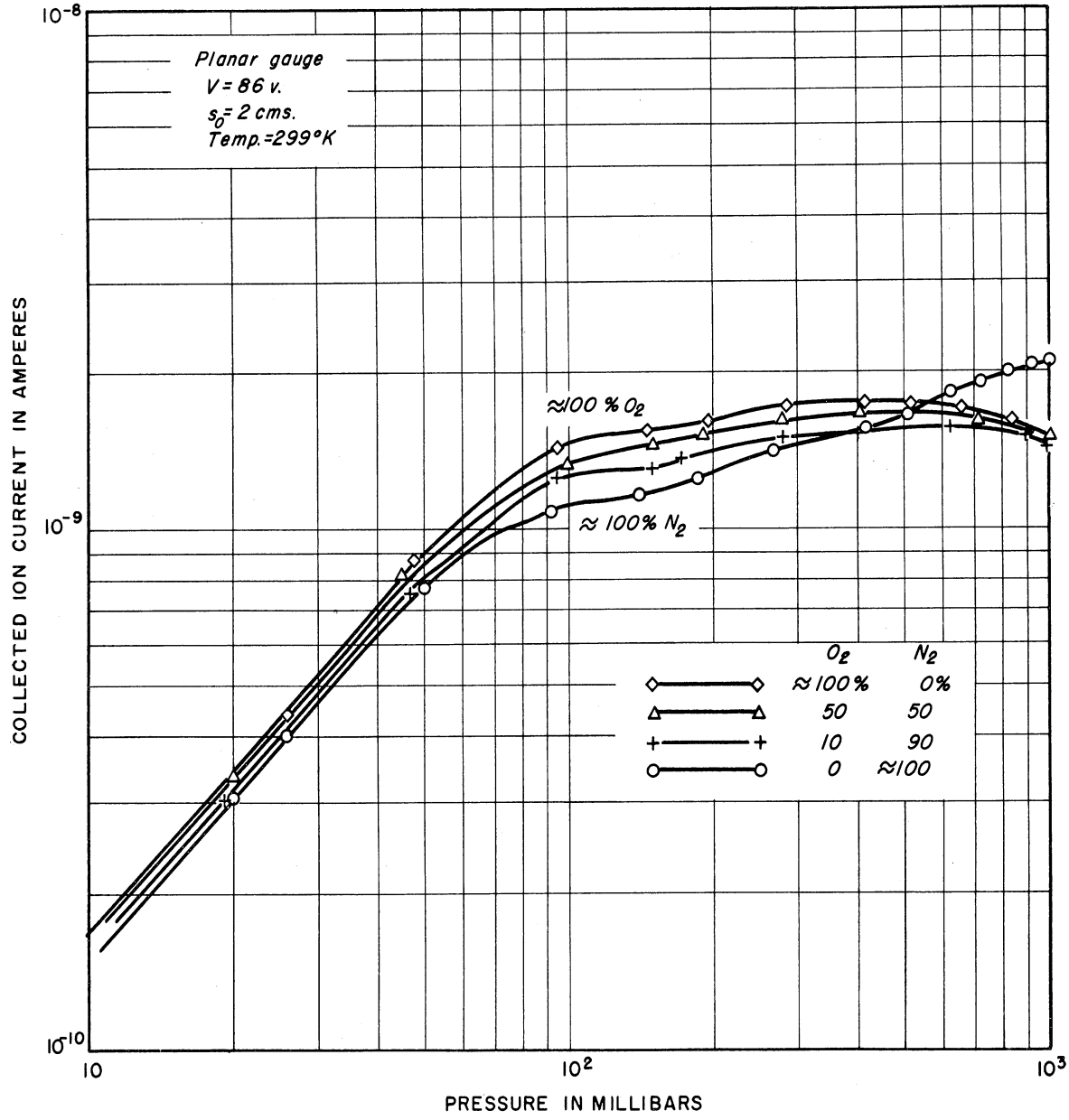

Fig. 4.19. Experimental i-P curves for different mixtures of nitrogen and oxygen at room temperature—planar gauge.

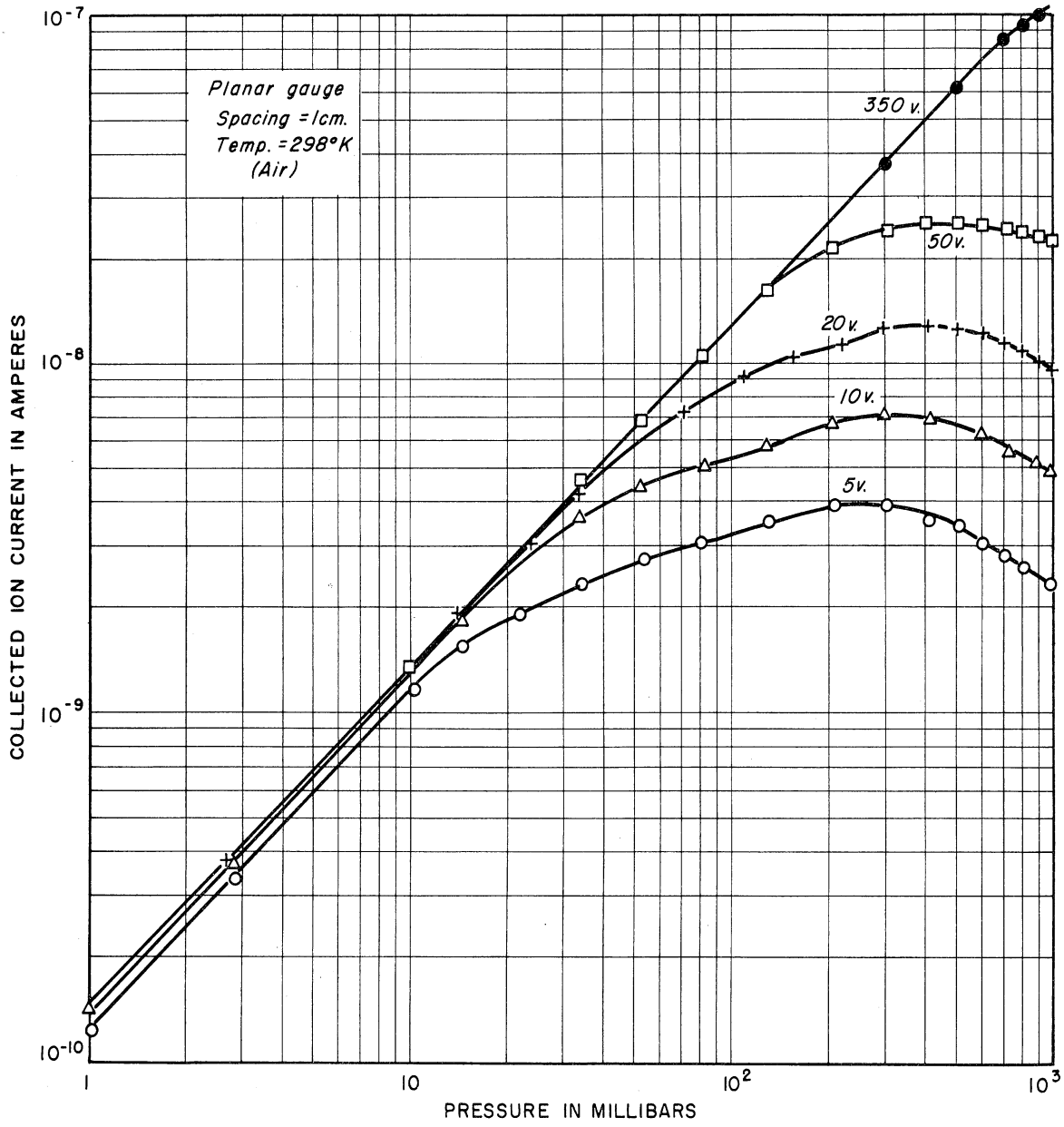

Fig. 4.20. Variation of recombination dip with plate voltage.

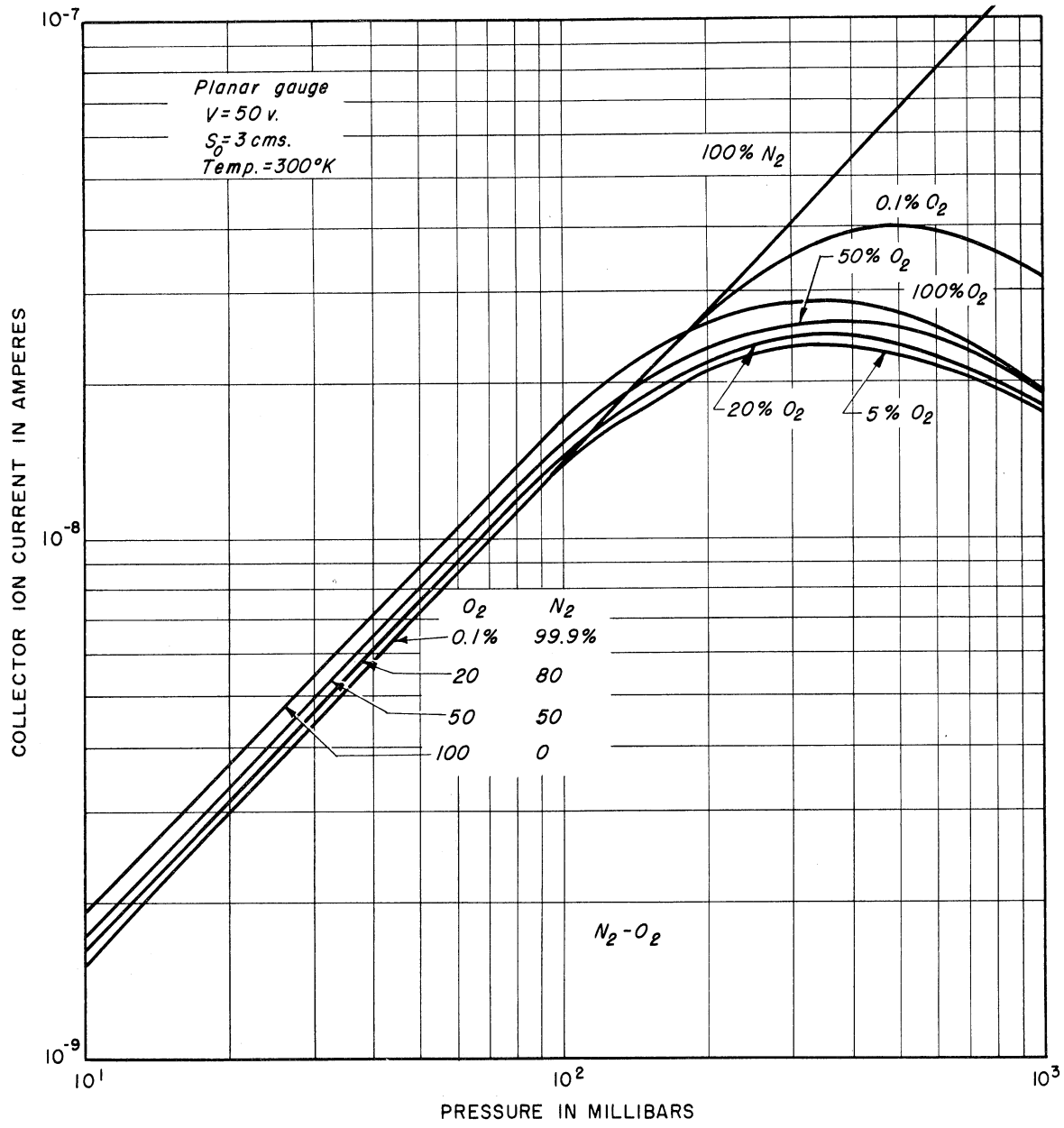

Fig. 4.21. Theoretical i-P curves for several mixtures of nitrogen and oxygen using Bradbury's experimental values of δ_e.

but could also be taken as evidence in favor of Bloch and Bradbury's theory of electron attachment in diatomic molecules.[39] They confirm the steep rise of the attachment coefficient, δ_e, at low energies and point to the existence of a peak value as predicted by the theory, and illustrated in Fig. 2.13. The general agreement between the theoretical results of Fig. 3.14 and the experimental of Fig. 4.19 also supports the validity of the approximate analysis presented in Chapter III.

4.6. DESCRIPTION OF TWO PROTOTYPE RADIOACTIVE IONIZATION GAUGES

In an effort to realize a radioactive ionization pressure gauge suitable for rocket measurements, two different gauges were designed in the light of knowledge and experience gained in the studies reported above. In designing such a device, one must consider the operating limitations imposed by the rigors of a rocket flight. Consequently, these gauges should meet the following requirements:

1. Adequate output current for measurement by ordinary d-c electrometer.
2. Linear response at least within the required range of measurements.
3. Short response time for transporting gas out of or into the gauge; the chamber volume should consequently be kept to a minimum.
4. Large area-to-volume ratio to facilitate adequate accommodation coefficient.

Consideration of the above requirements led to the design of two successfully used gauges. In one, alpha particles from radium alloy were the ionizing agents; in the other, beta particles from a tritium source were used. Each gauge is briefly described below.

4.6.1. Radium Prototype Gauge.—The first gauge, which was designed for the use of radium as the ionization source, had a basically planar configuration in which the source formed one of the plates (the positive electrode), and the ion collector, the other electrode. The main constructional details of this gauge are shown in Fig. 4.22.

It was possible, with this arrangement, to achieve an almost linear response between 300 and 1 x 10^{-1} mb, pressures attained typically in the rocket experiment at altitudes of approximately 15 and 80 km. It is clear from Fig. 4.23 that the gauge is still useful at lower altitudes (higher densities), but with some sacrifice in the linearity and consequently a reduction of the output current due to the loss of some ions by recombination.

The linearity of the resulting i-P characteristic could have been extended up to atmospheric pressure ($\approx$ 1000 mb) by applying a higher voltage. This practice was not adopted on account of the gas amplification by electron collision which would occur at low pressures in the presence of high accelerating fields. The voltage between the plates, however, could have been varied so as to maintain a linear response throughout the range of interest. However, the data below 10 km were not sufficiently important to the experimental program to justify the

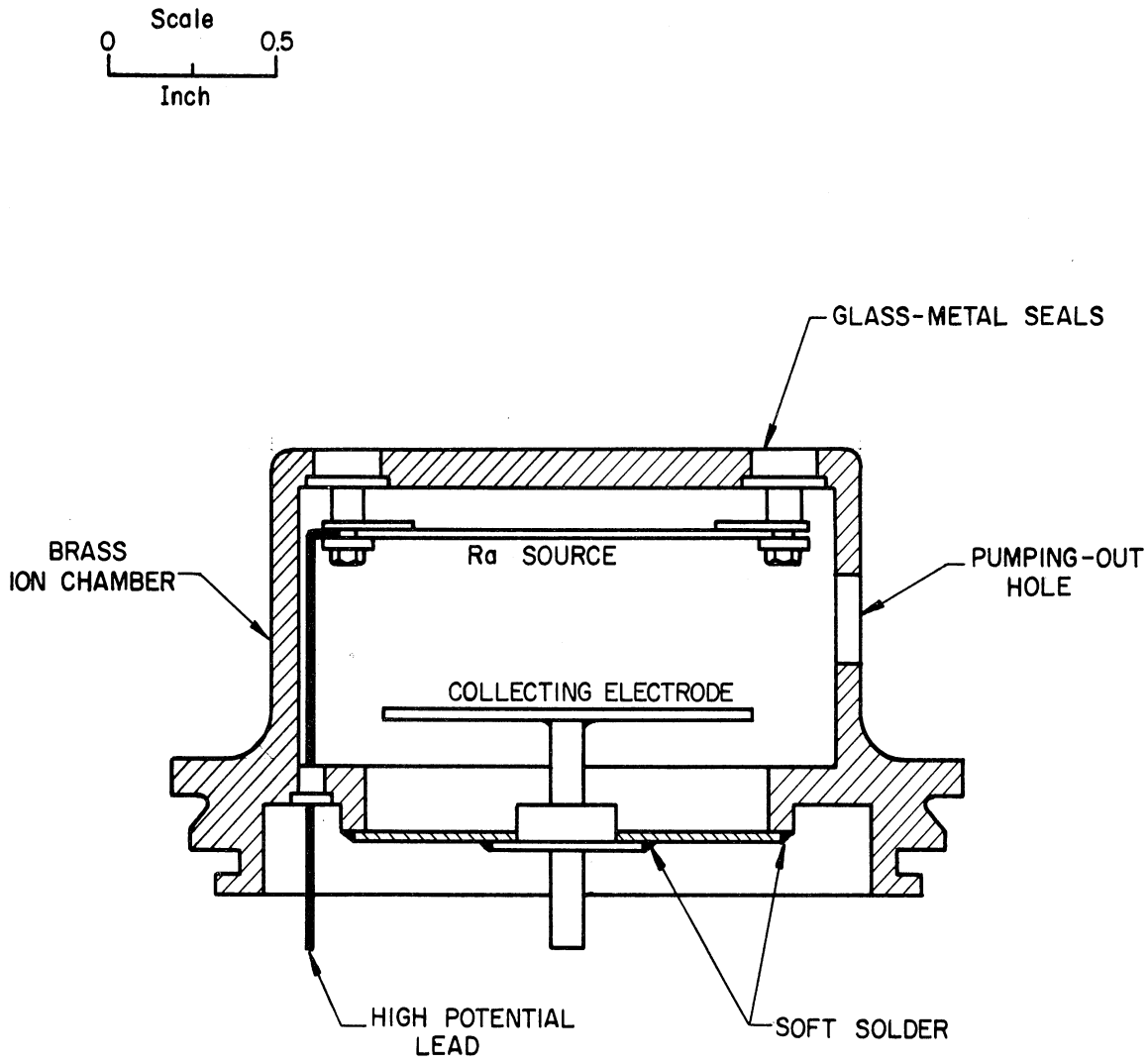

Fig. 4.22. Radium prototype gauge.

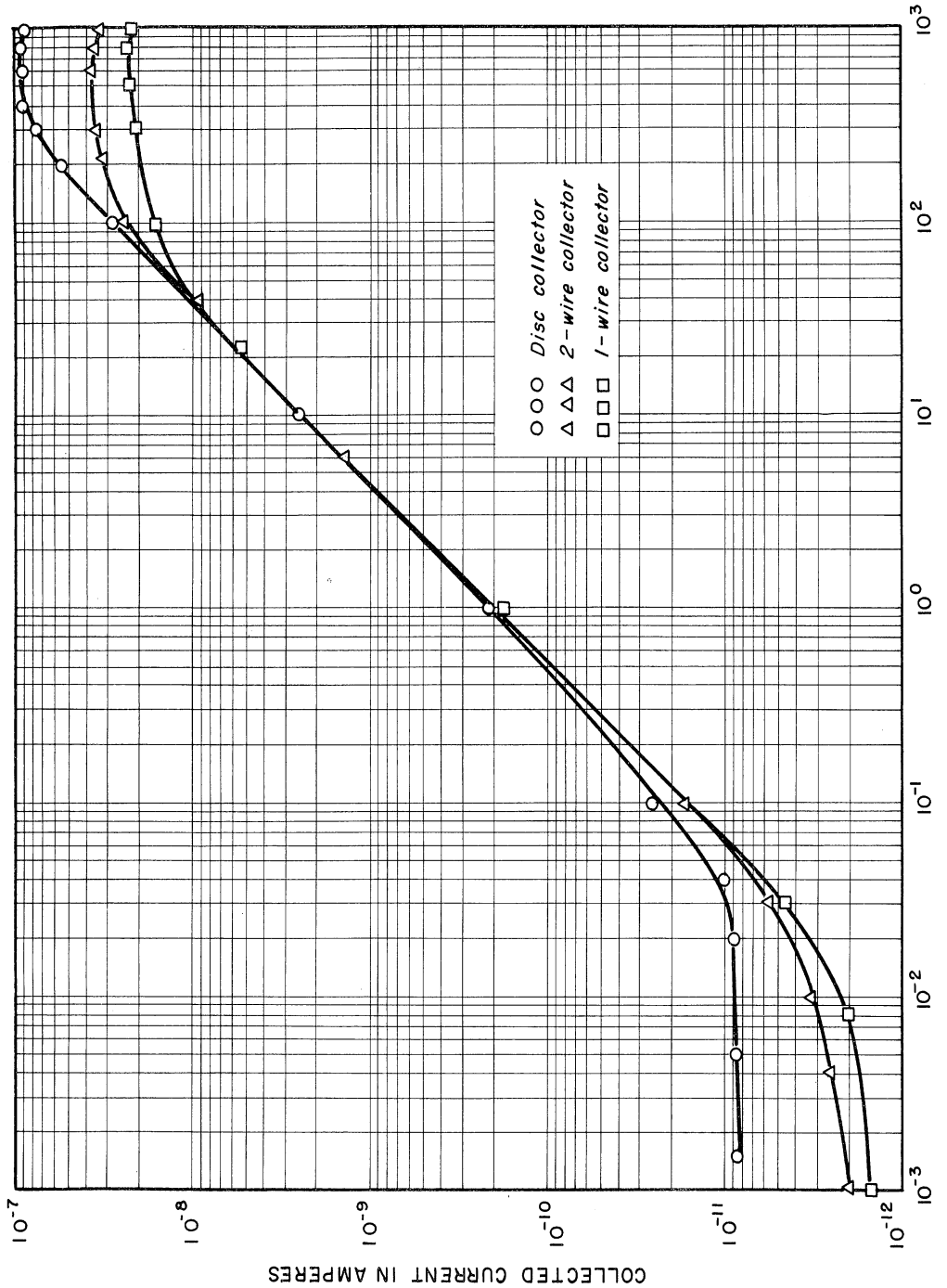

Fig. 4.23. Typical i-P curves for radium prototype gauge.

complexity that such voltage adjustment would require in the associated circuits. Of course, the gauge sensitivity might have been increased by the use of sources of higher intensity, but possible improvement would be limited chiefly to the high-pressure range, since an increase in radiation often offsets the lowest measurable pressure as a result of the relatively high dark current produced. Another drawback in using a stronger radium source would be the gamma radiation from this source, which would constitute a health hazard. This is completely eliminated in the gauge next described, in which the tritium source, (H^3), emits beta particles only.

4.6.2. Tritium Prototype Gauge.—As stated above, the radium gauge was useful only for altitudes up to about 80 km. The carrying rockets, however, were capable of attaining altitudes of about 150 or 200 km, the lower altitude for the Nike-Cajun type, and the higher for the Aerobee. It was naturally desirable to extend the useful range of the radioactive prototype gauge to higher altitudes. This required an increase in the current sensitivity at higher altitudes (lower pressures) with less dark current effect.

These requirements, as well as those discussed in the previous section for the planar radium gauge, were realized to a substantial degree in the new design illustrated in Fig. 4.24, which shows a completed chamber with an attached low-leakage ceramic wafer and associated high-megohm resistors.[2]

Here tritium was adopted as a source material. Tritium is a high-

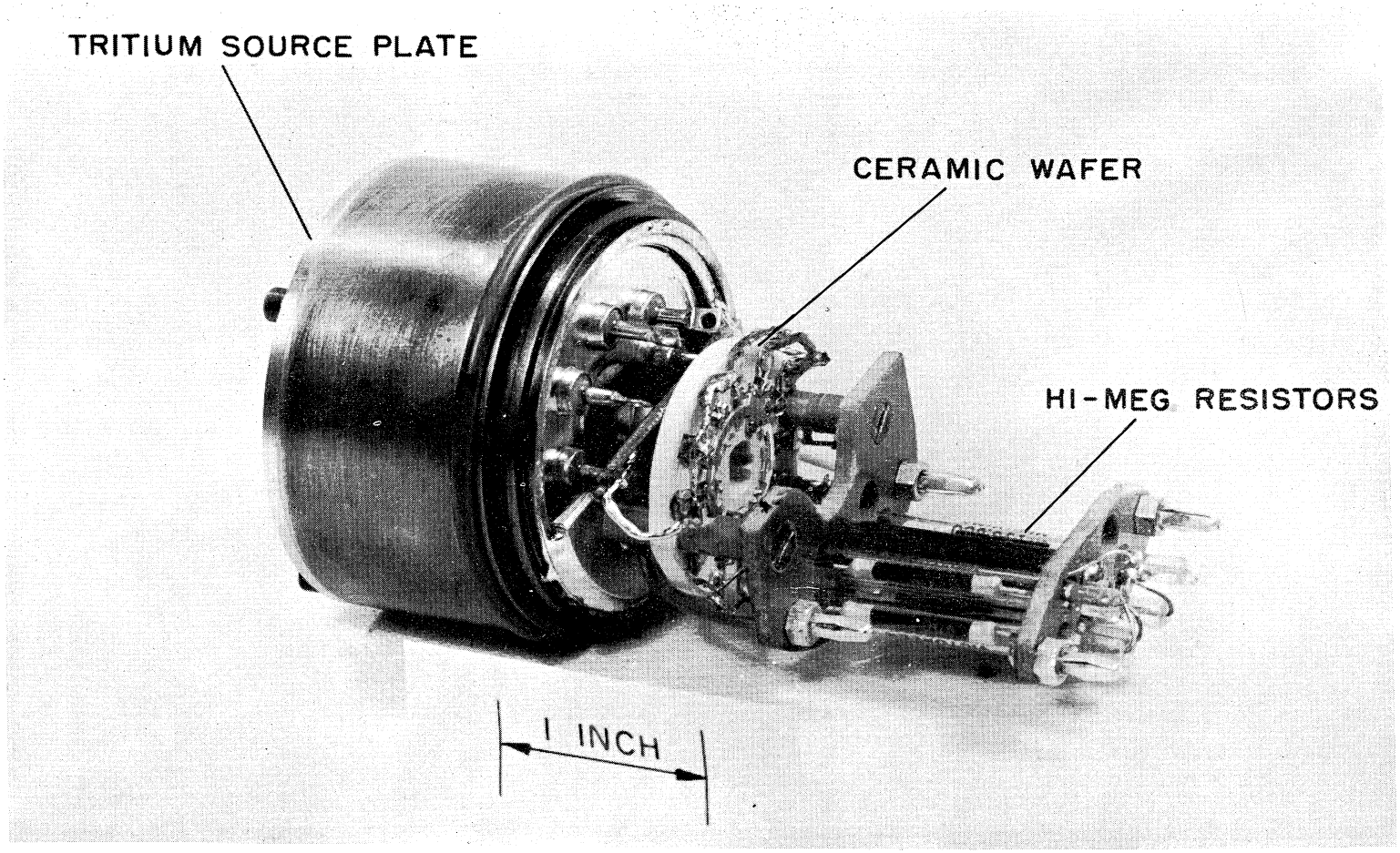

Fig. 4.24. Assembled ionization chamber with attached low-leakage wafer and high-megohm resistors.

activity beta source, emitting 18-kev electrons and no gamma radiation. It has a half-life of twelve years, which is long enough so that calibration is adequately constant. This is very desirable for the present application. Under normal conditions tritium exists as a gas, which readily combines with titanium to become solid titanium tritide. Figure 4.25 shows the titanium-tritide—stainless-steel foil source secured to an ionization-chamber end plate. It was estimated from chamber measurements that an effective activity of approximately 1 curie per square inch (1 curie = 3.7×10^{10} disintegrations per second) was attained.

The physical aspects of the ionization chamber are shown in Figs. 4.24 - 4.29. The chamber consists of an outer stainless-steel cylinder closed at the bottom by a disc carrying several glass-to-metal seals to provide for external electrical connections and element assembly mounting. The top is closed by the source-bearing end plate, fastened by four screws.

Internally the gauge consists of a cylindrical polarizing electrode (Fig. 4.27) and a collector assembly (Fig. 4.28) which supports two collectors, one for the high-pressure end of the range, the other for the low-pressure end. The source faces the open end of the polarizing cylinder, directly adjacent to the high-pressure collector, which is the circularly formed wire shown in Fig. 4.29. This collector is supported on two glass-to-metal seals, which in turn are supported by a bridge which spans the open end of the polarizing electrode. The low-pressure collector is supported by another glass-to-metal seal in the center of

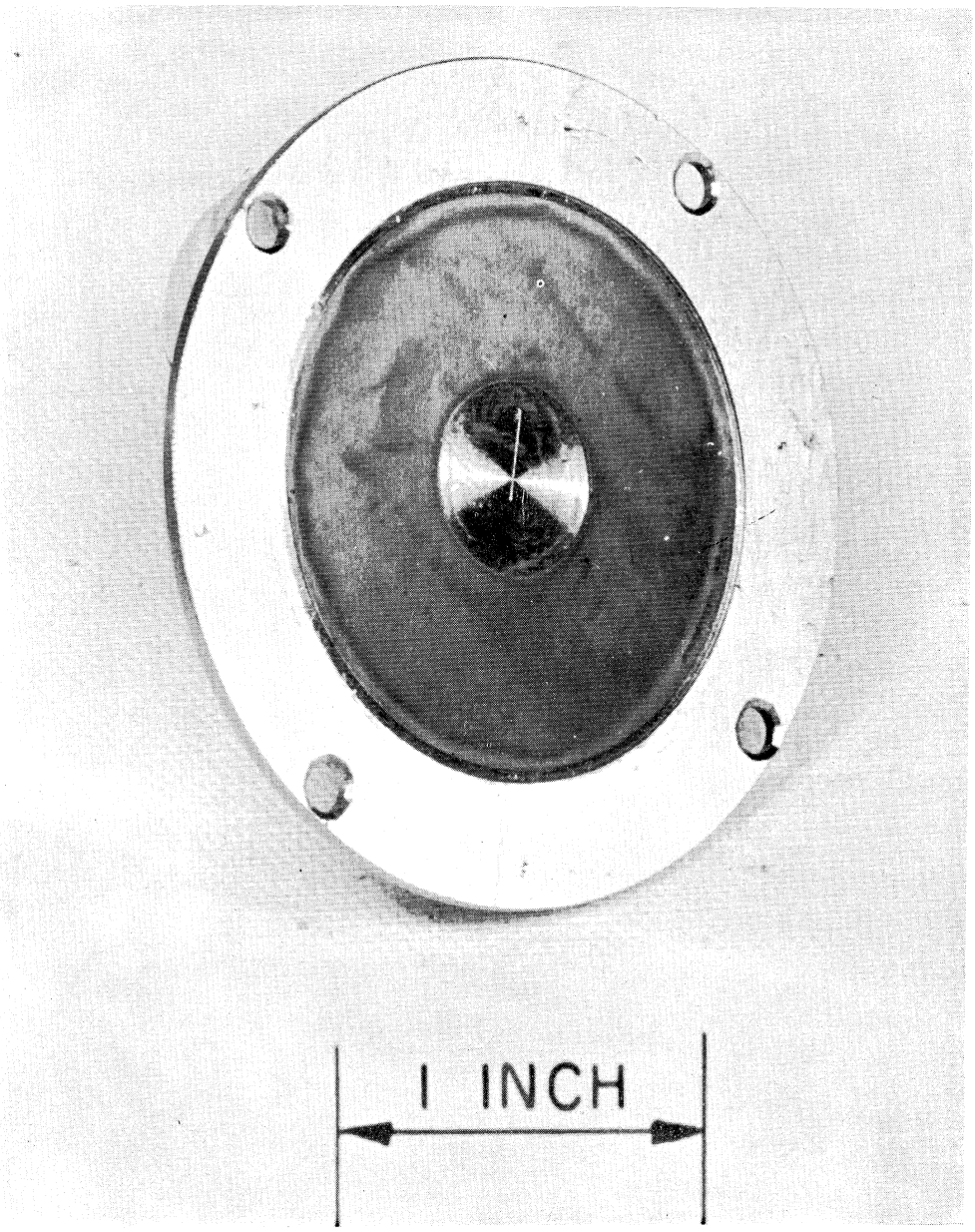

Fig. 4.25. End plate of ionization chamber showing titanium tritide source.

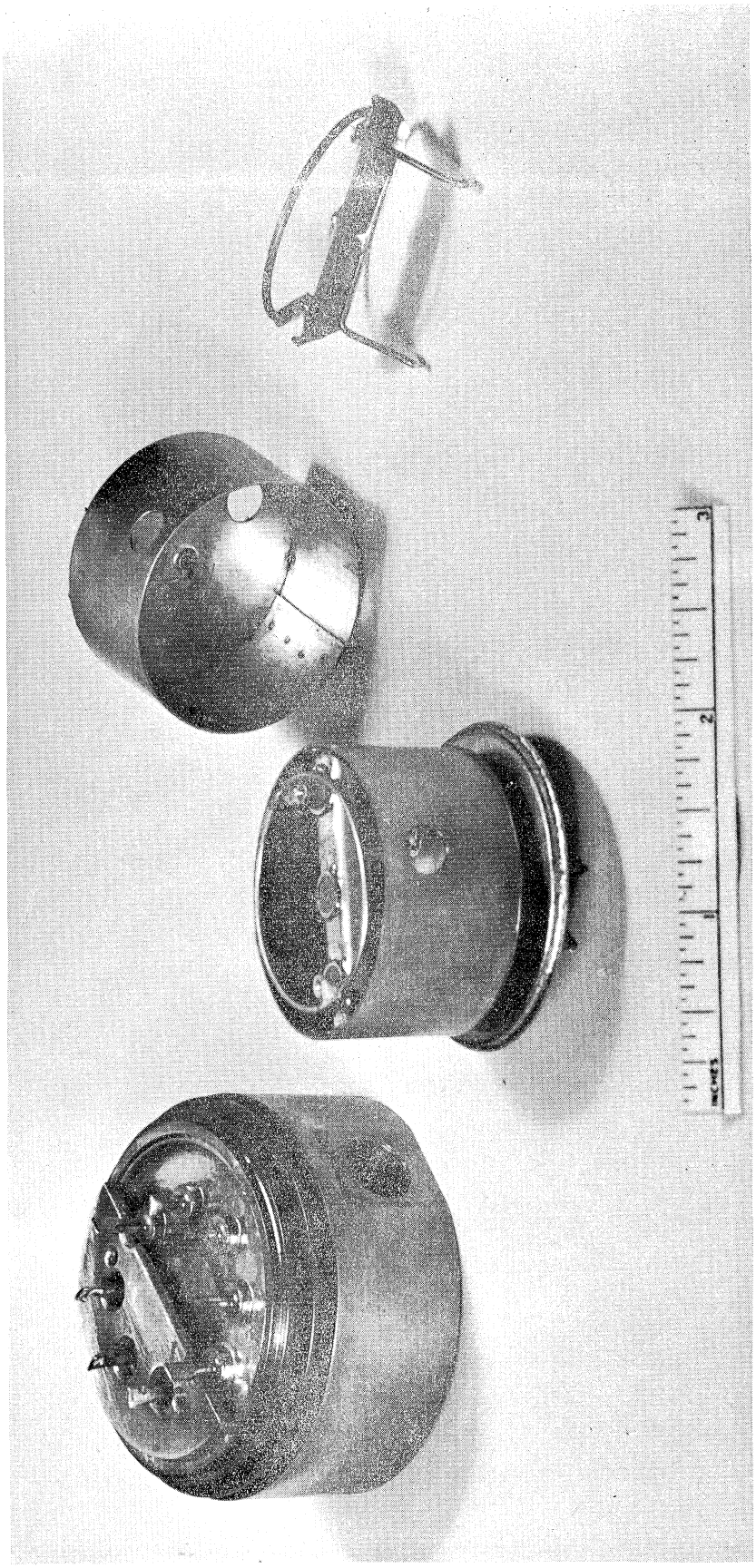

Fig. 4.26. Ionization-chamber elements.

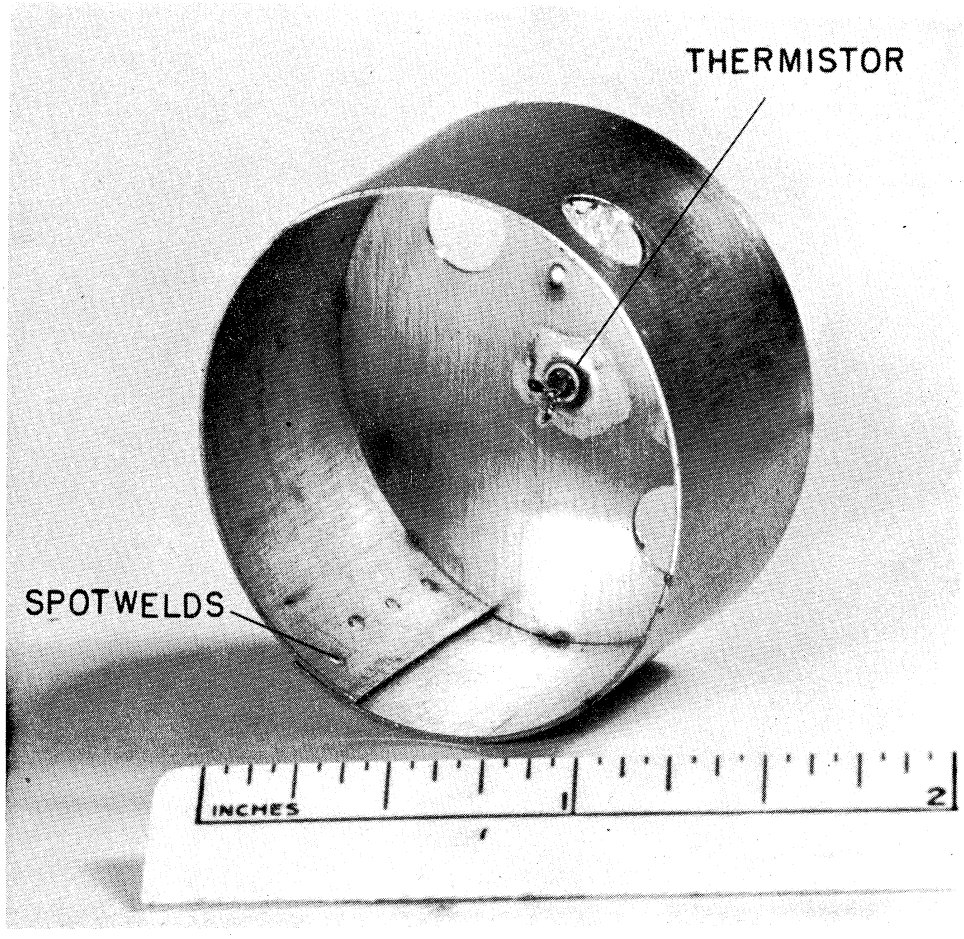

Fig. 4.27. Ionization-chamber polarizing electrode.

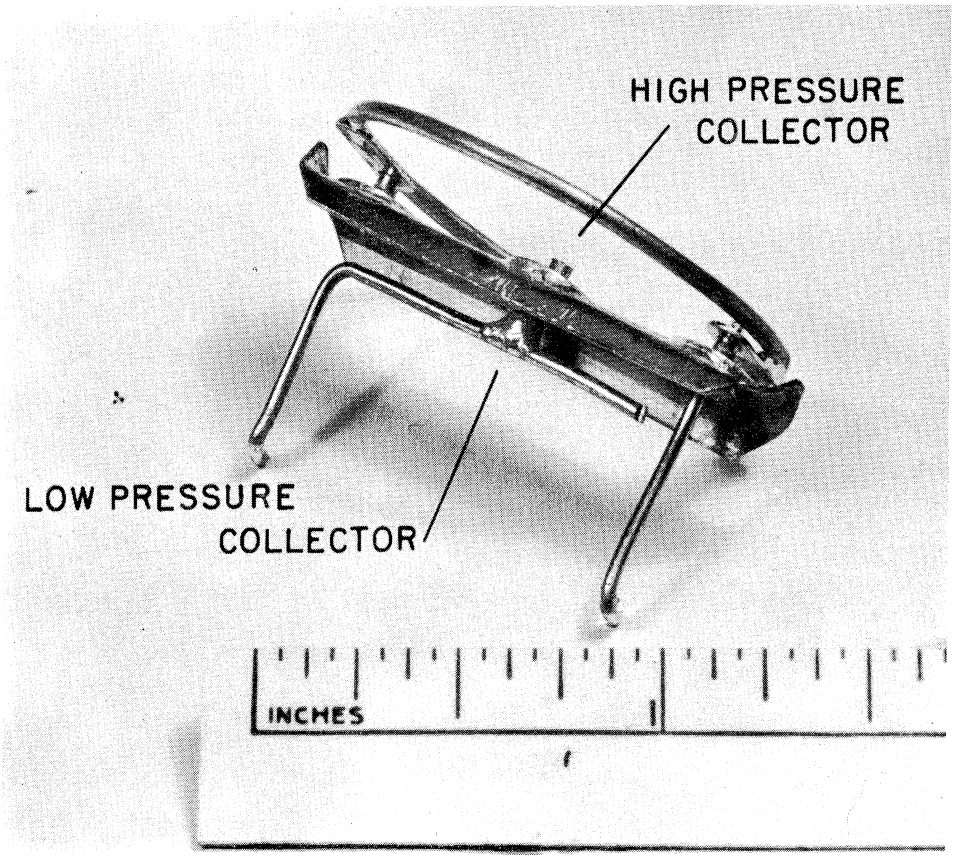

Fig. 4.28. Ionization-chamber collector assembly.

Fig. 4.29. Ionization-chamber element assembly.

the bridge, and is shielded from direct source radiation by the bridge itself. The area of this collector is also minimized to reduce electron emission that occurs due to X-ray radiation from the surface of the polarizing cylinder under the influence of the impinging beta particles as discussed above. These precautions substantially reduced the dark current, thus extending the gauge applicability to lower pressures.

The relatively low energy of the ionizing particles means that their path length in air decreases sharply as the density increases. Thus at higher densities, little ionization is produced in the vicinity of the low-pressure collector, so that an alternative collector near the source must be employed. Thus the chamber is provided with both a low- and high-pressure collector. They are proportioned so that in their linear region, near 1 mb, the currents are roughly equivalent, eliminating a step when changing from one to the other. Typical i-P characteristics of each are shown in Fig. 4.30, and a compositive curve, in Fig. 4.31.

The chamber elements are fashioned from stainless steel; spot welding is employed in the assembly of the structure. Two thermistors are usually employed during flight measurements, one in air, visible in Fig. 4.27, the other held in a small depression in the outside of the polarizing electrode end plate; the depression is visible in Fig. 4.27. These thermistors permit the gas temperature in the chamber to be estimated.

The above gauge proved to be adequate for pressure measurements up to altitudes of about 100 km, beyond which the mean free path of the gas particles becomes long with respect to the gauge dimensions. This would

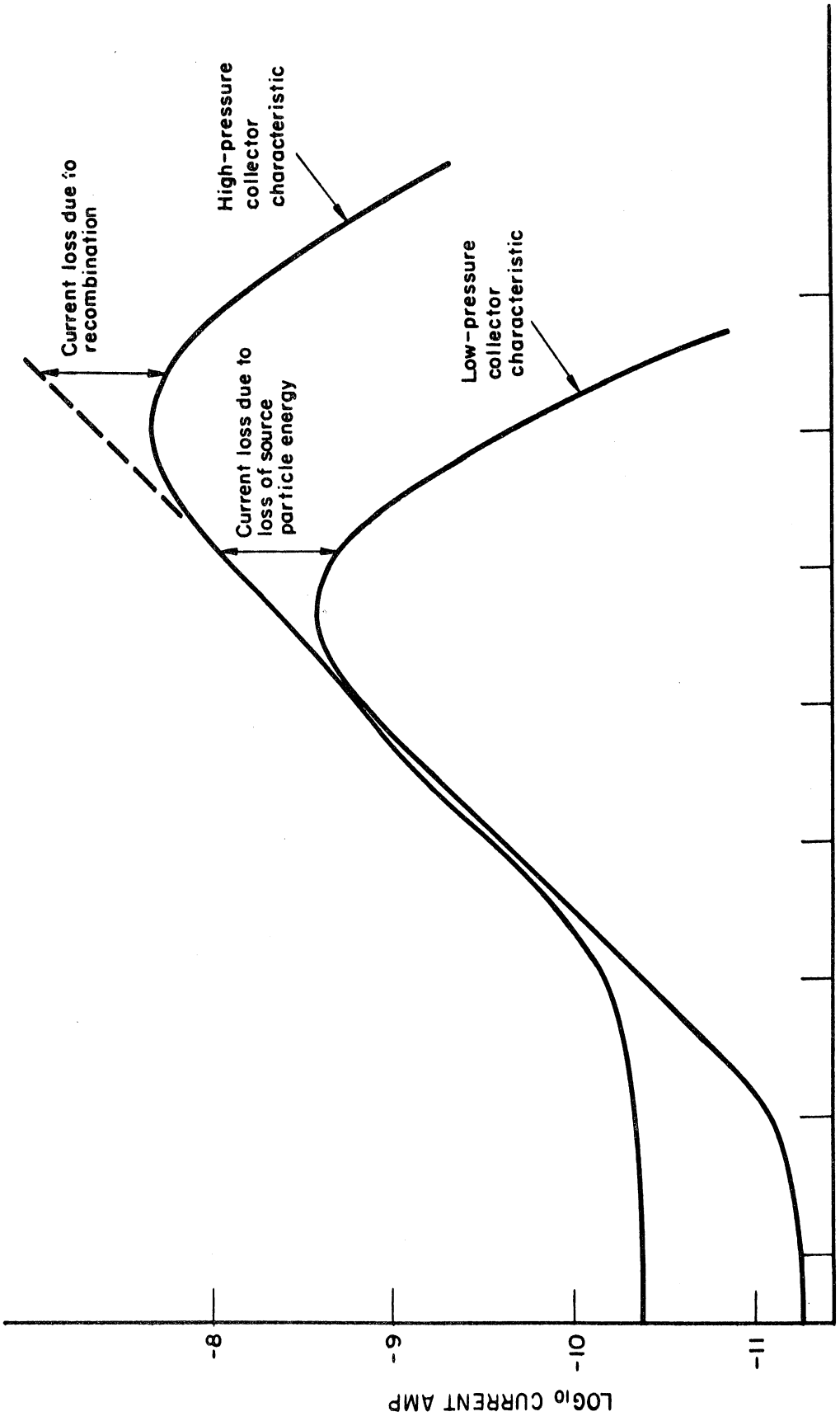

Fig. 4.30. i-P curve of typical ionization chamber showing low-pressure and high-pressure characteristics.

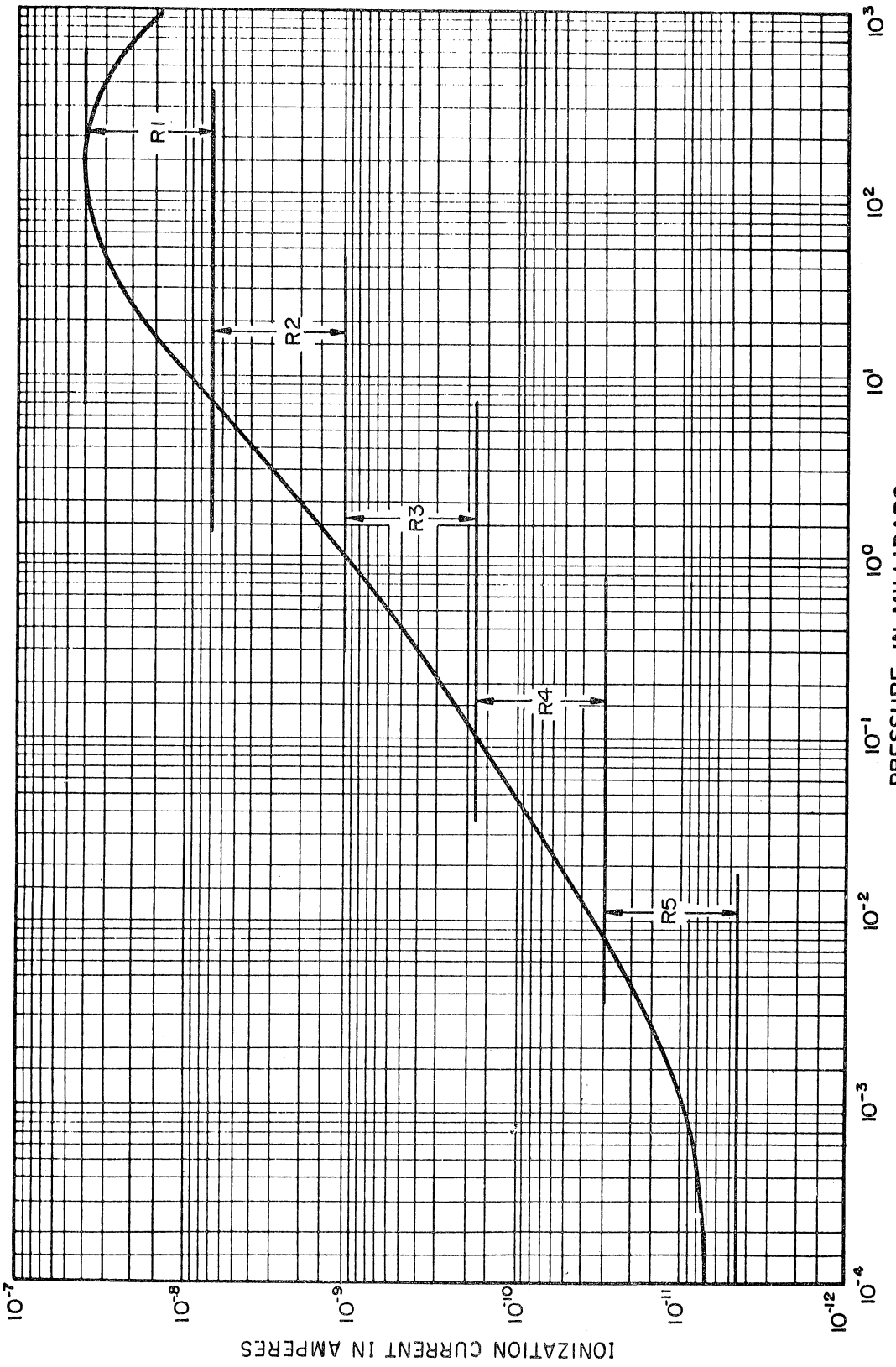

Fig. 4.31. Typical composite i-P curve for ionization chamber showing corresponding load resistances.

require a quite different method of interpreting measurements from the one employed in the instrumentation dealt with here.

4.6.3. The Amplifier.—A detailed description of the amplifier, switching circuit, and power supply can be found in Ref. 2. A schematic diagram of the amplifier section is shown in Fig. 4.32. The amplifier consists of three direct-coupled stages with an electrometer input and a cathode follower output. The ionization current (ranging from 10^{-12} to 10^{-8} amp) passes through the appropriate high-megohm resistor, causing a voltage drop which appears as a portion of the voltage in the feedback loop of the amplifier for which the feedback factor is unity. Thus a voltage change effected at the output of the amplifier is nearly equivalent in magnitude to the voltage change across the high-megohm resistor but opposite in sense. The amplifier, therefore, acts as an impedance matching device.

The complete schematic and assembly are shown in Figs. 4.33 and 4.34, respectively.

4.7. THE VACUUM SYSTEM

Figures 4.35 and 4.36 show the vacuum system used to determine the previous experimental data and to calibrate the prototype radioactive ionization pressure gauges. The system was capable of producing and enabling the measurement of a wide range of pressures from about 10^{-6} mb to atmospheric (1013 mb).

The vacuum system consisted of mechanical pumps, an oil diffusion

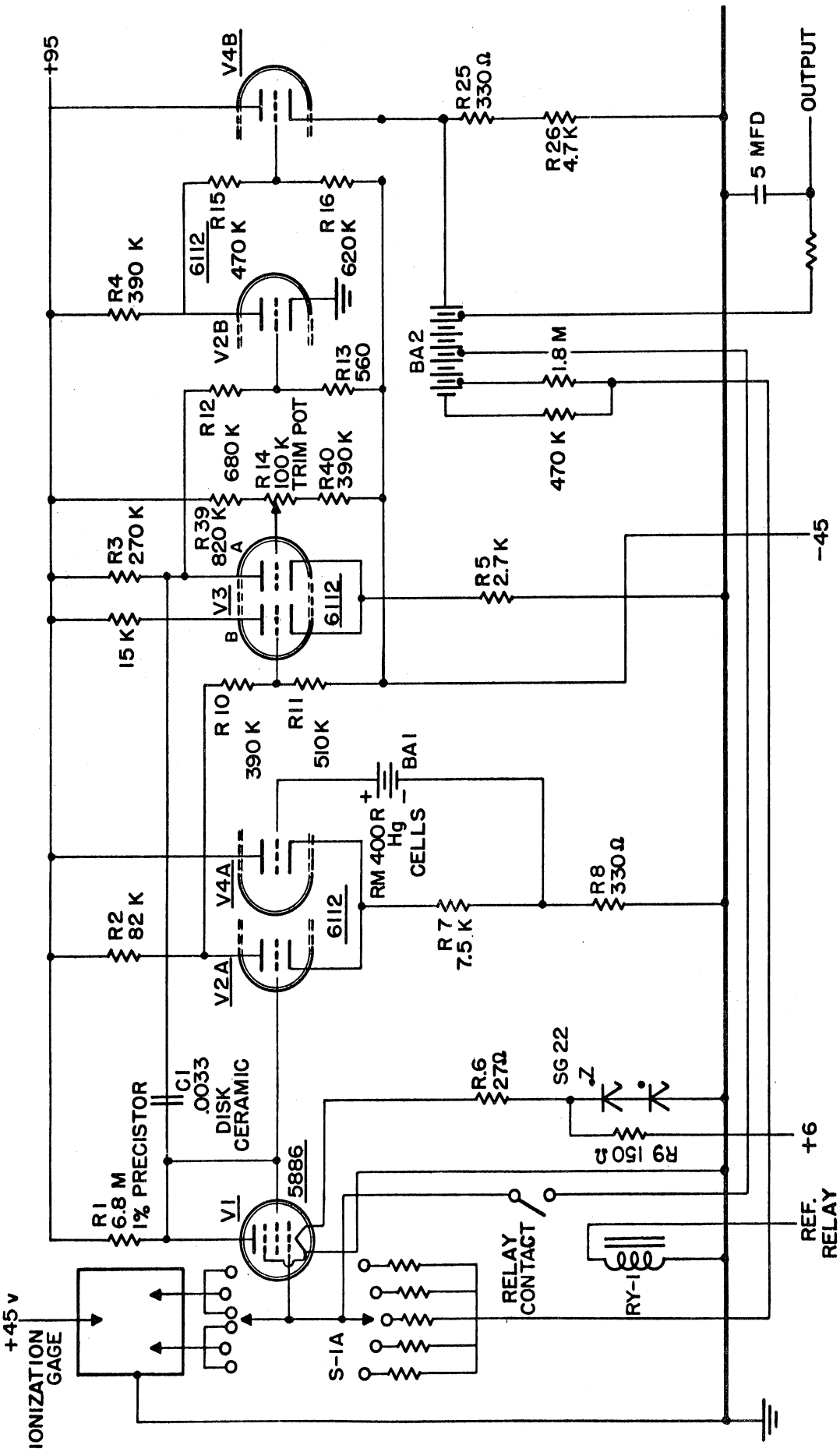

Fig. 4.32. Amplifier schematic diagram.

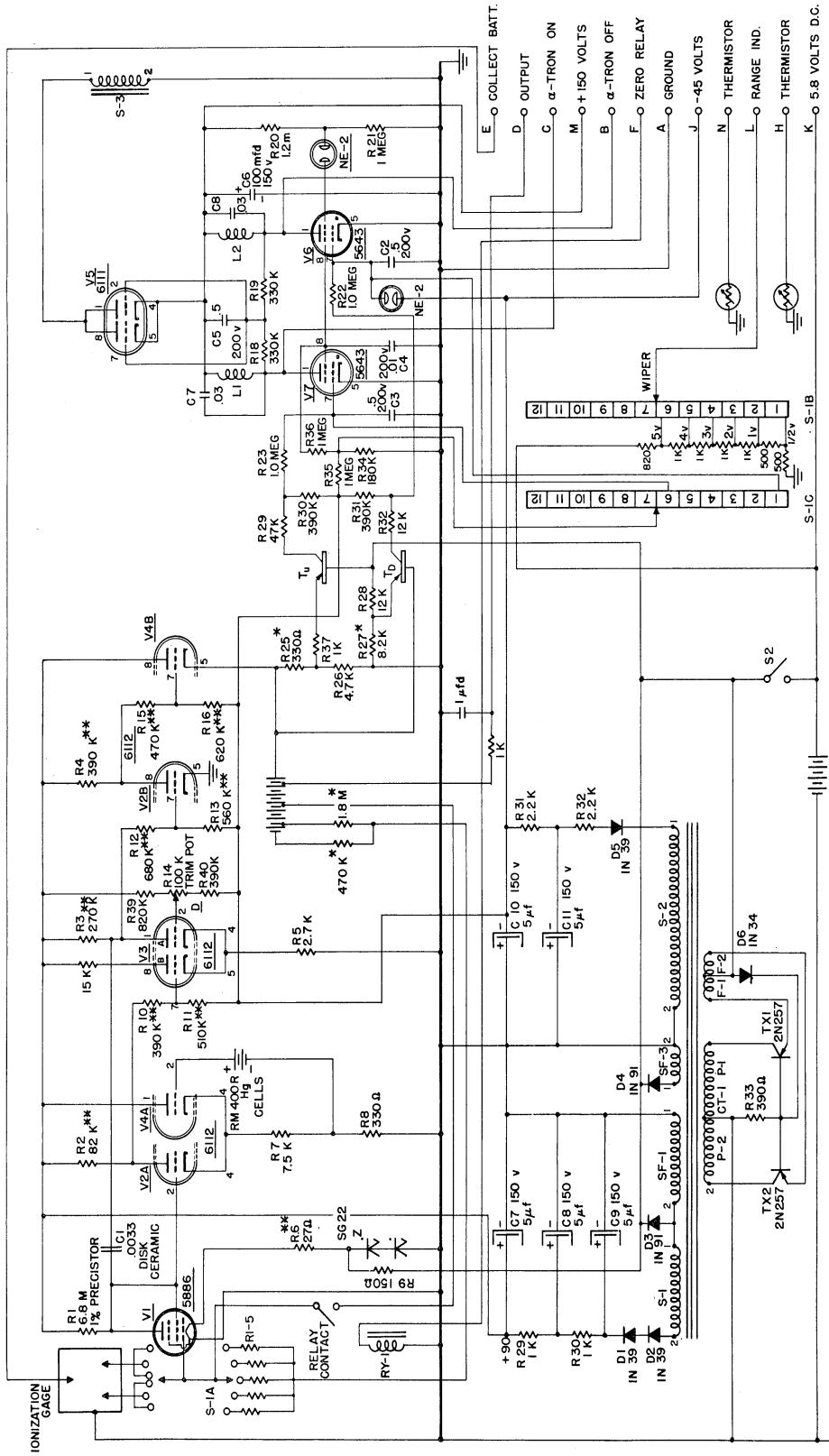

Fig. 4.33. System schematic diagram.

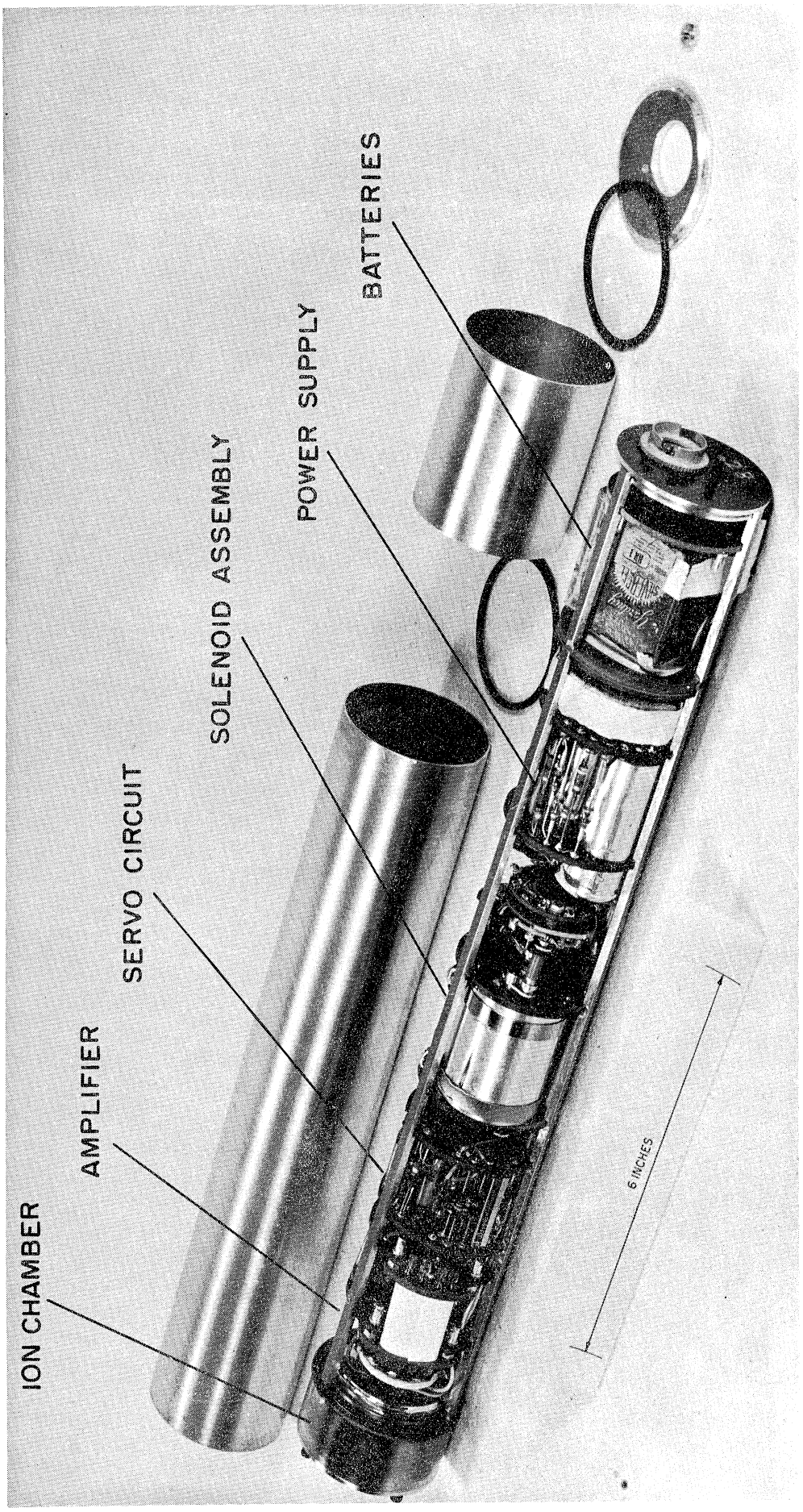

Fig. 4.34. Complete system out of enclosing tubing.

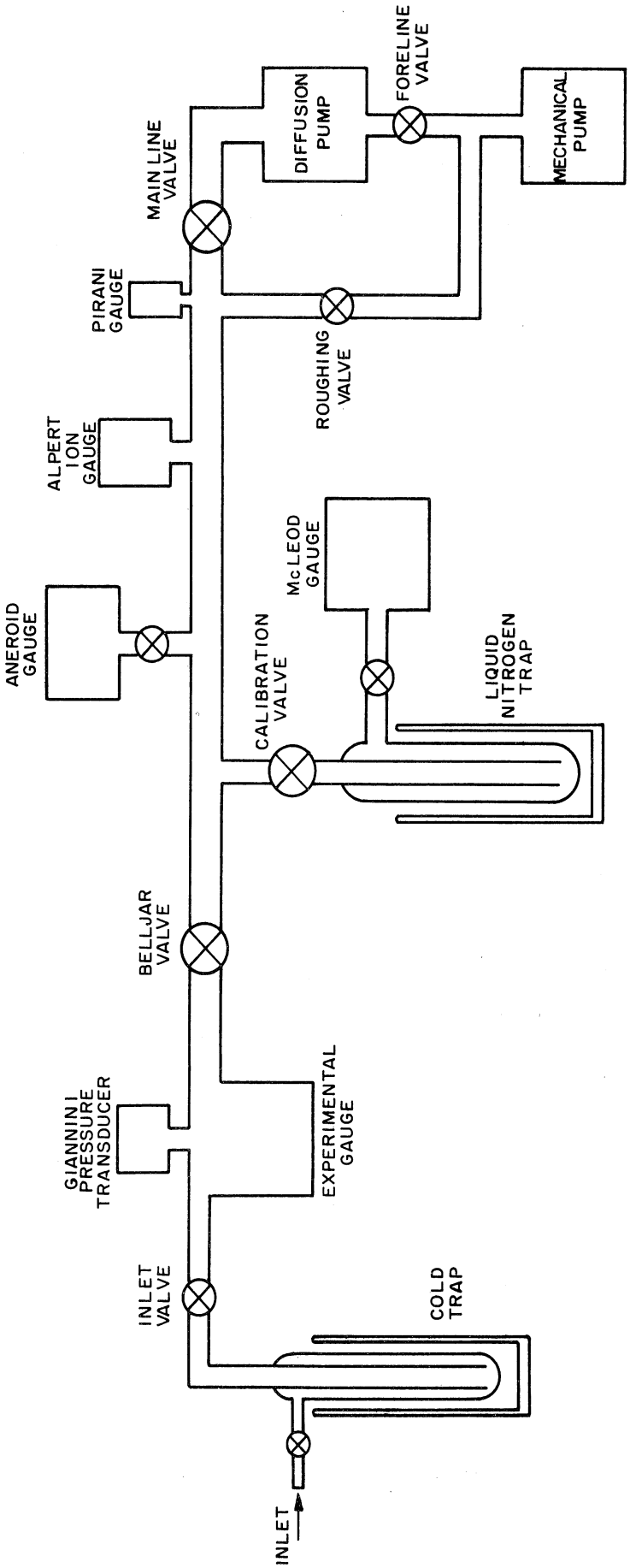

Fig. 4.35. Vacuum system layout.

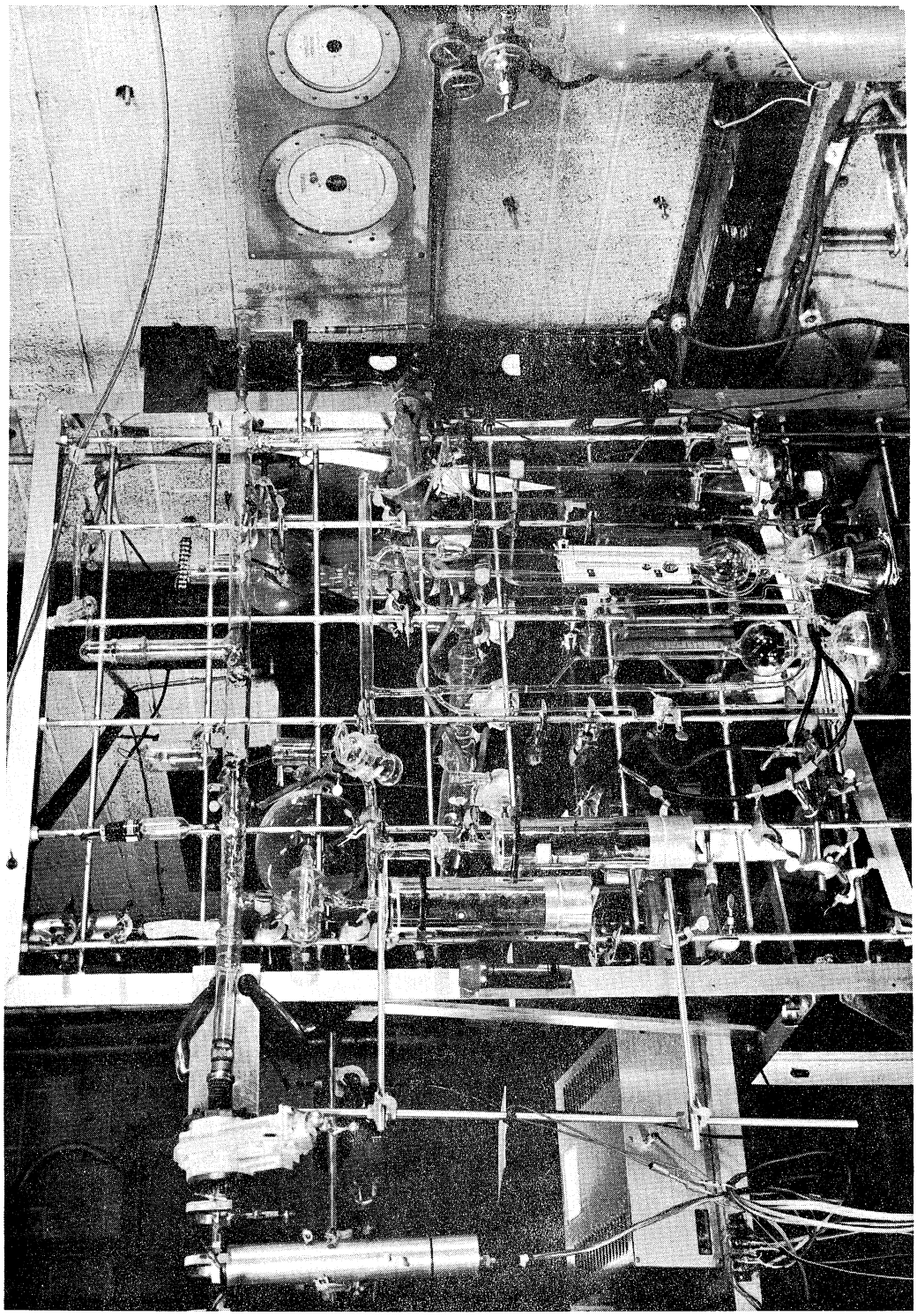

Fig. 4.36. Vacuum system used for calibrating pressure-measurement system.

pump, and a number of different types of pressure-measuring devices. It was also equipped with typical accessories for rough pressure indication, protection in the event of glass breakage, air dryer inlets, and cold traps.

For pressures lower than 10^{-3} mb, an Alpert ion gage was employed, whereas a three-range McLeod gauge served for pressures between 10^{-3} mb and 5 mb. Two Wallace and Tiernen aneroid gauges were used to cover pressures greater than 1 mb.

CHAPTER V

CONCLUSIONS

An analytical as well as an experimental study of a radioactive ionization pressure gauge has been made in an effort to acquire a better understanding of the properties of such a device in measuring pressure. Some of the conclusions drawn have a direct bearing on the particular gauge under investigation; other conclusions, although closely related to the gauge, are also of general interest. These conclusions are summarized below.

1. An approximate relationship between the ionization current and the gas pressure, developed analytically for a planar radioactive ionization gauge, and taking into consideration the variation of electron attachment as a function of field-to-pressure ratio, was found to be in general agreement with experiment, thus verifying the validity of the assumptions made there.
2. There is a strong indication that the hysteresis phenomenon may be caused by one or both of the following factors:
   a. The temperature dependence of the main electronic processes inside the gauge.
   b. A variation in the environmental conditions which may result in a change in the composion of the

present electronegative gases.

3. The primary ionization in a gauge varies with the temperature of a gas under constant density. The variation is such that more ionization current is collected with decreasing temperature.

4. The planar gauge used would be a useful tool in the study of ionization by electron collisions in gases.

5. Some of the experimental results obtained confirm the existence of a peak value for electron attachment at low energies, as predicted theoretically by Bloch and Bradbury for diatomic molecules.

APPENDIX

ANALYTICAL INVESTIGATION OF SOURCE STABILITY

The disintegration of radium and its decay products results in the emission of alpha, beta, and gamma rays which, in their passage through gases, produce ionization. The specific ionization varies greatly for the three products, roughly in the ratio 10,000 : 100 : 1, respectively. We need, therefore, concern ourselves with the alpha particles only.

The successive transformations of radium and its decay products are illustrated in Fig. A.1 which shows the type and range, in standard air, of particles emitted, as well as the half-life time of the successive elements. All the decay products of radium (Ra) are solid substances except radon (Rn) which is gaseous under normal conditions.

CASE I

Since the half-life time of disintegration of radium is considerably long (1620 years), it is perfectly justifiable to assume that, for an interval of a few days, the disintegration of radium (Ra) takes place at a constant rate, n_o particles per second. This also means that radon gas is emanating from radium at the same rate, n_o particles per second.

It is known that the rate of disintegration of any radioactive material depends on the amount as well as the kind of material. This could be expressed as

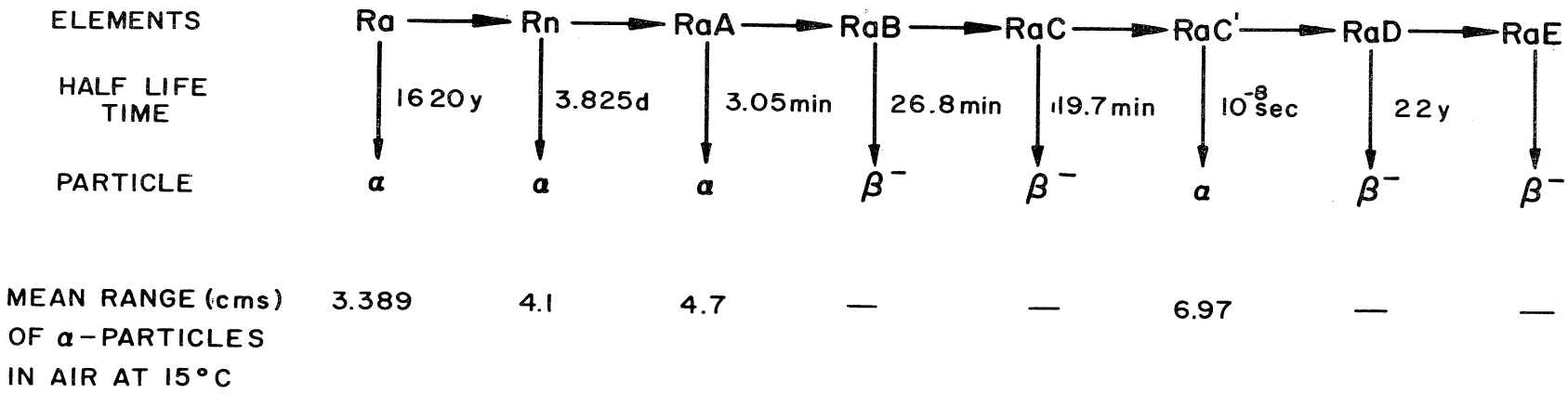

Fig. A.1. Radioactive transformation of radium and its decay products.

$$\frac{dN}{dt} = -\lambda N \quad ,$$

where N is the number of particles at any instant, t, and λ is the decay constant, a characteristic of each element and independent of all physical and chemical conditions.

The net change of radon (dp) in an interval dt is then given by

$$dp = (n_o - \lambda_1 p)\, dt \quad ,$$

or

$$\frac{dp}{dt} + \lambda_1 p = n_o \quad ,$$

where p is the amount of radon present at any instant and λ_1 is the characteristic constant for the same material. Assuming radon was initially absent, then p is given by

$$p = \frac{n_o}{\lambda_1}(1 - e^{-\lambda_1 t}) \quad .$$

Similarly for Ra A

$$\frac{dq}{dt} = \lambda_1 p - \lambda_2 q \quad ,$$

where q is the amount of Ra A at any instant and λ_2 is the characteristic constant of Ra A.

Substituting for p and transposing, we get

$$\frac{dq}{dt} + \lambda_2 q = n_o (1 - e^{-\lambda_1 t}) \quad .$$

Considering Ra A initially absent, then the solution for q is

$$q = \frac{n_o}{\lambda_2} - \frac{n_o}{\lambda_2 - \lambda_1} e^{-\lambda_1 t} - \frac{n_o \lambda_1}{\lambda_2(\lambda_1 - \lambda_2)} e^{-\lambda_2 t} \quad .$$

In the same way the values of Ra B and Ra C are, respectively,

$$r = \frac{n_0}{\lambda_3} - \frac{n_0 \lambda_2}{(\lambda_2-\lambda_1)(\lambda_3-\lambda_1)} e^{-\lambda_1 t} - \frac{n_0 \lambda_1}{(\lambda_1-\lambda_2)(\lambda_3-\lambda_2)} e^{-\lambda_2 t} - \frac{n_0 \lambda_1 \lambda_2}{\lambda_3(\lambda_1-\lambda_3)(\lambda_2-\lambda_3)} e^{-\lambda_3 t}$$

and

$$s = \frac{n_0}{\lambda_4} - \frac{n_0 \lambda_2 \lambda_3}{(\lambda_2-\lambda_1)(\lambda_3-\lambda_1)(\lambda_4-\lambda_1)} e^{-\lambda_1 t} - \frac{n_0 \lambda_1 \lambda_3}{(\lambda_1-\lambda_2)(\lambda_3-\lambda_2)(\lambda_4-\lambda_2)} e^{-\lambda_2 t}$$

$$- \frac{n_0 \lambda_1 \lambda_2}{(\lambda_1-\lambda_3)(\lambda_2-\lambda_3)(\lambda_4-\lambda_3)} e^{-\lambda_3 t} - \frac{n_0 \lambda_1 \lambda_2 \lambda_3}{\lambda_4(\lambda_1-\lambda_4)(\lambda_2-\lambda_4)(\lambda_3-\lambda_4)} e^{-\lambda_4 t}$$

Since the half-life time of Ra C is very small, 10^{-6} seconds, no further calculations are needed beyond Ra C to account for the fourth alpha particle. Therefore, the build-up of the alpha activity N(t) of the sealed source becomes

$$N(t) = n_0 + \lambda_1 p + \lambda_2 q + \lambda_4 s \quad \text{alpha/sec}$$

or

$$N(t) = n_0 [4 - a_1 e^{-\lambda_1 t} - a_2 e^{-\lambda_2 t} - a_3 e^{-\lambda_3 t} - a_4 e^{-\lambda_4 t}] ,$$

where

$$a_1 = 1 + \frac{\lambda_2}{\lambda_2-\lambda_1} + \frac{\lambda_2 \lambda_3 \lambda_4}{(\lambda_2-\lambda_1)(\lambda_3-\lambda_1)(\lambda_4-\lambda_1)} ,$$

$$a_2 = \frac{\lambda_1}{\lambda_1-\lambda_2} + \frac{\lambda_1 \lambda_3 \lambda_4}{(\lambda_1-\lambda_2)(\lambda_3-\lambda_2)(\lambda_4-\lambda_2)} ,$$

$$a_3 = \frac{\lambda_1 \lambda_2 \lambda_4}{(\lambda_1-\lambda_3)(\lambda_2-\lambda_3)(\lambda_4-\lambda_3)} , \text{ and}$$

$$a_4 = \frac{\lambda_1 \lambda_2 \lambda_3}{(\lambda_1-\lambda_4)(\lambda_2-\lambda_4)(\lambda_3-\lambda_4)} .$$

At the steady state,

$$n_0 = \lambda_1 P_0 = \lambda_2 Q_0 = \lambda_3 R_0 = \lambda_4 S_0 ,$$

where P_o, Q_o, R_o, and S_o are, respectively, the contents of radon, Ra A, Ra B, and Ra C, when they all attain the same rate of disintegration as that of radium, n_o. A radium source, as such, is often said to be in equilibrium with its daughter products.

CASE II

In this case it is considered that the source is not perfectly sealed under vacuum; consequently the alpha activity will be partially affected as a result of the continuous loss in the active radon. The source, however, is assumed to be well sealed under atmospheric pressure. Because of the loss in radon through the seal, the rate of supply of radon is taken as $n_o e^{-\alpha t}$, where α is a constant, for mathematical simplicity, and $\alpha < \lambda_1$.

The source activity, in this case, undergoes two different changes: (a) during the pumping out period the activity is continuously affected by loss of part of the radon generated, and (b) under atmospheric pressure no further losses are assumed and the source starts to build up its activity.

To summarize the procedure carried out in Case II: (i) one starts with a source under equilibrium, i.e., with

$$P_o = \frac{n_o}{\lambda_1}, \quad Q_o = \frac{n_o}{\lambda_2}, \quad R_o = \frac{n_o}{\lambda_3}, \text{ and } \quad S_o = \frac{n_o}{\lambda_4},$$

as the initial contents of Rn, Ra A, Ra B, and Ra C, respectively; (ii) the source is then kept under vacuum for an interval of time T, at the end of which the radioactive contents, as a result of radon loss, will

have the values P_T, Q_T, R_T, and S_T, respectively; (iii) radon loss is then assumed to stop after exposing and keeping the source under atmospheric pressure for a long period during which it builds up its activity with P_T, Q_T, R_T, and S_T as the new initial contents.

To find p, q, r, and s under vacuum, one follows the same procedure used in Case I with P_0, Q_0, R_0, S_0, the equilibrium contents, as initial values for radon, Ra A, Ra B, and Ra C, respectively, and $n_0 e^{-\alpha t}$ instead of n_0 as the rate of production of radon. Then the instantaneous values of radon, Ra A, Ra B, Ra C, respectively, are:

$$p(t) = \frac{n_0}{\lambda_1-\alpha} e^{-\alpha t} + N e^{-\lambda_1 t} ,$$

$$q(t) = \frac{n_0 \lambda_1}{(\lambda_1-\alpha)(\lambda_2-\alpha)} e^{-\alpha t} + \frac{\lambda_1 N}{\lambda_2-\lambda_1} e^{-\lambda_1 t} + A e^{-\lambda_2 t} ,$$

$$r(t) = \frac{n_0 \lambda_1 \lambda_2}{(\lambda_1-\alpha)(\lambda_2-\alpha)(\lambda_3-\alpha)} e^{-\alpha t} + \frac{\lambda_1 \lambda_2 N}{(\lambda_2-\lambda_1)(\lambda_3-\lambda_1)} e^{-\lambda_1 t} + \frac{\lambda_2 A}{\lambda_3-\lambda_2} e^{-\lambda_2 t} + B e^{-\lambda_3 t} ,$$

and

$$s(t) = \frac{n_0 \lambda_1 \lambda_2 \lambda_3}{(\lambda_1-\alpha)(\lambda_2-\alpha)(\lambda_3-\alpha)(\lambda_4-\alpha)} e^{-\alpha t} + \frac{\lambda_1 \lambda_2 \lambda_3 N}{(\lambda_2-\lambda_1)(\lambda_3-\lambda_1)(\lambda_4-\lambda_1)} e^{-\lambda_1 t}$$

$$+ \frac{\lambda_2 \lambda_3 A}{(\lambda_3-\lambda_2)(\lambda_4-\lambda_2)} e^{-\lambda_2 t} + \frac{\lambda_3 B}{(\lambda_4-\lambda_3)} e^{-\lambda_3 t} + C e^{-\lambda_4 t} ,$$

where

$$N = \frac{n_0}{\lambda_1} - \frac{n_0}{\lambda_1-\alpha} ,$$

$$A = \frac{n_0}{\lambda_2} - \frac{\lambda_1 N}{\lambda_2-\lambda_1} - \frac{n_0 \lambda_1}{(\lambda_1-\alpha)(\lambda_2-\alpha)} ,$$

$$B = \frac{n_0}{\lambda_3} - \frac{\lambda_2 A}{\lambda_3-\lambda_2} - \frac{\lambda_1 \lambda_2 N}{(\lambda_3-\lambda_1)(\lambda_2-\lambda_1)} - \frac{n_0 \lambda_1 \lambda_2}{(\lambda_1-\alpha)(\lambda_2-\alpha)(\lambda_3-\alpha)} , \text{ and}$$

$$C = \frac{n_0}{\lambda_4} - \frac{\lambda_3 B}{\lambda_4-\lambda_3} - \frac{\lambda_2 \lambda_3 A}{(\lambda_3-\lambda_2)(\lambda_4-\lambda_2)} - \frac{\lambda_1 \lambda_2 \lambda_3 N}{(\lambda_2-\lambda_1)(\lambda_3-\lambda_1)(\lambda_4-\lambda_1)} - \frac{\lambda_1 \lambda_2 \lambda_3 n_0}{(\lambda_1-\alpha)(\lambda_2-\alpha)(\lambda_3-\alpha)(\lambda_4-\alpha)} .$$

P_T, Q_T, R_T, and S_T could then be calculated by substituting T for t.

Now, on raising the pressure to atmospheric and assuming no further loss of radon under these conditions, the activity of the source as an alpha emitter could be evaluated by following exactly the same lines as before. In this case the total activity is given by the sum of the activity in Case I and that of radon, Ra A, Ra B, and Ra C with P_T, Q_T, R_T, and S_T as initial amounts, respectively.

Then the activity of the source becomes:

$$N'(t) = 4\, n_0 - a_1(n_0-\lambda_1)P_T e^{-\lambda_1 t} - \left[n_0 a_2 - \lambda_2 Q' - \frac{\lambda_2\,\lambda_3\,\lambda_4\,Q'}{(\lambda_3-\lambda_2)(\lambda_4-\lambda_2)}\right] e^{-\lambda_2 t}$$

$$- \left[n_0 a_3 - \frac{\lambda_3\,\lambda_4}{\lambda_4-\lambda_3} R'\right] e^{-\lambda_3 t} - [n_0 a_4 - \lambda_4 S'] e^{-\lambda_4 t} \quad ,$$

where a_1, a_2, a_3, a_4 are the same as in Case I,

$$Q' = Q_T - \frac{\lambda_1}{\lambda_2-\lambda_1} P_T \quad ,$$

$$R' = R_T - \frac{\lambda_2}{\lambda_3-\lambda_2} Q' - \frac{\lambda_1\,\lambda_2}{(\lambda_3-\lambda_1)(\lambda_2-\lambda_1)} P_T \quad , \text{ and}$$

$$S' = S_T - \frac{\lambda_3\,R'}{\lambda_4-\lambda_3} - \frac{\lambda_2\,\lambda_3\,Q'}{(\lambda_3-\lambda_2)(\lambda_4-\lambda_2)} - \frac{\lambda_1\,\lambda_2\,\lambda_3\,P_T}{(\lambda_4-\lambda_1)(\lambda_3-\lambda_1)(\lambda_2-\lambda_1)} \quad .$$

The result of some numerical examples is shown in Fig. A.2, where three cases are considered:

(A) T = 72 hours, $\alpha = 0.2\,\lambda_1$,

(B) T = 72 hours, $\alpha = 0.6\,\lambda_1$,

(C) T = 240 hours, $\alpha = 0.6\,\lambda_1$.

The values of λ_1, λ_2, λ_3, and λ_4 are the conventional values for radon, Ra A, Ra B, and Ra C, respectively.[4]

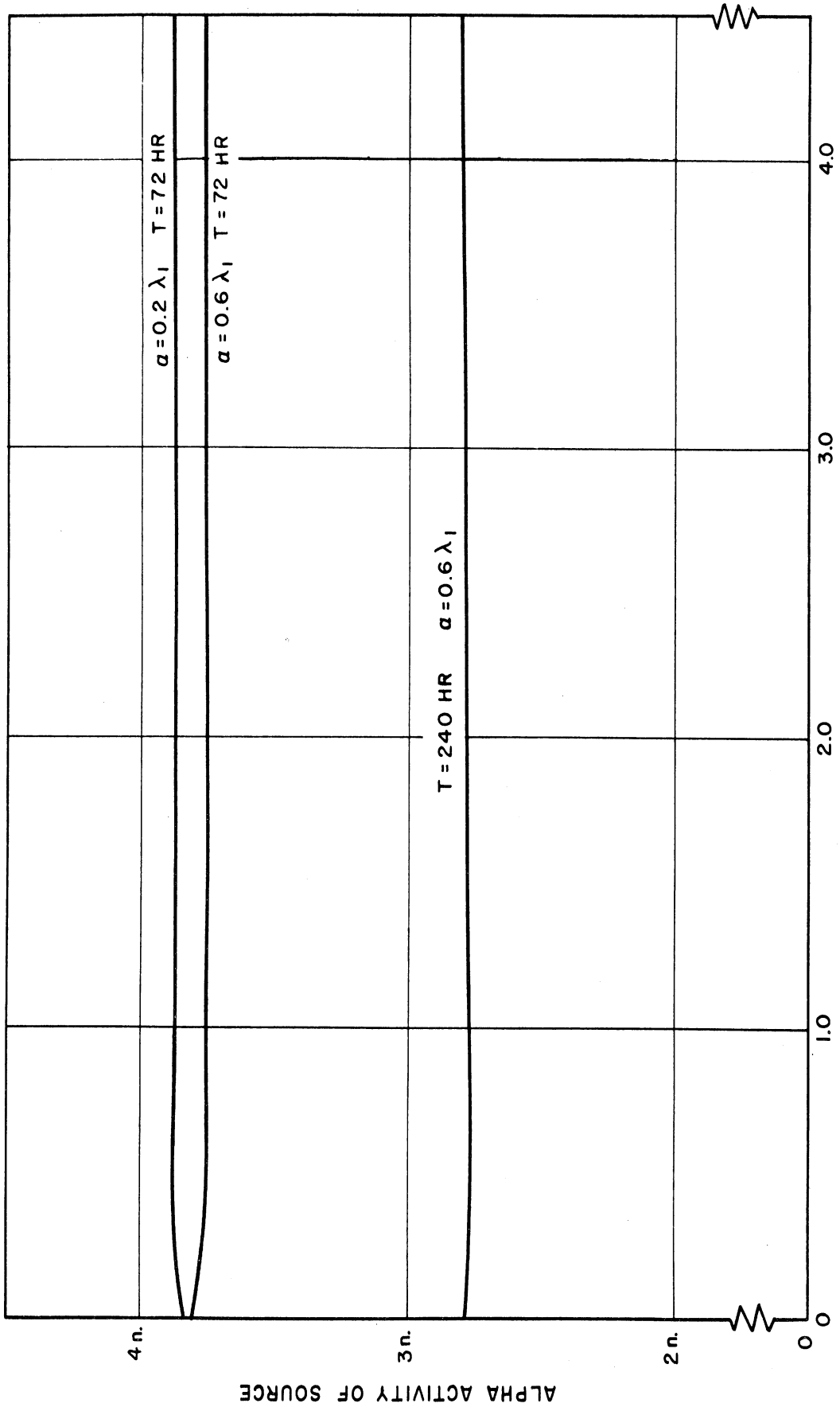

Fig. A.2. Calculated alpha activity of a poorly sealed source

REFERENCES

1. Sicinski, H. S., Spencer, N. W., and Dow, W. G., "Rocket Measurements of Upper Atmosphere Ambient Temperatures and Pressure in the 30-75 km Region," Jour. App. Phys., 25, 161 (1954).

2. Spencer, N. W., Boggess, R. L., Brace, L. H., and El-Moslimany, M. A., A Radioactive Ionization-Gage Pressure-Measurement System, Univ. of Mich. Eng. Res. Inst. Scientific Report 2597-3-S, Ann Arbor, May, 1958.

3. Laby, T. H., and Kaye, G.W.C., "Gaseous Ionization and Pressure," Phil. Mag., S.6, 16, 879 (1908).

4. Rutherford, E., Chadwick, J., and Ellis, C. D., Radiations from Radioactive Substances, Cambridge University Press, New York, 1951.

5. Downing, J. R., and Mellen, G., "A Sensitive Vacuum Gauge with Linear Response," Rev. Sci. Instr., 17, 218 (1946).

6. Bateman, H., "The Solution of a System of Different Equations Occurring in the Theory of Radioactive Transformations," Proc. Camb. Phil. Soc., 15, 423 (1910).

7. Fowler, R. H., "Contribution to the Theory of the Motion of Alpha-Particles Through Matter. Part I. Ranges. Part II. Ionizations," Proc. Camb. Phil. Soc., 21, 521, 531 (1923).

8. Crowther, J. A., Ions, Electrons and Ionizing Radiations, Edward Arnold and Co., London, 1946.

9. Rossi, B., High-Energy Particles, Prentice-Hall, New York, 1952.

10. Jaffé, G., "Zur Theorie der Ionization in Kolonnen," Ann. d. Physik, 43, 303 (1913); "Sur l'Ionization des Diélectriques Liquides par l'Emanation du Radium," Le Radium, 10, 126 (1913).

11. Schemel, J., "Über Trägerrekombination in Gasen," Ann. D. Physik, 85, 137 (1928).

12. Langevin, M. P., "Une Formule Fondamentale de Theorie Cinétique," Ann. de Chem. et Phys., S.8, 5, 245 (1905).

13. Hasse, H. R., "Langevin's Theory of Ionic Mobility," Phil. Mag., S.7, 1, 139 (1926).

14. Hasse, H. R., and Cook, W. R., "The Calculation of the Mobility of Monocmolecular Ions," Phil Mag., S.7, 12, 554 (1931).

15. Loeb, L. B., "Gas Ion Mobilities and Their Independence of the Nature of Ion," Phil. Mag., S.6, 48, 446 (1924).

16. Loeb, L. B., "Gas Ion Mobilities," Letter to the Editors, Phil. Mag., S.6, 49, 517 (1925).

17. Ramsauer, C., "Uber den Wirkungsquerschnitt der Gasmolekule gegenuber langsamen Electronen," Ann. d. Physik, F.4, 64, 513 (1921).

18. Normand, C. E., "The Absorption Coefficient for Slow Electrons in Gases," Phys. Rev., S.2, 35, 1217 (1930).

19. Brode, R. B., "The Quantitative Study of the Collisions of Electrons with Atoms," Rev. Mod. Phys., 5, 257 (1933).

20. Compton, K. T., and Langmuir, I., "Electrical Discharges in Gases--Part I. Survey of Fundamental Processes," Rev. Mod. Phys., 2, 123 (1930).

21. Bradbury, N. E., and Nielsen, R. A., "Absolute Values of the Electron Mobility in Hydrogen," Phys. Rev., S.2, 49, 388 (1936).

22. Nielsen, R. A., "Absolute Values of the Electron Drift Velocity in Nitrogen, Helium, Neon, and Argon," Phys. Rev., S.2, 50, 950 (1936).

23. Nielson, R. A., and Bradbury, N. E., "Electron and Negative Ion Mobilities in Oxygen, Air, Nitrous Oxide and Ammonia," Phys. Rev., S.2, 51, 69 (1937).

24. Loeb, L. B., Basic Processes of Gaseous Electronics, University of California Press, Berkeley, 1955.

25. Moulin, M. M., "Recherches sur l'Ionisation Produite par les Rayons α," Ann. Chem. Phys., 21, 550 (1910); and 22, 26 (1911).

26. Thomson, J. J., "Recombination of Gaseous Ions, the Chemical Combination of Gases, and Monomolecular Reactions," Phil. Mag., S.6, 47, 337 (1924).

27. Dow, W. G., Fundamentals of Engineering Electronics (second ed.), John Wiley and Sons, Inc., New York, 1952.

28. Cobine, J. D., Gaseous Conductors, Theory and Engineering Applications, McGraw-Hill Book Co., New York, 1941.

29. Persson, K. B., Sixth Conference on Gaseous Electronics, Washington, D.C., October 22-24, 1953.

30. Loeb, L. B., "Formation of Negative Ions," Handbuch der Physik, Vol. XXI (Springer-Verlag, Berlin, 1956), p. 445.

31. Massey, H.S.W., Negative Ions (second ed.), Cambridge University Press, New York, 1950.

32. Branscomb, L., "Negative Ions," Advances in Electronics, Vol. IX, Academic Press, New York, 1957.

33. Dalgarno, A., and McDowell, M.R.C., "Charge Transfer and Mobility of H^- Ions in Atomic Hydrogen," Proc. Phys. Soc. (London), A69, 615 (1956).

34. Thomson, J. J., "The Mobility of Negative Ions at Low Pressures," Phil. Mag., S.6, 30, 321 (1915).

35. Brown, C. B., and Rose D. J., "Methods of Measuring the Properties of Ionized Gases at High Frequencies. I - Measurements of Q," J. Appl. Phys., 23, 711 (1952); "II - Measurements of Electric Fields," J. Appl. Phys., 23, 719 (1952).

36. Bradbury, N. E., "Electron Attachment and Negative Ion Formation in Oxygen and Oxygen Mixtures," Phys. Rev., 44, 883 (1933).

37. Cravath, A. M., "The Rate of Formation of Negative Ions by Electron Attachment," Phys. Rev., 33, 605 (1929).

38. Bradbury, N. E., "Photoelectric Currents in Gases Between Parallel Plates as a Function of the Potential Difference," Phys Rev., S.2, 40, 980 (1932).

39. Bloch, F., and Bradbury, N. E., "On the Mechanism of Unimolecular Electron Capture," Phys. Rev., S.2, 48, 689 (1935).

40. Hine, G. J., and Brownell, G. L. (eds.), Radiation Dosimetry, Academic Press, New York, 1956.

41. Boag, J. W., and Wilson, T., "The Saturation Curve at High Ionization Intensity," Brit. J. Appl. Phys., 3, 222 (1952).

42. Thomson, J. J., "On the Theory of the Conduction of Electricity Through Gases by Charged Ions," Phil. Mag., S.5, 47, 253 (1899).

43. Thomson, J. J., Conduction of Electricity Through Gases, Vol. I, University Press, Cambridge, England, 1933.

44. Walker, G. W., "On Saturation Currents in Ionization," Phil. Mag., S.6, 8, 653 (1904).

45. Robb, A. A., "On the Conduction of Electricity Through Gases Between Parallel Plates - Parts I and II," Phil Mag., S.6, 10, 237, 664 (1905).

46. Dwight, H. B., Tables of Integrals and Other Mathematical Data (revised ed.), The MacMillan Company, New York, 1947.

47. Bortner, T. E., and Hurst, G. S., "Ionization of Pure Gases and Mixtures of Gases by 5-Mev Alpha Particles," Phys. Rev., S.2, 93, 1236 (1954).

48. Geballe, R., and Harrison, M. A., "Negative Ion Formation in Oxygen," Phys. Rev., S.2, 85, 372 (1952).

49. Harrison, M. A., and Geballe, R., "Simultaneous Measurement of Ionization and Attachment Coefficients," Phys. Rev., S.2, 91, 1 (1953).

50. Geballe, R., and Reeves, M. I., "A Condition on Uniform Field Breakdown in Electron-Attaching Gases," Phys. Rev., S.2, 92, 867 (1953).

51. Sayers, J., "Ionic Recombination in Air," Proc. Roy. Soc., A.169, 83 (1938).

52. Gardner, M. E., "The Recombination of Ions in Pure Oxygen as a Function of Pressure and Temperature," Phys. Rev., S.2, 53, 75 (1938).